

National Aeronautics and Space Administration



Scaled CMOS Technology Reliability Users Guide

Mark White
Jet Propulsion Laboratory
Pasadena, California

Jet Propulsion Laboratory
California Institute of Technology
Pasadena, California

JPL Publication 09-33 01/10



Scaled CMOS Technology Reliability Users Guide

NASA Electronic Parts and Packaging (NEPP) Program
Office of Safety and Mission Assurance

Mark White
Jet Propulsion Laboratory
Pasadena, California

NASA WBS: 724297.40.43
JPL Project Number: 103982
Task Number: 03.02.02

Jet Propulsion Laboratory
4800 Oak Grove Drive
Pasadena, CA 91109

<http://nepp.nasa.gov>

This research was carried out at the Jet Propulsion Laboratory, California Institute of Technology, and was sponsored by the National Aeronautics and Space Administration Electronic Parts and Packaging (NEPP) Program.

Reference herein to any specific commercial product, process, or service by trade name, trademark, manufacturer, or otherwise, does not constitute or imply its endorsement by the United States Government or the Jet Propulsion Laboratory, California Institute of Technology.

Copyright 2010. California Institute of Technology. Government sponsorship acknowledged.

ABSTRACT

The desire to assess the reliability of emerging scaled microelectronics technologies through faster reliability trials and more accurate acceleration models is the precursor for further research and experimentation in this relevant field. The effect of semiconductor scaling on microelectronics product reliability is an important aspect to the high reliability application user. From the perspective of a customer or user, who in many cases must deal with very limited, if any, manufacturer's reliability data to assess the product for a highly-reliable application, product-level testing is critical in the characterization and reliability assessment of advanced nanometer semiconductor scaling effects on microelectronics reliability. A methodology on how to accomplish this and techniques for deriving the expected product-level reliability on commercial memory products are provided.

Competing mechanism theory and the multiple failure mechanism model are applied to the experimental results of scaled SDRAM products. Accelerated stress testing at multiple conditions is applied at the product level of several scaled memory products to assess the performance degradation and product reliability. Acceleration models are derived for each case. For several scaled SDRAM products, retention time degradation is studied and two distinct soft error populations are observed with each technology generation: early breakdown, characterized by randomly distributed weak bits with Weibull slope $\beta=1$, and a main population breakdown with an increasing failure rate.

Retention time soft error rates are calculated and a multiple failure mechanism acceleration model with parameters is derived for each technology. Defect densities are calculated and reflect a decreasing trend in the percentage of random defective bits for each successive product generation.

A normalized soft error failure rate of the memory data retention time in FIT/Gb and FIT/cm² for several scaled SDRAM generations is presented revealing a power relationship. General models describing the soft error rates across scaled product generations are presented. The analysis methodology may be applied to other scaled microelectronic products and their key parameters.

Table of Contents

List of Tables	vi
List of Figures	vii
Chapter 1: Overview	1
1.1 Background	1
1.1.1 Aerospace Vehicle Systems Institute (AVSI) Consortium	3
1.1.2 Lifetime Enhancement through Derating	4
1.1.3 Derating Factor	6
1.1.4 Failure Mechanism Simulation	7
1.1.5 Micro-Architectural Level Reliability Modeling	8
1.1.6 Circuit-Level Reliability Modeling and Simulation	11
1.1.7 Deep Submicron CMOS VLSI Circuit Reliability Modeling and Simulation	12
1.1.8 Physics-of-Failure Based VLSI Circuits Reliability Simulation and Prediction	15
1.1.9 Product Reliability	16
1.2 CMOS Technology Scaling and Impact	18
1.2.1 MOS Scaling Theory	18
1.2.2 Moore's Law	20
1.2.3 Scaling to Its limits	21
1.2.4 Scaling Impact on Circuit Performance	23
1.2.5 Scaling Impact on Power Consumption	24
1.2.6 Scaling Impact on Circuit Design	25
1.2.7 Scaling Impact on Parts Burn-in	27
1.2.8 Scaling Impact on Long Term Microelectronics Reliability	28
1.3 Physics-of-Failure (PoF) Methodology	31
1.3.1 Competing Mechanism Theory	32
1.3.2 Intrinsic Failure Mechanism Overview	32
1.3.3 Hot Carrier Injection and Statistical Model	33
1.3.4 Electromigration and Statistical Model	35
1.3.5 Negative Bias Temperature Instability and Statistical Model	36
1.3.6 Time-Dependent Dielectric Breakdown and Statistical Model	37
1.3.7 Multiple Failure Mechanism Model	38
1.3.8 Acceleration Factor	40
1.4 Motivation and Objectives	43
1.4.1 Motivation	43
1.4.2 Objectives	47
Chapter 2: Scaling Impact on SDRAM	48
2.1 Overview	48
2.2 Design of Experiments	52
2.2.1 Electrical Test Flow	57
2.2.2 Electrical Test Conditions and Limits	58
2.3 Technology and Construction Analysis	62

2.4	Device Characterization.....	64
2.4.1	Voltage Breakdown	64
2.4.2	Minimum Frequency Operation Characterization	65
2.5	Stress Test Results	65
2.5.1	Stress Test Results (I_{ddo})	66
2.5.2	Retention Time Degradation (Tret)	69
Chapter 3:	SDRAM Degradation and Predictive Model	73
3.1	Acceleration Model.....	73
3.1.1	Life Distribution.....	74
3.1.2	Multivariable Life-Stress Relationship	75
3.2	Data Analysis	81
3.3	Degradation Model	97
Chapter 4:	Physics-of-Failure & Systems Approach	101
4.1	Overview.....	101
4.2	Failure Mechanisms	103
4.3	Discussion.....	103
4.3.1	Randomness	112
4.4	Retention Time Early Breakdown	113
4.5	Power Relationship as a Function of Scaling	117
4.6	Physical Failure Model	120
4.7	DRAM Scaling and Defect Density.....	124
4.8	Soft Error Failure Rate.....	128
Chapter 5:	Conclusion.....	134
5.1	Background.....	134
5.2	Conclusion	134
5.3	Future Work.....	139
Appendix A	140
References	164

List of Tables

Table 1.	Impact of Different Scaling Related Parameters on Intrinsic Failure Mechanisms	9
Table 2.	Experimental Baseline.....	54
Table 3.	Experimental Stress Test Matrix.....	54
Table 4.	Test Conditions and BI Board Layout.....	56
Table 5.	DC Tests, Conditions and Limits.....	59
Table 6a.	Iddo Performance Summary.....	67
Table 6b.	Iddo Performance Characterization Drifts.....	68
Table 7.	T-NT Weibull Model Distribution Parameters – 4.0V	91
Table 8.	T-NT Weibull Model Distribution Parameters – 2.5V	92
Table 9.	Exponential Model Parameters.....	98
Table 10.	Data Retention TTF (t 0.1 Point).....	99
Table 11.	Q-Ratio t_1/t_m at Initial Test Point.....	102
Table 12.	Retention Time Soft Error Rate Calculations.....	113
Table 13a.	130nm Retention Time SER Matrix for Early Failures.....	116
Table 13b.	110nm Retention Time SER Matrix for Early Failures.....	116
Table 13c.	90nm Retention Time SER Matrix for Early Failures.....	116
Table 14.	DRAM Chip and Cell Characteristics.....	125
Table 15.	Normalized Soft Error Failure Rate for Scaled DRAM (FIT/Gb).....	130
Table 16.	Normalized Soft Error Failure Rate for Scaled DRAM (FIT/cm ²).....	131

List of Figures

Figure 1.	<i>D_f</i> versus <i>D_{voltage}</i> with Constant Operating Temperature and Frequency	7
Figure 2.	FIT Values for Processor W/C Conditions.	9
Figure 3.	MaCRO Flow of Lifetime, Failure Rate and Reliability Trend Prediction.	14
Figure 4.	Intrinsic FM Models as a Function of Operating Stress.	16
Figure 5.	Moore's Law.	21
Figure 6.	Trends of Power Supply Voltage, Threshold Voltage, and Gate Oxide Thickness vs. Channel Length for CMOS Logic Devices.	22
Figure 7.	CMOS Performance, Power Density and Circuit Density Trends.	23
Figure 8.	Active and Leakage Power for a Constant Die Size.	24
Figure 9.	CMOS Intrinsic Wearout Failure Mechanisms.	28
Figure 10.	1T1C DRAM Cell.	49
Figure 11a-b.	Current DRAM Trends.	51
Figure 11c.	Current DRAM Trends.	52
Figure 12.	Sapphire S ATE.	55
Figure 13.	National Instruments PCI-6542.	55
Figure 14.	Stress Burn-in Boards.	56
Figure 15.	512Mb SDRAM Functional Block Diagram.	64
Figure 16a-b.	Operating Current and Refresh Current Degradation.	66
Figure 17a-b.	Effect of Temperature on Data Retention for 90nm Technology.	70
Figure 17c-d.	Effect of Temperature on Data Retention for 110nm Technology.	71
Figure 17e-f.	Effect of Temperature on Data Retention for 130nm Technology.	72
Figure 18a.	90nm T-NT/Weibull Initial and 1,000 hr. Stress Plots at Fixed Voltage.	83
Figure 18b.	90nm T-NT/Weibull Initial and 1,000 hr. Stress Plots at Fixed Temperature.	84
Figure 19a.	110nm T-NT/Weibull Initial and 1,000 hr. Stress Plots at Fixed Voltage.	85
Figure 19b.	110nm T-NT/Weibull Initial and 1,000 hr. Stress Plots at Fixed Temperature.	86
Figure 20a.	130nm T-NT/Weibull Initial and 1,000 hr. Stress Plots at Fixed Voltage.	87
Figure 20b.	130nm T-NT/Weibull Initial and 1,000 hr. Stress Plots at Fixed Temperature.	88
Figure 21.	90nm T-NT/Weibull Initial and 1,000 hr. Use Level Plots at Fixed 398.15K and 4.05V.	93
Figure 22.	90nm T-NT/Weibull Initial and 1,000 hr. Reliability Plots at Fixed 398.15K and 4.05V.	94
Figure 23.	90nm T-NT/Weibull Initial and 1,000 hr. FR Plots at Fixed 398.15K and 4.05V.	95
Figure 24.	90nm T-NT/Weibull Initial and 1,000 hr. SD Plots at Fixed 398.15K and 4.05V.	96
Figure 25.	Tret Degradation Prediction at Accelerated Conditions.	100

Figure 26.	130nm Bit Failure Distribution at Initial Time (t_1), 125°C/4.0V.....	106
Figure 27.	130nm Bit Failure Distribution at Time (t_2)	107
Figure 28.	110nm Bit Failure Distribution at Initial Time (t_1), 125°C/4.0V.....	108
Figure 29.	110nm Bit Failure Distribution at Time (t_2)	109
Figure 30.	90nm Bit Failure Distribution at Initial Time (t_1), 125°C/4.0V.....	110
Figure 31.	90nm Bit Failure Distribution at Time (t_2)	111
Figure 32.	Optical Overview of Memory Block Layout.....	112
Figure 33a.	130nm System Retention Time SER (95%CL, 1,000hrs).	114
Figure 33b.	110nm System Retention Time SER (95%CL, 1,000hrs).	115
Figure 33c.	90nm System Retention Time SER (95%CL, 1,000hrs).	115
Figure 34.	DRAM Metal Bit Line.....	124
Figure 35.	Random Defective Bits per Product Generation.....	126
Figure 36.	Normalized Soft Error Failure Rate for Scaled DRAM (FIT/Gb).....	129
Figure 37.	Generalized Soft Error Failure Rate for Scaled DRAM (FIT/Gb)	130
Figure 38.	Normalized Soft Error Failure Rate for Scaled DRAM (FIT/cm ²).....	131
Figure 39.	Generalized Soft Error Failure Rate for Scaled DRAM (FIT/cm ²)	132

Chapter 1: Overview

1.1 Background

NASA, the aerospace community, and other high reliability (hi-rel) users of advanced microelectronic products face many challenges as technology scales into deep sub-micron feature sizes. 90nm and 65nm technologies are now being assessed for product reliability as the desire for higher performance, lower operating power, and lower stand-by power characteristics continue to be sought after in hi-rel space systems. International Technology Roadmap for Semiconductors (ITRS) predictions over the next few years will drive manufacturers to reach both physical and material limitations as technology continues to scale. As a result, new materials, designs and processes will be employed to keep up with the performance demands of the industry. While target product lifetimes for mil-product have generally been ten years at maximum rated junction temperature, leading edge commercial-off-the-shelf (COTS) microelectronics may be somewhat less due to reduced cost consumer electronics and reduced safety and reliability margins, including design life. Therefore, reliability uncertainties through the introduction of new materials, processes and architectures, coupled with the economic pressures to design for 'reasonable life,' pose a concern to the hi-rel user of advanced scaled microelectronics technologies. These aspects, in addition to higher power and thermal densities, increase the risk of introducing new failure mechanisms and accelerating known failure mechanisms.

The desire to assess the reliability of emerging technologies through faster reliability trials and more accurate acceleration models is the precursor for further research and experimentation in this field. Semiconductor scaling effects on microelectronics reliability prediction, qualification strategies and derating criteria for space applications is an area where ongoing research is warranted. Ramp-voltage and constant-voltage stress tests to determine voltage-to-breakdown and time-to-breakdown, coupled with temperature acceleration, can be effective methods to identify and model critical stress levels and the reliability of emerging deep-sub micron microelectronics. Here, an overview of product reliability trends, emerging issues with scaling, derating approaches and physics-of-failure (PoF) considerations for reliability assessment of advanced scaled microelectronics technologies for hi-rel space applications will be presented.

Derating microelectronic devices and their critical stress parameters in aerospace applications has been common practice for decades to improve device reliability and extend operating life in critical missions [1]. Derating is the intentional reduction of key parameters, e.g., supply voltage and junction temperature, to reduce internal stresses and increase device lifetime and reliability. Semiconductor technology scaling and process improvements, however, compel us to reevaluate common failure mechanisms, application and stress conditions, reliability trends, and common derating principles to provide affirmation that adequate derating criteria is applied to current technologies destined for high reliability space systems. It is incumbent upon the user to develop an understanding of advanced technology failure mechanisms through modeling, accelerated testing, and failure analysis prior to the infusion of new nano-scale CMOS products in critical high reliability environments. NASA needs PoF based derating guidance for advanced scaled microelectronic technologies for long-term critical missions. Semiconductor manufacturers in

general do not publish their reliability reports for fear of losing their competitive edge, and customers are often forced into making assumptions with the performance and reliability trade-offs.

There has been steady progress over the years in the development of a physics-of-failure understanding of the effect that various stress drivers have on semiconductor structure performance and wearout. This has resulted in better modeling and prediction capabilities. Applying a PoF approach to reliability prediction and derating of EEE parts for NASA flight projects is an improvement in device reliability assessment on the basis of environmental and operating stresses. The benefit to NASA flight projects as a result of this work include a more technically sound predictive reliability models and derating guidance for the reliable application of flight electronic parts based on a PoF derating approach, particularly for emerging scaled microelectronic technologies.

1.1.1 Aerospace Vehicle Systems Institute (AVSI) Consortium

Some of the more relevant work in this area of research was initiated by the Aerospace Vehicle Systems Institute (AVSI) Consortium in 2002. AVSI Project #17 – *Methods to Account for Accelerated Semiconductor Device Wearout* was established to investigate, understand and address the impacts of microelectronic nanometer technology and its implication on device lifetime as a result of device wearout. The project was oriented toward avionics applications, however, all high-reliability users of scaled microelectronics will benefit from this work. In his thesis, *Methods to Account for Accelerated Semiconductor Device Wearout in Long life*

Aerospace Applications [2], J. Walter supported some of the primary objectives of the AVSI project, including:

- 1) Determination of likely failure mechanisms of future semiconductor devices in avionics applications;
- 2) Development of models to estimate expected lifetimes of future avionics; and
- 3) Development of device assessment methods and avionics system design guidelines.

Walter discussed failure mechanism lifetime models and derating modeling approaches with an emphasis on systems engineering methodologies, impact of scaling, and mitigating the impact of decreasing device reliability in aerospace applications.

1.1.2 Lifetime Enhancement through Derating

A semiconductor device's lifetime may be affected by changing its operating parameters, specifically junction temperature, because of heat activated mechanisms and supply voltage. A semiconductor device's operating voltage (V_{dd}) directly affects many of its parameters. These include current density (j_e) and the electric field (E_{ox}) across the gate dielectric. Supply voltage also has a significant effect on junction temperature (T_j). Junction temperature is the internal operating temperature of a device. It is dependent on the power dissipated from the device (P_D), the ambient operating temperature (T_a), and the sum of the thermal impedances between the die and ambient environment (θ_{ja}). An engineer can exercise some control over each of these factors in a system design.

The relationship for determining the junction temperature is [3]:

$$T_j = \theta_{ja} * P_D + T_a \quad (1.1)$$

The power dissipated in the T_j equation is determined by [4]:

$$P_D = K * C * V_{dd}^2 * f + i_l V_{dd} \quad (1.2)$$

where V_{dd} is the supply voltage, f is the switching frequency, K is the switching factor and C is the average node capacitance. The power dissipated is the sum of both dynamic and static power dissipation. In CMOS circuits, dynamic power is the dominant factor, accounting for at least 90% of the power dissipation [5]. Therefore a first order approximation of the power dissipation is given by:

$$P_D \sim P_{dynamic} = C_{eff} * V_{dd}^2 * f \quad (1.3)$$

where C_{eff} combines the physical capacitance and activity (number of active nodes) to account for the average capacitance charged during each $1/f$ period. While the above equation shows that V_{dd} has a direct impact on junction temperature, V_{dd} has a further impact in that frequency is proportional to it as well. In a CMOS circuit, a reduction in V_{dd} results in a near linear reduction in circuit delay [6].

1.1.3 Derating Factor

The term *Derating Factor* (D_f) is synonymous with *Acceleration Factor* (A_f), but is defined as the ratio of measured MTTF of a semiconductor at its manufacturer rated operating conditions to the measured MTTF of identical devices operating at derated conditions. This is described as:

$$D_f = \left(\frac{MTTF_{derated}}{MTTF_{rated}} \right) \quad (1.4)$$

The desired values for D_f are greater than zero ($D_f > 0$), with larger values providing a longer operational life. Therefore, the derated lifetime is described as:

$$MTTF_{derated} = D_f \times MTTF_{rated} \quad (1.5)$$

Walter [2] went on to model the individual and combined electromigration (EM), hot carrier degradation (HCD), time-dependent-dielectric-breakdown (TDDB), and derating factor vs. derated voltage while keeping operating temperature and frequency constant in Figure 1. In the case of the three intrinsic wearout mechanisms discussed, the combined total derating factor is described by Walter as:

$$D_f = \frac{\lambda}{\frac{\lambda_{EM}}{D_{JEM}} + \frac{\lambda_{HCD}}{D_{JHCD}} + \frac{\lambda_{TDDB}}{D_{JTDDB}}} \quad (1.6)$$

where λ can represent either the total failure rate or the sum of the failure rates of the wearout mechanisms. This will result in two different answers, the total derating factor and wearout derating factor respectively.

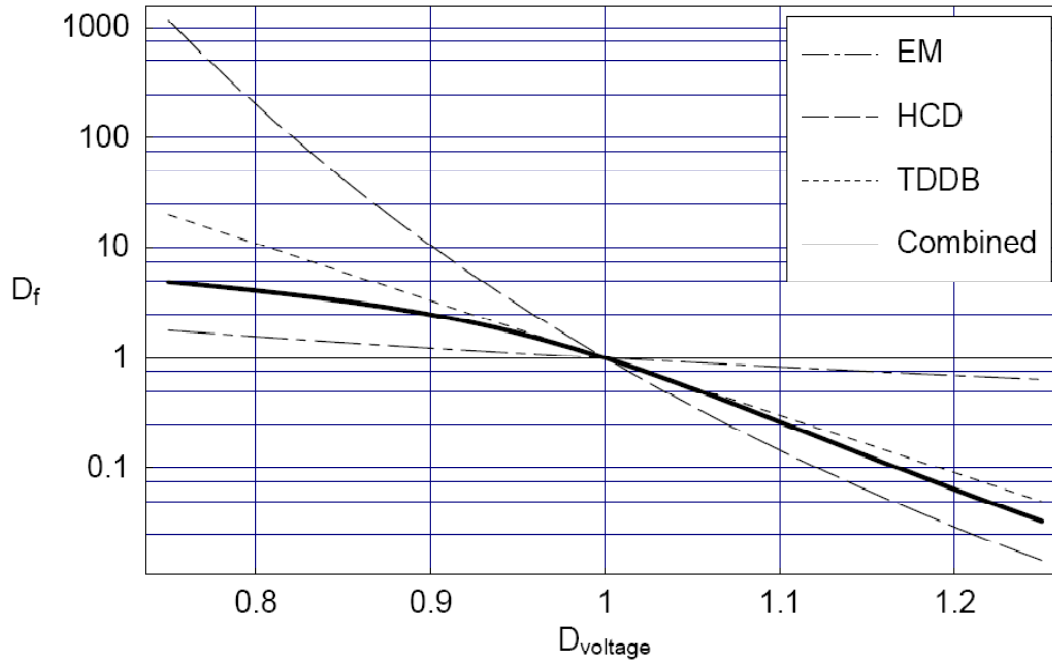


Figure 1. D_f versus $D_{voltage}$ with Constant Operating Temperature and Frequency.

$\lambda_{EM} = \lambda_{TDDDB} = \lambda_{HCD}$, $T_j = 85^\circ\text{C}$, $T_a = 20^\circ\text{C}$, $V_{dd,max} = 3.3\text{V}$, $V_{th} = 0.8\text{V}$, $E_{aEM} = 0.8\text{ eV}$, $n = 2$, $B = 70$, $E_{aTDDDB} = 0.75\text{ eV}$, $E_{ox} = 4\text{ MV/cm}$, $g = 3\text{ Naperians per MV/cm}$.

Due to the low failure rates of semiconductor devices, a device's failure rate is normally determined through accelerated life testing and then extrapolated back to at-use conditions, using an acceleration factor, in order to approximate an MTTF. When accelerated life testing is used to determine the rated lifetime of a device, care must be taken to ensure that all the relevant failure mechanisms are accelerated in order to make a reasonable extrapolation of the device's failure rate.

1.1.4 Failure Mechanism Simulation

Over the years, there has been a significant amount of simulation work that focuses on individual failure mechanisms and their impact on semiconductor reliability. Of note, Hsu, et al. [7] and

Chun, et al. [8] developed CAD tools for hot carrier induced damage effects in VLSI circuits; Alam, et. al. [9] developed models to simulate microelectronic reliability from electromigration damage; and P.C. Li, et al. [10] studied the effect of oxide failure on microelectronic reliability using simulation. Electromigration and hot-carrier effects on performance degradation of a 2-stage op-amp were simulated on a CAD reliability tool integrated with a Cadence Spectre simulator by Xuan and Chatterjee [11].

Attempts have been made over the years to simulate multiple failure mechanisms in microelectronics. Some of the earlier ones include Lathrop, et al. [12] who provided an investigative program using a CAD tool to improve microelectronic reliability by generating failure information due to electromigration, charge injection and electrostatic discharge; in 1992, Hu [13] developed a circuit reliability simulation model called BERT, that simulates the hot electron effect, oxide time-dependent breakdown, electromigration, bipolar transistor gain degradation, and radiation effects on microelectronics as part of the design process. As simulators became more advanced, more sophisticated approaches to modeling device performance and reliability were developed.

1.1.5 Micro-Architectural Level Reliability Modeling

While junction temperature reduction has traditionally been the primary derating focus, various SRAM field studies of commercial devices, and experimental research and modeling of the effects of duty cycle and V_{dd} stresses on the device, suggest that derating these elements with T_j can provide an order of magnitude or more improvement in reliability (FIT) [14-16]. The circuit design and application, however, must be robust enough to operate at the lower end of the device

performance and specification limits. In 2004, J. Srinivasan and the University of Illinois [17] conducted processor RAMP modeling which provided FIT estimates across 180nm to 65nm technologies for a processor operating at worst case conditions. The impact of different scaling related parameters on intrinsic failure mechanisms is presented in Table 1 [17]. FIT estimates for TDDB, EM, Stress Migration (SM) and Thermal Cycling (TC) related failure mechanisms, and their relative contribution to total FIT are summarized in Figure 2. On average, the simulated failure rate (FR) of a scaled 65nm processor may be as high as 316% higher than a similarly pipelined 180nm device [17].

Table 1. Impact of Different Scaling Related Parameters on Intrinsic Failure Mechanisms.

Failure Mech.	Major temperature dependence	Voltage dependence	Feature size dependence
EM	$e^{-\frac{E_{aEM}}{kT}}$		wh
SM	$ T - T_0 ^{-m} e^{-\frac{E_{aSM}}{kT}}$		
TDDB	$e^{-\frac{(X + \frac{Y}{T} + ZT)}{kT}}$	$(\frac{1}{V})^{(a-bT)}$	$10^{\frac{\Delta t_{op}}{0.22}}$
TC	$\frac{1}{T^q}$		

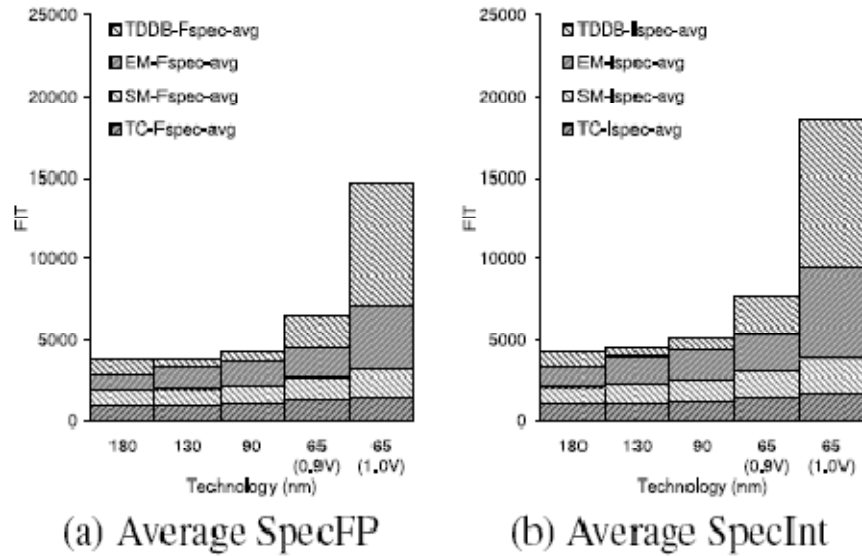


Figure 2. FIT Values for Processor W/C Conditions. Application for Model (a) and Model (b) with Relative Contribution of Each Mechanism.

Generally accepted models for MTTF due to EM, SM, TDDB and TC used in Srinivasan's model have been published in JEDEC Publication JEP122-A [18] and are recapitulated here for completeness:

$$t_{fEM} \propto (J)^{-n} \exp \frac{E_{aEM}}{kT} \quad (1.7)$$

where J is the current density in the interconnect, E_{aEM} is the activation energy for electromigration, k is Boltzmann's constant, and T is absolute temperature in Kelvin. n and E_{aEM} are constants that depend on the interconnect metal used.

$$t_{fSM} \propto |T_o - T|^{-m} \exp \frac{E_{aSM}}{kT} \quad (1.8)$$

where T is the absolute temperature in Kelvin, T_o is the stress free temperature of the metal (the metal deposition temperature), and m and E_{aSM} are material dependent constants.

$$t_{fTDDB} \propto \left(\frac{1}{V} \right)^{a-bT} \exp \frac{\left(X + \frac{Y}{T} + ZT \right)}{kT} \quad (1.9)$$

where T is the absolute temperature in Kelvin, a , b , X , Y , and Z are fitting parameters, and V is the voltage.

$$t_{fTC} \propto \left(\frac{1}{T_{average} - T_{ambient}} \right)^q \quad (1.10)$$

where $T_{ambient}$ is the ambient temperature in Kelvin, $T_{average} - T_{ambient}$ is the average large thermal cycle experienced by a structure on a chip, and q is the Coffin-Manson exponent, an empirically determined material-dependent constant.

Srinivasan makes two specific contributions. First, he describes an architecture-level model and its implementation, called RAMP, which can dynamically track lifetime reliability responding to changes in application behavior. RAMP is based on state-of-the-art device models for different wearout mechanisms. Second, he proposes dynamic reliability management (DRM) - a technique where a processor can respond to changing application behavior to maintain its lifetime reliability target. Contrary to current worst-case behavior based reliability qualification methodologies, DRM allows processors to be qualified for reliability at lower (but more likely) operating points than the worst case.

1.1.6 Circuit-Level Reliability Modeling and Simulation

There has been work over the years that has focused on the impact of intrinsic failure mechanisms on the circuit. Kumar, et al. [19] modeled NBTI degradation of threshold voltage and static noise margin (SNM) on 100nm and 70nm SRAM cells. In 2002, Reddy, et al. [20] demonstrated that SNM of an SRAM memory cell degrades on an 130nm CMOS process by NBTI and that the relative degradation increases as the operating voltage decreases. This was confirmed by measuring an increase in the relative frequency degradation of an NBTI stressed ring oscillator as the operating voltage dropped. Jha, et al. [21] later attempted to quantify circuit level degradation due to NBTI by simulating a variety of analog/mixed signal circuits.

In addition to hot carrier effects on circuit level reliability, thin oxide reliability in scaled CMOS devices has been modeled to predict breakdown at the device level and to determine the impact on circuit performance. J. Stathis describes this approach in [22] and explains how soft breakdown is the most common mode for a constant-current stress, while hard breakdown generally occurs during constant-voltage stress. Rosenbaum, et al. [23] also developed a circuit reliability simulator oxide breakdown module.

Khin, et al. [24] worked on a circuit reliability simulator for interconnects and contact electromigration.

1.1.7 Deep Submicron CMOS VLSI Circuit Reliability Modeling and Simulation

A new SPICE reliability simulation methodology that shifts the focus of reliability analysis from device wearout to circuit functionality was developed in 2005 by X. Li [25]. A set of accelerated lifetime models and failure equivalent circuit models were proposed for the most common MOSFET intrinsic wearout mechanisms, including hot carrier injection (HCI), negative bias temperature instability (NBTI), and TDDB. The accelerated lifetime models help to identify the most degraded transistors in a circuit in terms of the device's terminal voltage and current waveforms. Corresponding failure equivalent circuit models are then incorporated into the circuit to substitute the identified transistors. Finally, SPICE simulation is performed again to check circuit functionality and analyze the impact of device wearout on circuit operation. Device wearout effects are lumped into a very limited number of failure equivalent circuit model parameters, and circuit performance degradation and functionality are determined by the magnitude of these parameters.

In Li's approach, it is unnecessary to perform a large number of small-step SPICE simulation iterations, making simulation time much shorter in comparison to other tools. In addition, a reduced set of failure equivalent circuit model parameters, rather than a large number of device SPICE model parameters, need to be accurately characterized at each interim wearout process. Thus, device testing and parameter extraction work are also significantly simplified. The Maryland Circuit Reliability Oriented (MaCRO) SPICE simulation methodology flow is summarized in Figure 3 [25].

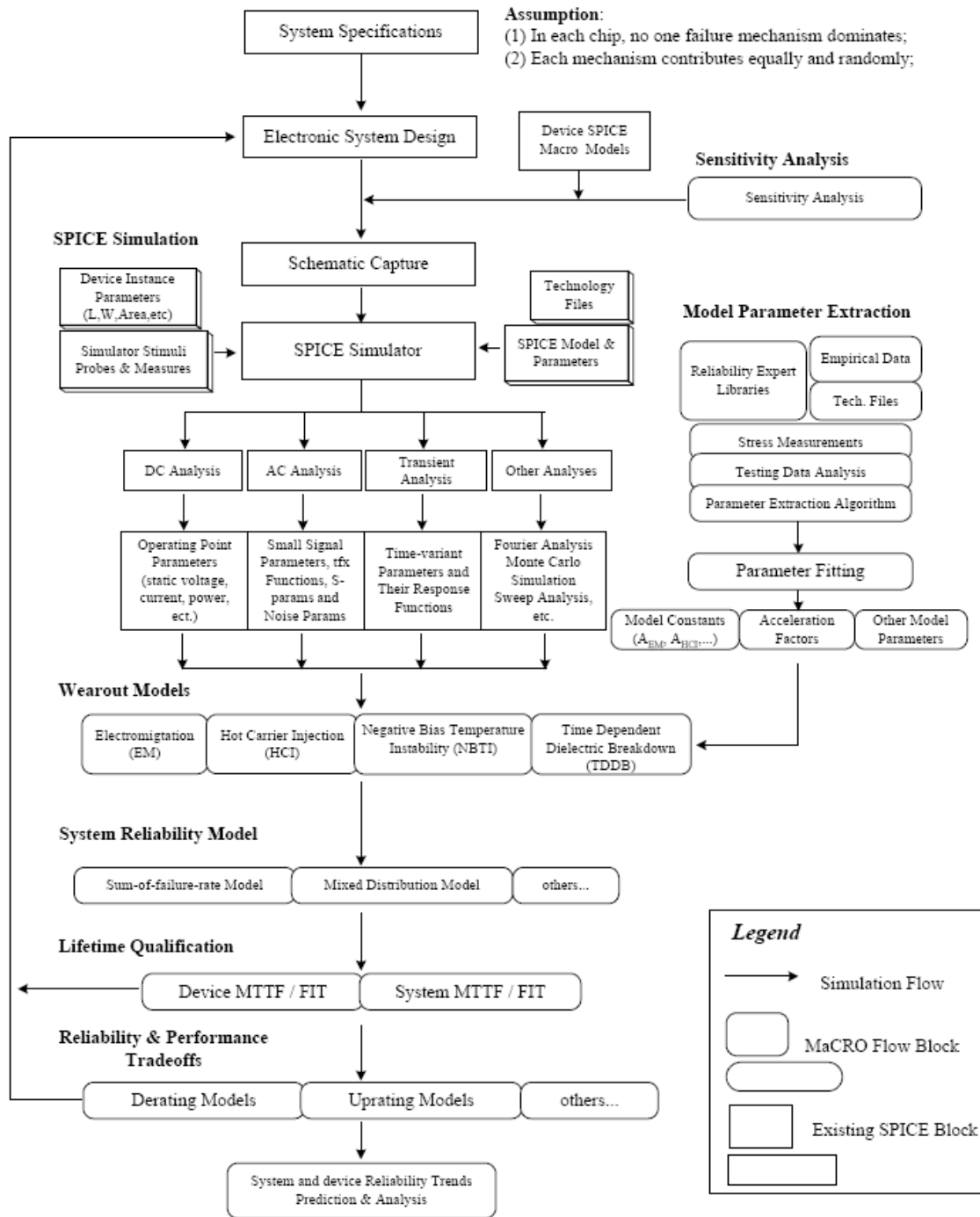


Figure 3. MaCRO Flow of Lifetime, Failure Rate and Reliability Trend Prediction.

1.1.8 Physics-of-Failure Based VLSI Circuits Reliability Simulation and Prediction

Most recently, J. Qin [26] proposed a physics-of-failure based statistical reliability prediction methodology to simplify the modeling and simulation complexity of the effect of multiple intrinsic failure mechanisms on semiconductor devices. Dynamic stress modeling utilizing PoF models for each failure mechanism with the best-fit lifetime distribution provided a reliability prediction for a 90nm SRAM module case study. With a specified application profile, simulation results revealed that TDDDB was the most serious reliability concern for the SRAM bit cell, NBTI was the second dominating mechanism, and HCI had a negligible degradation effect. The memory core's reliability prediction showed that the memory core had a constant failure rate up to 60,000 hours, and an increasing failure rate beyond 60,000 hours. Figure 4 provides a graphical representation of how intrinsic failure mechanisms may be modeled as a function of operating stresses.

The MaCRO simulation models proposed by Li and Qin may become useful to properly derate device and operating parameters to improve reliability and predict reliability trends in scaled technologies. This PoF approach to derating can become an important framework for hi-rel application users to derate product level voltages and temperatures to achieve the desired reliability of current scaled COTS microelectronics.

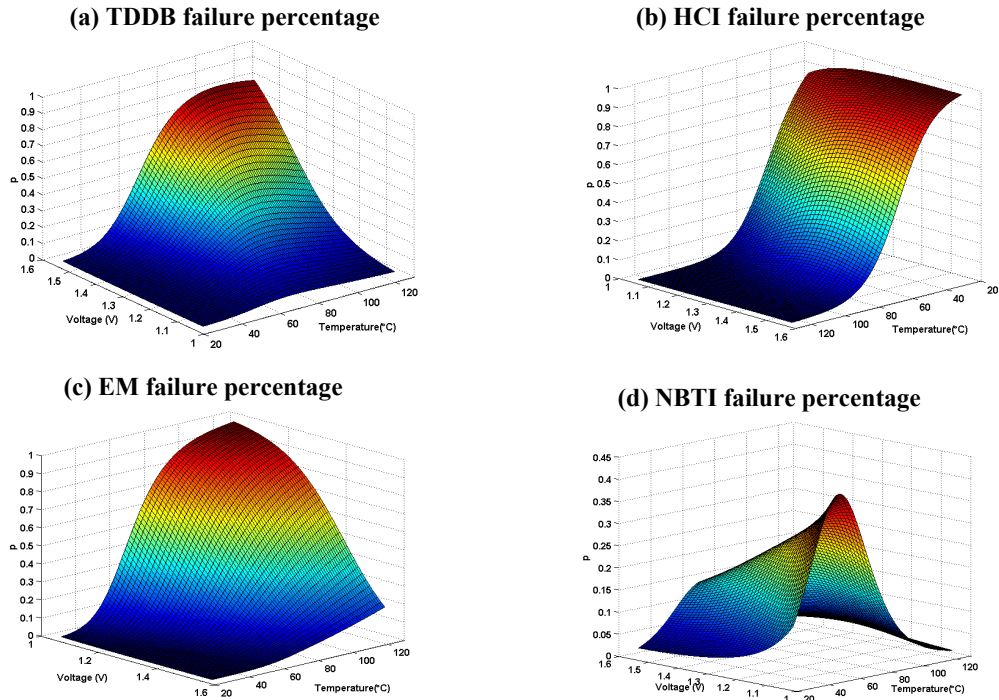


Figure 4. Intrinsic Failure Mechanism Models as a Function of Operating Stress.

1.1.9 Product Reliability

There has been a limited amount of product reliability data and studies published driving the need for independent assessment of the wearout and degradation characteristics of scaled technologies from a PoF standpoint. Most product reliability data is kept proprietary by the manufacturers in an effort to maintain their competitive edge. However, understanding the product reliability and performance metrics throughout the useful life and how best to mitigate the effects of degradation and failure in the application is essential.

One approach to product lifetime reliability accelerated testing is described by Mazzuchi and Soyer [27] in their Bayes method for assessing product reliability. In their approach, relevant information on both failure probabilities and the reliability growth process is used to develop the prior joint distribution for the probability of failure type over the testing range. The results are

then used at a particular test stage to update the knowledge of the probability of each failure type and the product reliability of the current test stage and subsequent test stages. Jee, et al. [28] developed an approach to optimize test coverage and test application time of an embedded SRAM using a defect-based approach, e.g., shorts and opens in a memory cell array. In their approach, faults are extracted and analyzed from a representative portion of the array, and the results are replicated for the entire memory array to reduce test time.

Estimating long-term performance of scaled microelectronic products can be difficult because accelerated life testing (ALT) involving elevated stresses can often result in either too few or no failures to make realistic predictions or inferences. Tang, et al. [29] describes a methodology to overcome this problem by using accelerated degradation testing (ADT) as a means to predict performance in such cases. By identifying key performance measures which are expected to degrade over time, product reliability can be inferred by the degradation paths without observing actual physical failures. Using this approach, the user defines a failure as the first time a key performance measure exceeds a pre-specified threshold, and then the degradation path is correlated to product reliability.

Krasich [30] and Turner [31] discuss product reliability and accelerated testing in their work, and Turner addresses failure mitigation and challenges as microelectronics scale to 90nm and beyond. Other notable accelerated degradation modeling methodologies include: the statistical methods of using degradation measures to estimate the time-to-fail distribution for a variety of degradation models developed by Lu and Meeker [32]; a model for analyzing linear degradation data proposed by Lu, et al. [33]; and the method to handle degradation failures developed by Guo

and Mettas [34] by applying amplification factors with control factors to model the degradation process.

1.2 CMOS Technology Scaling and Impact

Over the past three decades, CMOS technology scaling has been a primary driver of the electronics industry and has provided a path toward both denser and faster integration [35-47]. The transistors manufactured today are twenty times faster and occupy less than 1% of the area of those built twenty years ago. Predictions of size reduction limits have proven to elude the most insightful scientists and researchers. The predicted ‘limit’ has been dropping at nearly the same rate as the size of the transistors.

The number of devices per chip and the system performance has been improving exponentially over the last two decades. As the channel length is reduced, the performance improves, the power per switching event decreases, and the density improves. But the power density, total circuits per chip, and the total chip power consumption have been increasing. The need for more performance and integration has accelerated the scaling trends in almost every device parameter, such as lithography, effective channel length, gate dielectric thickness, supply voltage, and device leakage. Some of these parameters are approaching fundamental limits, and alternatives to the existing material and structures may need to be identified in order to continue scaling.

1.2.1 MOS Scaling Theory

During the early 1970s, both Mead [35] and Dennard [36] noted that the basic MOS transistor structure could be scaled to smaller physical dimensions. One could postulate a “scaling factor”

of λ , the fractional size reduction from one generation to the next generation, and this scaling factor could then be directly applied to the structure and behavior of the MOS transistor in a straightforward multiplicative fashion. For example, a CMOS technology generation could have a minimum channel length L_{min} , along with technology parameters such as the oxide thickness t_{ox} , the substrate doping N_A , the junction depth x_j , the power supply voltage V_{dd} , the threshold voltage V_{th} , etc. The basic “mapping” to the next process, $L_{min} \rightarrow \lambda L_{min}$, involved the concurrent mappings of $t_{ox} \rightarrow \lambda t_{ox}$, $N_A \rightarrow \lambda N_A$, $x_j \rightarrow \lambda x_j$, $V_{dd} \rightarrow \lambda V_{dd}$, and $V_{th} \rightarrow \lambda V_{th}$. Thus, the structure of the next generation process could be known beforehand, and the behavior of circuits in that next generation could be predicted in a straightforward fashion from the behavior in the present generation. The scaling theory developed by Mead and Dennard is solidly grounded in the basic physics and behavior of the MOS transistor. Scaling theory allows a “photocopy reduction” approach to feature size reduction in CMOS technology, and while the dimensions shrink, scaling theory causes the field strengths in the MOS transistor to remain the same across different process generations. Thus, the “original” form of scaling theory is constant field scaling.

Constant field scaling requires a reduction of the power supply voltage with each technology generation. In the 1980s, CMOS adopted the 5V power supply, which was compatible with the power supply of bipolar TTL logic. Constant field scaling was replaced with constant voltage scaling, and instead of remaining constant, the fields inside the device increased from generation to generation until the early 1990s, when excessive power dissipation and heating, gate dielectrics TDDB, and channel hot carrier aging caused serious problems with the increasing electric field. As a result, constant field scaling was applied to technology scaling in the 1990s.

Constant field scaling requires that the threshold voltage be scaled in proportion to the feature size reduction. However, ultimately threshold voltage scaling is limited by the sub-threshold slope of the MOS transistor, which itself is limited by the thermal voltage kT/q , where the Boltzmann constant, k and the electron charge, q are fundamental constants of nature and cannot be changed. The choice of the threshold voltage in a particular technology is determined by the off-state current goal per transistor and the sub-threshold slope. With off-current requirements remaining the same (or even tightening) and the sub-threshold slope limited by basic physics, the difficulty with scaling the threshold voltage is clear. Because of this, the power supply voltage decreased corresponding with the constant field scaling, but the threshold voltage was unable to scale as aggressively. This situation worsens as feature sizes and power supply voltages continue to scale. This is a fundamental problem with further CMOS technology scaling.

1.2.2 Moore's Law

It was the realization of scaling theory and its usage in practice which has made possible the better-known "Moore's Law." Moore's Law is a phenomenological observation that the number of transistors on integrated circuits doubles every two years, as shown in Figure 5. It is intuitive that Moore's Law cannot be sustained forever. However, predictions of size reduction limits due to material or design constraints, or even the pace of size reduction, have proven to elude the most insightful scientists. The predicted 'limit' has been dropping at nearly the same rate as the size of the transistors.

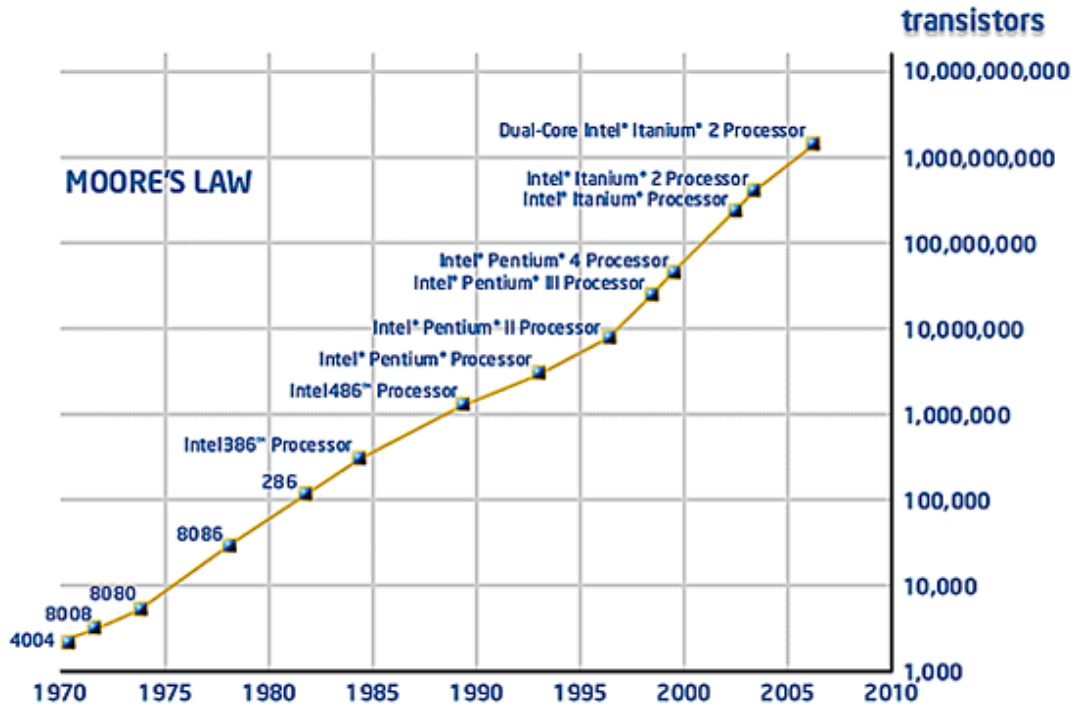


Figure 5. Moore's Law.

1.2.3 Scaling to its Limits

There does not seem to be any fundamental physical limitation that would prevent Moore's Law from characterizing the trends of integrated circuits. However, sustaining this rate of progress is not straightforward [39].

Figure 6 shows the trends of power supply voltage, threshold voltage, and gate oxide thickness versus channel length for high performance CMOS logic technologies [40]. Sub-threshold non-scaling and standby power limitations bound the threshold voltage to a minimum of 0.2V at the operating temperature. Thus, a significant reduction in performance gains is predicted below 1.5V due to the fact that the threshold voltage decreases more slowly than the historical trend, leading to more aggressive device designs at higher electric fields.

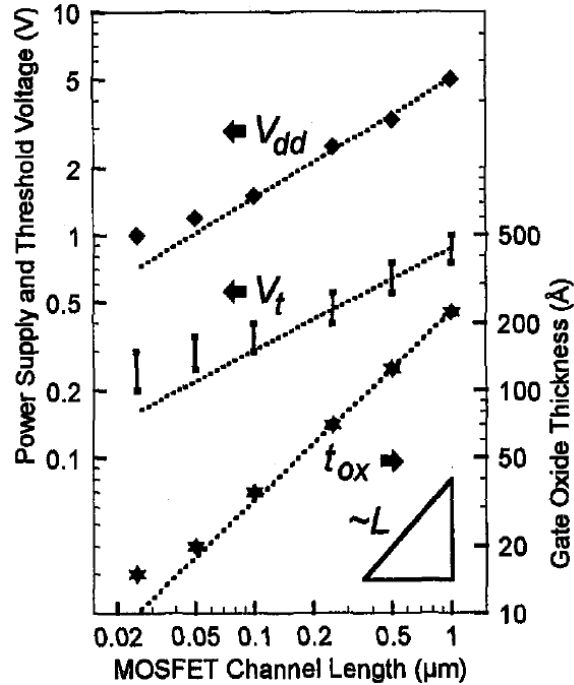


Figure 6. Trends of Power Supply Voltage V_{dd} , Threshold Voltage V_{th} , and Gate Oxide Thickness t_{ox} , versus Channel Length for CMOS Logic Technologies.

Further technology scaling requires major changes in many areas, including: 1) improved lithography techniques and non-optical exposure technologies; 2) improved transistor design to achieve higher performance with smaller dimensions; 3) migration from current bulk CMOS devices to novel materials and structures, including silicon-on-insulator, strained Si and novel dielectric materials; 4) circuit sensitivity to soft errors from radiation; 5) smaller wiring for on-chip interconnection of the circuits; 6) stable circuits; 7) more productive design automation tools; 8) denser memory cells, and 9) manageable capital costs. Metal gate and high-k gate dielectrics were introduced into production in 2007 to maintain technology scaling trends [48].

In addition, packaging technology needs to progress at a rate consistent with on-going CMOS technology scaling at sustainable cost/performance levels. This requires advances in I/O density,

bandwidth, power distribution, and heat extraction. System architecture will also be required to maximize the performance gains achieved in advanced CMOS and packaging technologies.

1.2.4 Scaling Impact on Circuit Performance

Transistor scaling is the primary factor in achieving high-performance microprocessors and memories. Each 30% reduction in CMOS IC technology node scaling has [41, 49]: 1) reduced the gate delay by 30% allowing an increase in maximum clock frequency of 43%; 2) doubled the device density; 3) reduced the parasitic capacitance by 30%; and 4) reduced energy and active power per transition by 65% and 50%, respectively. Figure 7 shows CMOS performance, power density and circuit density trends, indicating a linear circuit performance as a result of technology scaling [41].

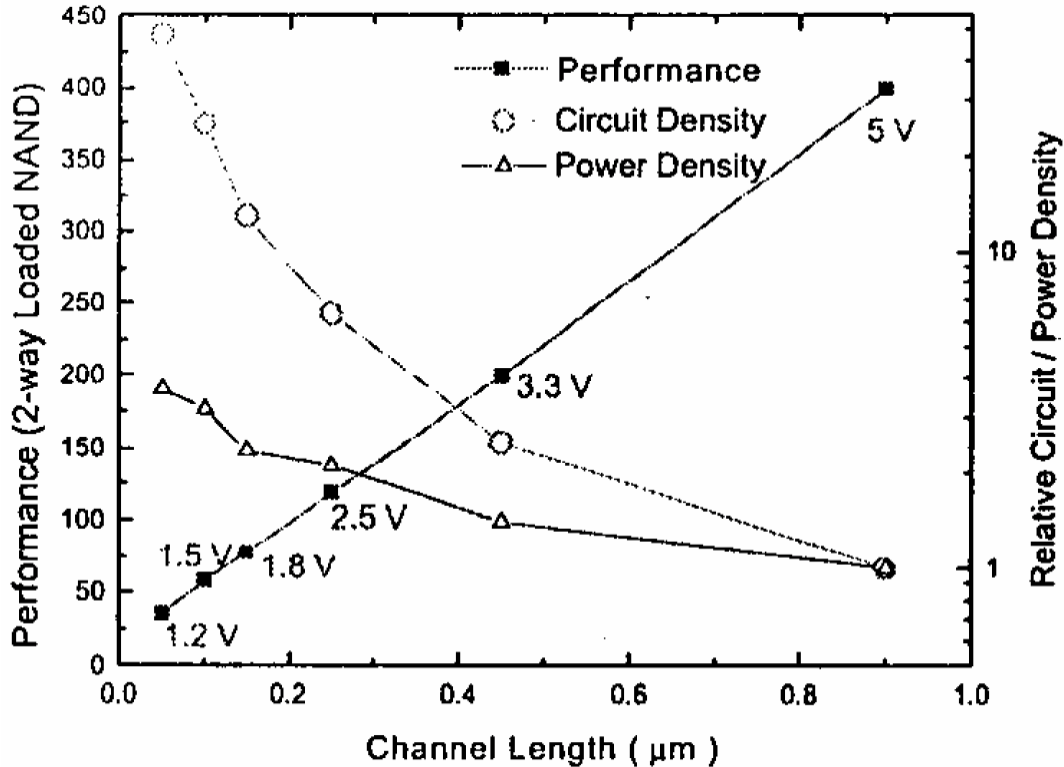


Figure 7. CMOS Performance, Power Density and Circuit Density Trends.

1.2.5 Scaling Impact on Power Consumption

Dynamic power and leakage current are the major sources of power consumption in CMOS circuits. Leakage related power consumption has become more significant as threshold voltage scales with technology. There are several studies that deal with the impact of technology scaling in various aspects of CMOS VLSI design [39, 47, 50-52].

Figure 8 [51] illustrates how the dynamic and leakage power consumption vary across technologies, where P_{act} is the dynamic power consumption and P_{leak} is the leakage power consumption. The estimates have only captured the influence of sub-threshold currents since they are the dominant leakage mechanism. For sub-100nm technologies, temperature has a much greater impact on the leakage power consumption than the active power consumption for the same technology. In addition, the leakage power consumption increases almost exponentially.

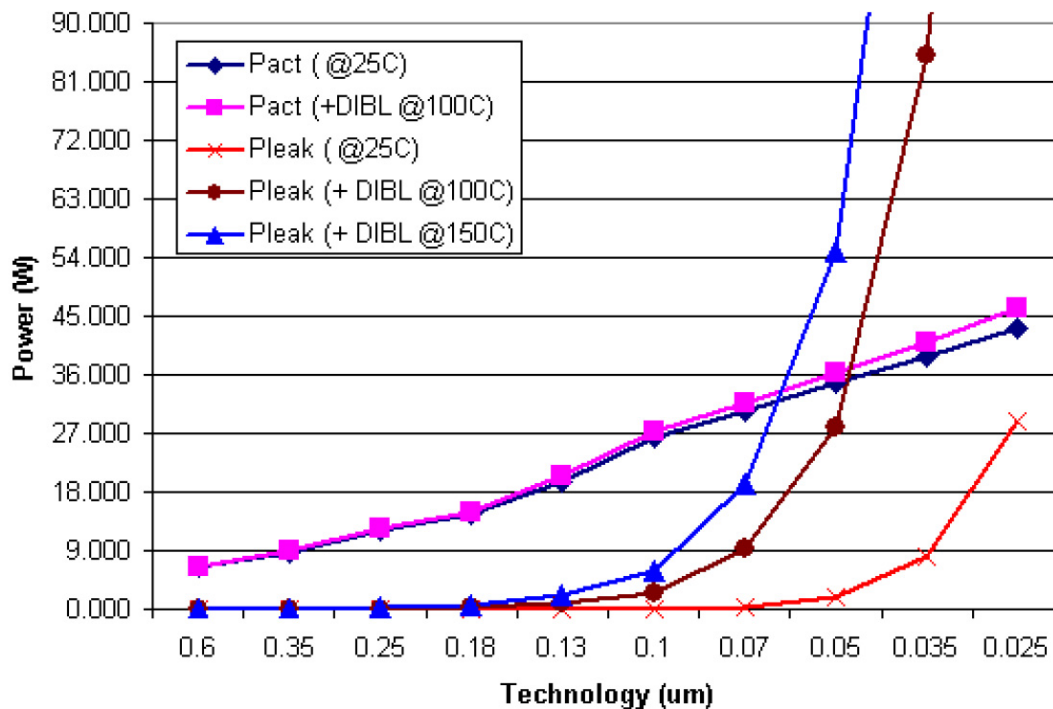


Figure 8. Active and Leakage Power for a Constant Die Size.

1.2.6 Scaling Impact on Circuit Design

With continuing aggressive technology scaling, it is increasingly difficult to sustain supply and threshold voltage scaling to provide the required performance increase, limit energy consumption, control power dissipation, and maintain reliability. These requirements pose several difficulties across a range of disciplines. On the technology front, the question arises whether we can continue along the traditional CMOS scaling path – reducing effective oxide thickness, improving channel mobility, and minimizing parasitics. On the design front, researchers are exploring various circuit design techniques to deal with process variation, leakage and soft errors [41, 47].

For CMOS technologies beyond 90nm, leakage power is one of the most crucial design components which must be efficiently controlled in order to utilize the performance advantages of these technologies. It is important to analyze and control all components of leakage power, placing particular emphasis on sub-threshold and gate leakage power. A number of issues must be addressed, including low voltage circuit design under high intrinsic leakage, leakage monitoring and control, effective transistor stacking, multi-threshold CMOS, dynamic threshold CMOS, well biasing techniques, and design of low leakage data-paths and caches.

While supply voltage scaling becomes less effective in providing power savings as leakage power becomes larger due to scaling, it is suggested that the goal is to no longer have simply the highest performance, but instead have the highest performance within a particular power budget by considering the physical aspects of the design. In some cases, it may be possible to balance the benefit of using high threshold devices from a low leakage process running at the higher

possible frequency at a full V_{dd} , as opposed to using faster but leakier devices which require more voltage scaling in order to reach the desired power budget.

Nanometer design technologies must work under tight operating margins, and are therefore highly susceptible to any process and environmental variability. Traditional sources of variation due to circuit and environmental factors, such as cross capacitance, power supply integrity, multiple inputs switching, and errors arising due to tools and flows, affect circuit performance significantly. To address environmental variation, it is important to build circuits that have well-distributed thermal properties, and to carefully design supply networks to provide reliable V_{dd} and ground levels throughout the chip.

With technology scaling, process variation has become more of a concern and has received an increased amount of attention from the design automation community. Several research efforts have addressed the issue of process variation and its impact on circuit performance [49, 53-55]. A worst-case approach was first used to develop the closed form models for sensitivity due to different parameter variations for a clock tree [53], and was further developed to include interconnect and device variation impact on timing delay due to technology scaling [49]. The impact of systematic variation sources was then considered in [54]. Finally, an integrated variation analysis technique was developed in [55], which considers the effects of both systematic and random variation in both interconnect and devices simultaneously. The design community has realized that in order to address the process-induced variations and to ensure the final circuit reliability, instead of treating timing in a worst-case manner, as is conventionally done in static timing analysis, statistical techniques need to be employed that directly predict the

percentage of circuits that are likely to meet a timing specification. The effects of uncertainties in process variables must be modeled using statistical techniques, and they must be utilized to determine variations in the performance parameters of a circuit.

1.2.7 Scaling Impact on Parts Burn-In

Power supply voltage in scaled technologies must be lowered for two main reasons [56]: 1) to reduce the device internal electric fields and 2) to reduce active power consumption since it is proportional to V_{dd}^2 . As V_{dd} scales, then V_{th} must also be scaled to maintain drain current overdrive to achieve higher performance. Lower V_{th} leads to higher off-state leakage current, which is the major problem with burn-in of scaled nanometer technologies.

The total power consumption of high-performance microprocessors increases with scaling. Off-state leakage current is a higher percentage of the total current at the sub-100nm nodes under nominal conditions. The ratio of leakage to active power becomes worse under burn-in conditions and the dominant power consumption is from the off-state leakage. Typically, clock frequencies are kept in the tens of megahertz range during burn-in, resulting in a substantial reduction in active power. Conversely, the voltage and temperature stresses cause the off-state leakage to be the dominant power component.

Stress during burn-in accelerates the defect mechanisms responsible for early-life failures. Thermal and voltage stresses increase the junction temperature resulting in accelerated aging. Elevated junction temperature, in turn, causes leakages to further increase. In many situations, this may result in positive feedback leading to thermal runaway. Such situations are more likely

to occur as technology is scaled into the nanometer region. Thermal runaway increases the cost of burn-in dramatically. To avoid thermal runaway, it is crucial to understand and predict the junction temperature under normal and stress conditions. Junction temperature, in turn, is a function of ambient temperature, package to ambient thermal resistance, package thermal resistance, and static power dissipation. Considering these parameters, one can optimize the burn-in environment to minimize the probability of thermal runaway while maintaining the effectiveness of burn-in test.

1.2.8 Scaling Impact on Long Term Microelectronics Reliability

The major long-term reliability concerns include the intrinsic wear-out mechanisms of time dependent dielectric breakdown (TDDB) of gate dielectrics, hot carrier injection (HCI), negative bias temperature instability (NBTI), and electromigration (EM). For microelectronics, the primary intrinsic wearout failure mechanisms are illustrated in Figure 9.

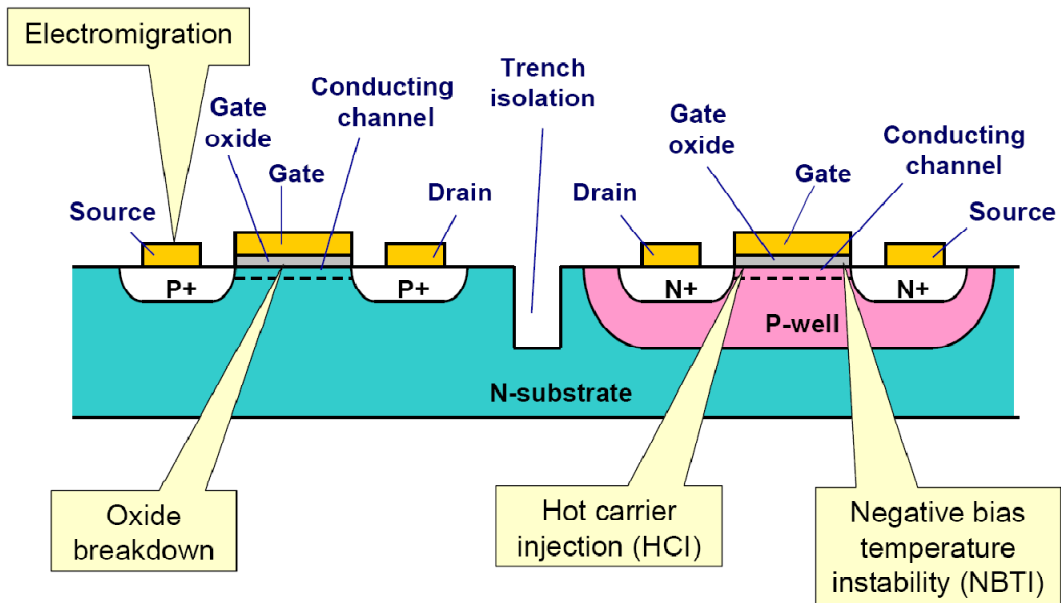


Figure 9. CMOS Intrinsic Wearout Failure Mechanisms.

The drivers & effects of the primary intrinsic failure mechanisms of concern are as follows:

Hot Carrier Injection (HCI):

- Drivers: Channel length & width, oxide thickness, operating voltage, and low temperature.
- Effect: Increased substrate current (I_{sub}), saturation drain current degradation (I_{DSAT}), and increase in V_{th} .
- Impact of Scaling: The rate of hot carrier degradation is directly related to the length of the channel, the oxide thickness, and the voltage of the device. Hot carrier effects are expected to be a growing concern.

Electromigration (EM):

- Drivers: High temperature and current density in metal interconnects.
- Effect: Metal migration leading to increased resistance and open or short circuit.
- Impact of Scaling: Energy densities within interconnects are expected to grow as device features become smaller.

Negative Bias Temperature Instability (NBTI):

- Drivers: Oxide thickness and high temperature.
- Effect: Degraded (I_{DSAT}) and transconductance (g_m), and an increase in I_{off} and V_{th} .
- Impact of Scaling: NBTI is a growing concern as devices continue to scale. As feature sizes scaled through 0.13 μ m, devices required much thinner gate oxides and introduced nitrides in the SiO₂.

Time-Dependent-Dielectric-Breakdown (TDDB):

- Drivers: Oxide thickness, gate voltage, and high electric field.
- Effect: Anode to cathode short through the dielectric.
- Impact of Scaling: TDDB is expected to accelerate as gate oxide thicknesses decrease with continued device scaling.

The physics and the reliability characterization and modeling of each mechanism have been major research topics for the past three decades. There has been an abundant amount of research in this area, including [57].

Among the wear-out mechanisms, TDDB and NBTI seem to be the major reliability concerns as devices scale. The gate oxide has been scaled down to only a few atomic layers thick with significant tunneling leakage. While the gate leakage current may be at a negligible level compared with the on-state current of a device, it will first have an effect on the overall standby power. For a total active gate area of 0.1 cm^2 , chip standby power limits the maximum tolerable gate leakage current to approximately $1\text{-}10 \text{ A/cm}^2$, which occurs for gate oxides in the range of $15\text{-}18\text{ \AA}$ [40].

Scaling impact of TDDB and NBTI on digital, analog and RF circuit reliability has been an important topic during past years [58-69]. Either TDDB, NBTI, or both were found to contribute to digital circuit speed degradation [58, 62], FPGA delay increase [65], SRAM minimum operating voltage V_{min} shift measurement [64, 66, 67], RF circuit parametric drifts [60, 61], and analog circuit mismatch [59, 63]. It appears that SRAM minimum operating voltage V_{min} shift

due to TDDB and NBTI is one of the effects that has been tested and characterized most. For example, it is shown [66] that transistor shifts due to NBTI manifest themselves as population tails in the product's minimum operating voltage distribution. TDDB manifests itself as single-bit or logic failures that constitute a separate sub-population. NBTI failures are characterized by Log-normal statistics combined with a slower degradation rate, which is in contrast to TDDB failures that follow extreme-value statistics and exhibit a faster degradation rate. Most of the studies seem to indicate that the advanced technology parts may experience intrinsic or wear-out mechanisms induced circuit parametric shifts during operating life time, especially at higher operating voltages and temperature conditions.

1.3 Physics-of-Failure (PoF) Methodology

The PoF methodology may be summarized as follows:

- Identify potential failure mechanisms (e.g., chemical, electrical, physical, mechanical, structural, or thermal processes leading to failure) and the likely failure sites on each device.
- Expose the product to highly accelerated stresses to find the dominant root-cause of failure.
- Identify the dominant failure mechanism as the weakest link.
- Model the dominant mechanism (what and why the failure takes place).
- Combine the data gathered from the acceleration tests and statistical distributions, e.g., Weibull, lognormal distributions.

- Develop an equation for the dominant failure mechanism at the site and its time-to-failure (TTF).
- Extrapolate to use conditions.

This process is used to assess the retention time reliability of three progressive DRAM technologies described in Chapter 2.

1.3.1 Competing Mechanism Theory

While the failure rate qualification has not improved over the years, the semiconductor industry understanding of reliability physics of semiconductor devices has increased tremendously. Failure mechanisms are well understood and the manufacturing and design processes are so tightly controlled that electronic components are designed to perform with reasonable life and with no single dominant failure mechanism. In practice, however, highly accelerated stress testing is used to determine the life limiting failure mechanism and the weakest link.

1.3.2 Intrinsic Failure Mechanism Overview

The potential intrinsic wearout failure mechanisms considered include Hot Carrier Injection (HCI), Electromigration (EM), Negative Bias Temperature Instability (NBTI), and Time-Dependent-Dielectric-Breakdown (TDDB). Much work has been done on the physics of these failure mechanisms in the past including [70], a primary deliverable for the Aerospace Vehicles Space Institute (AVSI) Consortium Project 17: Methods to Account for Accelerated Semiconductor Wearout. Therefore; only a brief overview will be presented here.

1.3.3 Hot Carrier Injection and Statistical Model

The switching characteristics of a MOSFET can degrade and exhibit instabilities due to the charge that is injected into the gate oxide. The typical effect of hot carrier, or hot electron, degradation is to reduce the on-state current in an n-channel MOSFET and increase the off-state current in a p-channel MOSFET. The rate of hot carrier degradation is directly related to the length of the channel, the oxide thickness, and the voltage of the device. A measure of transistor degradation or lifetime is commonly defined in terms of percentage shift of threshold voltage, change in transconductance, or variation in drive or saturation current [71]. Several approaches to minimize HCI effects include: thermo-chemical processing to reduce the Si-SiO₂ interfacial trap density; introducing ion implanted regions of lighter doping between the channel and heavily doped drain regions to better distribute the electric field, reducing its peak value; adding nitride to the gate oxide so that it is more resistant to interface-trap generation; and reducing the transistor operating voltage [71].

There are three main types of hot carrier injection modes according to Takeda [72]:

1. Channel hot electron (CHE) injection.
2. Drain avalanche hot carrier (DAHC) injection.
3. Secondary generated hot electron (SGHE) injection.

CHE injection is due to the escape of “lucky” electrons from the channel, causing a significant degradation of the oxide and the *Si-SiO₂* interface, especially at low temperature (77K) [73]. Alternatively, DAHC injection results in both electron and hole gate currents due to impact ionization, giving rise to the most severe degradation around room temperature. SGHE injection

is due to minority carriers from secondary impact ionization or, more likely, bremsstrahlung radiation, and becomes a problem in ultra-small MOS devices.

The lognormal distribution is generally used to model hot carrier degradation [74]:

$$f(t) = \frac{1}{\sigma(2\Pi)^{1/2}} \exp\left[-\frac{1}{2}\left(\frac{\ln t - \mu}{\sigma}\right)^2\right]. \quad (1.11)$$

Hot carrier effects are enhanced at low temperature. The primary reason for this is an increase in electron mean free path and impact ionization rate at low temperature. As was shown in [75], substrate current at 77K is five times greater than that at room temperature, and CHE gate current is approximately 1.5 orders of magnitude greater than that at room temperature. At low temperature, the electron trapping efficiency increases and the effect of fixed charges becomes large [76]. This accelerates the degradation of G_m at low temperature. The degradation of V_{th} and G_m at low temperatures is more severely accelerated for CHE-induced effects than for DAHC. Hu [77] showed the temperature coefficient of CHE gate and substrate current to be negative. The lifetime model for HCI is commonly expressed as:

$$t_f = A_{HCI} \left(\frac{I_{sub}}{W}\right)^{-n} \exp\left(\frac{E_{aHCI}}{kT}\right), \quad (1.12)$$

where E_a has a value of approximately $-0.1 \text{ eV} \sim -0.2 \text{ eV}$ [78].

1.3.4 Electromigration and Statistical Model

Passage of high current densities through interconnects causes time-dependent mass transport effects that manifest as surface morphological changes. The resulting metal conductor degradation includes mass pileups in hillocks and whiskers, void formation and thinning, localized heating, and cracking of passivating dielectrics [71]. The scaling of interconnects to keep up with semiconductor scaling increases current densities and temperature, reducing median life. There are three properties having an immediate impact on EM reliability models:

- The orientation of the boundary with respect to the electric field.
- The angles of the grain boundaries with respect to each other.
- Changes in the number of the grains per unit area—grain density.

Each of these properties can give rise to the ion divergences necessary to create voids in metal strips and interconnects.

The lognormal failure distribution is often used to characterize EM lifetime [79]. The bimodal lognormal distribution is often seen in copper via EM tests. Lai [80] described two EM failure mechanisms: via related and metal-stripe related. Ogawa [81] reported two distinct failure modes in dual-damascene Cu/oxide interconnects. One model described void formation within the dual-damascene via; the other reflected voiding that occurs in the dual-damascene trench. These models formed a bimodal lognormal distribution.

The temperature acceleration factor is calculated from Black's equation and may be expressed as:

$$\frac{MTTF}{t_m} = \frac{1}{AF} = \left(\frac{j}{j_s}\right)^2 \exp\left(\frac{E_a}{k}\left(\frac{1}{T_1} - \frac{1}{T_2}\right)\right), \quad (1.13)$$

where t_m = test time to failure, j = current density, T_1 and T_2 are stress operating temperatures, and E_a is the activation energy for electromigration. Reported activation energies for EM range from approximately 0.35eV ~ 0.9eV depending on conductor grain size and metal alloy [82].

1.3.5 Negative Bias Temperature Instability and Statistical Model

NBTI occurs to p-channel MOS (PMOS) devices under negative gate voltages at elevated temperatures. Bias temperature stress under constant voltage (DC) causes the generation of interface traps (N_{IT}) between the gate oxide and silicon substrate, which causes device threshold voltage (V_t) to increase, and drain current (I_{dsat}) and transconductance (g_m) to decrease. The NBTI effect is more severe for PMOS than NMOS devices due to the presence of holes in the PMOS inversion layer that are known to interact with the oxide states. The degradation of device performance is a significant reliability concern for current ultrathin gate oxides where there are indications that NBTI worsens exponentially with thinning gate oxide. Degradation is commonly modeled with power-law time dependence and Arrhenius temperature acceleration. Degradation partially recovers once stress is removed [83]. Major drivers for NBTI degradation in PMOS devices are ultrathin gate oxide thickness and high temperature.

The lognormal failure distribution is often used to characterize NBTI lifetime and frequency degradation over time is best described as a power law of time (Time^β) with β values ranging from 0.25 to 0.4 [84, 85]. Activation energies for NBTI have been reported to be in the range of 0.18eV to 0.84eV [86, 87].

Improved models have been proposed after the simple power-law model. Considering temperature and gate voltage, the lifetime model for NBTI is commonly expressed as:

$$t_f = A_{NBTI} V_{gs}^{-\frac{1}{\beta}} \left[\frac{1}{1 + 2 \exp(-\frac{E_1}{kT})} + \frac{1}{1 + 2 \exp(-\frac{E_2}{kT})} \right]^{-\frac{1}{\beta}}, \quad (1.14)$$

where A and β are constants and V_{gs} is the applied gate voltage.

1.3.6 Time-Dependent Dielectric Breakdown and Statistical Model

TDDB is a wearout phenomenon of SiO_2 , the thin insulating layer between the control “gate” and the conducting “channel” of the transistor. SiO_2 has a very high bandgap (approximately 9eV) and excellent scaling and process integration capabilities, which makes it the key factor in the success of MOS-technology [88]. Dielectric layers as thin as 1.5 nm can be obtained in fully functioning MOSFETs with gate lengths of only 40 nm [89]. Although SiO_2 has many extraordinary properties, it is not perfect and suffers degradation caused by stress factors, such as a high oxide field. Oxide degradation has been the subject of numerous studies that were published over the past four decades. Even today, a complete understanding of TDDB has not yet been reached. Basic models, such as E model and 1/E model, have been proposed and are

still debated in the reliability community. Percolation theory has been successfully applied to the statistical description of TDDB. As oxide continues to scale down, new findings will help researchers gain a better understanding of this complicated process.

The statistical nature of TDDB is well described by the Weibull distribution, since TDDB is a “weakest link” type of failure mechanism. The activation energy for $T_{ox} < 10\text{nm}$ ranges from 0.6 to 0.9 eV.

Several lifetime models have been proposed for TDDB, these include: thermo- chemical model, anode hole injection model, IBM model, and two voltage driven models, including exponential and power law. The lifetime model commonly expressed for TDDB is:

$$t_f = A_{TDDB} \left(\frac{1}{A}\right)^{\frac{1}{\beta}} F^{\frac{1}{\beta}} V_{gs}^{a+bT} \exp\left(\frac{c}{T} + \frac{d}{T^2}\right). \quad (1.15)$$

1.3.7 Multiple Failure Mechanism Model

Standard High Temperature Operating Life (HTOL) tests can reveal multiple failure mechanisms during testing, which suggests that no single failure mechanism dominates the FIT rate in the field. Therefore, in order to make a more accurate model for FIT, a preferable approximation is that all failures are equally likely and the resulting overall failure distribution resembles a constant failure rate process that is consistent with the mil-handbook, FIT rate approach. The acceleration of a single failure mechanism is a highly non-linear function of temperature and/or voltage. The temperature acceleration factor (AF_T) and voltage acceleration factor (AF_V) can be

calculated separately and are the subject of most studies of reliability physics. The total acceleration factor of the different stress combinations are the product of the acceleration factors of temperature and voltage:

$$AF = \frac{\lambda(T_2, V_2)}{\lambda(T_1, V_1)} = AF_T \cdot AF_V = \exp\left(\frac{E_a}{k} \left(\frac{1}{T_1} - \frac{1}{T_2}\right)\right) \exp(\gamma_1(V_2 - V_1)). \quad (1.16)$$

This acceleration factor model is widely used as the industry standard for device qualification. However, it only approximates a single dielectric breakdown type of failure mechanism and does not correctly predict the acceleration of other mechanisms [90].

To be even approximately accurate, electronic devices should be considered to have several failure modes degrading simultaneously. Each mechanism ‘competes’ with the others to cause an eventual failure. When more than one mechanism exists in a system, then the relative acceleration of each one must be defined and averaged under the applied condition. Every potential failure mechanism should be identified and its unique AF should then be calculated for each mechanism at a given temperature and voltage so the FIT rate can be approximated for each mechanism separately. Then, the final FIT is the sum of the failure rates per mechanism, as described by:

$$FIT_{\text{total}} = FIT_1 + FIT_2 + \dots + FIT_i \quad (1.17)$$

where each mechanism leads to an expected failure unit per mechanism, FIT_i . Unfortunately, individual failure mechanisms are not uniformly accelerated by a standard HTOL test, and the

manufacturer is forced to model a single acceleration factor that cannot be combined with known physics of failure models [90].

1.3.8 Acceleration Factor

The qualification of device reliability, as reported by a FIT rate, must be based on an acceleration factor, which represents the failure model for the tested device. If we assume that there is no failure analysis (FA) of the devices after the HTOL test, or that the manufacturer does not report FA results to the customer, then a model should be made for the acceleration factor, AF , based on a combination of competing mechanisms [90].

Suppose there are two identifiable, constant rate competing failure modes (assume an exponential distribution). One failure mode is accelerated only by temperature. We denote its failure rate as $\lambda_1(T)$. The other failure mode is only accelerated by voltage, and the corresponding failure rate is denoted as $\lambda_2(V)$. By performing the acceleration tests for temperature and voltage separately, we can get the failure rates of both failure modes at their corresponding stress conditions. Then we can calculate the acceleration factor of the mechanisms. If for the first failure mode we have $\lambda_1(T_1)$, $\lambda_1(T_2)$, and for the second failure mode, we have $\lambda_2(V_1)$, $\lambda_2(V_2)$, then the temperature acceleration factor is:

$$AF_T = \frac{\lambda_1(T_2)}{\lambda_1(T_1)}, T_1 < T_2, \quad (1.18)$$

and the voltage acceleration factor is:

$$AF_V = \frac{\lambda_2(V_2)}{\lambda_2(V_1)}, V_1 < V_2. \quad (1.19)$$

The system acceleration factor between the stress conditions of (T_1, V_1) and (T_2, V_2) is:

$$AF = \frac{\lambda_1(T_2, V_2) + \lambda_2(T_2, V_2)}{\lambda_1(T_1, V_1) + \lambda_2(T_1, V_1)} = \frac{\lambda_1(T_2) + \lambda_2(V_2)}{\lambda_1(T_1) + \lambda_2(V_1)}. \quad (1.20)$$

The above equation can be transformed to the following two expressions:

$$AF = \frac{\lambda_1(T_2) + \lambda_2(V_2)}{\frac{\lambda_1(T_2)}{AF_T} + \frac{\lambda_2(V_2)}{AF_V}}, \quad (1.21)$$

or

$$AF = \frac{\lambda_1(T_1)AF_T + \lambda_2(V_1)AF_V}{\lambda_1(T_1) + \lambda_2(V_1)}. \quad (1.22)$$

These two equations can be simplified based on different assumptions. When $\lambda_1(T_1) = \lambda_2(V_1)$ where there is an equal probability under normal operating conditions:

$$AF = \frac{AF_T + AF_V}{2}. \quad (1.23)$$

Therefore, unless the temperature and voltage is carefully chosen so that AF_T and AF_V are very close, within a factor of about 2, then one acceleration factor will overwhelm the failures at the accelerated conditions. Similarly, when $\lambda_1(T_2) = \lambda_2(V_2)$ i.e., an equal probability during accelerated test condition, then the AF will take the form:

$$AF = \frac{2}{\frac{1}{AF_T} + \frac{1}{AF_V}}, \quad (1.24)$$

and the acceleration factor applied to normal operating conditions will be dominated by the individual factor with the greatest acceleration. In either situation, the accelerated test does not accurately reflect the correct proportion of acceleration factors based on the understood physics of failure mechanisms.

Suppose a device has n independent failure mechanisms, and λ_{LTFM_i} represents the i th failure mode at accelerated condition, λ_{useFM_i} represents the i th failure mode at normal condition, then the AF can be expressed in two forms [90].

If the device is designed, such that the failure modes have equal frequency of occurrence during normal operating conditions:

$$AF = \frac{\lambda_{useFM_1} \cdot AF_1 + \lambda_{useFM_2} \cdot AF_2 + \dots + \lambda_{useFM_n} \cdot AF_n}{\lambda_{useFM_1} + \lambda_{useFM_2} + \dots + \lambda_{useFM_n}} = \frac{\sum_{i=1}^n AF_i}{n}. \quad (1.25)$$

If the device is designed, such that the failure modes have equal frequency of occurrence during the test conditions:

$$AF = \frac{\lambda_{LTFM_1} + \lambda_{LTFM_2} + \dots + \lambda_{LTFM_n}}{\lambda_{LTFM_1} \cdot AF_1^{-1} + \lambda_{LTFM_2} \cdot AF_2^{-1} + \dots + \lambda_{LTFM_n} \cdot AF_n^{-1}} = \frac{n}{\sum_{i=1}^n \frac{1}{AF_i}}. \quad (1.26)$$

From these relations, it is clear that only if the acceleration factors for each mode are almost equal, i.e., $AF_1 \sim AF_2$, the total acceleration factor will be $AF = AF_1 = AF_2$, and certainly not the product of the two (as is currently the model used by industry). If, however, the acceleration of one failure mode is much greater than the second, the standard FIT calculation may be incorrect by several orders of magnitude.

1.4 Motivation and Objectives

1.4.1 Motivation

The motivation for further research of scaling effects on microelectronics reliability stems from industry scaling trends and the associated reliability implications:

- As devices are scaled down, they become more sensitive to defects and statistical process variations.
- The number of processing steps is increasing dramatically with each new generation (approximately 50 more steps per generation and a new metal level every two generations).
- New materials are being introduced with each new generation, replacing proven materials, e.g. Cu and low K inter-level dielectrics for Al and SiO₂.
- There is less time to characterize new materials than in the past, e.g., reliability issues with new materials and new potential failure modes.

- Manufacturers are trending toward providing ‘just enough’ lifetime, reliability, and environmental specifications for commercial applications, e.g., < five year product lifetimes, trading off ‘excess’ reliability margins for performance.
- There is a significant rise in the amount of proprietary technology and data developed by manufacturers, and there is a reluctance to share that information with hi-rel customers, e.g., process recipes, process controls, process flows, design margins, MTTF.
- There is a focus on the commercial customer, with little or no emphasis on the needs of the space customer, e.g., extended life, extreme environments, high reliability.
- There are increasingly difficult testability challenges due to part complexity.

Modern reliability approaches, including a PoF based reliability modeling strategy, are needed to better predict long term product reliability, operating margins, and performance of progressively scaled technologies in NASA applications. NASA and other hi-rel users must be able to reliably predict end-of-life characteristics and time-to-failure of these advanced scaled technologies for the next generation of flight avionics systems. Further research, modeling, accelerated testing, and failure analysis are needed to better understand the impact of nanometer semiconductor scaling on microelectronics reliability. The relationship between smaller technology feature sizes, device failure mechanisms, and activation energies must be further investigated to quantifiably assess the reliability of current microelectronic products across different stress conditions for hi-rel NASA space applications. Better predictive models explaining the anticipated behavior of advanced scaled microelectronic technologies, and the expected performance degradation over time are desired. Physics-of-failure derating guidance for advanced scaled microelectronics is needed. A qualification plan, based upon analysis from

testing at multiple stress conditions and the failure mechanism process rates, is sought after to better design for high reliability and long life.

While earlier AVSI sponsored work has produced some of the empirical models needed for a PoF based derating approach, and better simulation models have been developed to predict device wearout under various stress conditions, experimental verification and validation of the outputs of these models continues. This work will include a series of experiments to evaluate some of the more recent memory technologies to substantiate and validate proposed acceleration models for temperature and voltage life-stress relationships across scaled technologies. The purpose of this work is to develop a better understanding of the impact of nanometer technology scaling on microelectronics reliability, assess current trends, and provide an independent assessment of some of the proposed acceleration models so that we are able to better predict the reliability of scaled microelectronic technologies in hi-rel systems, and eventually apply PoF based derating models.

Empirical and computer-based modeling, simulation, and analyses are being employed to build PoF based FR estimation models to assess the impact of various failure mechanisms on product reliability, and extrapolate bathtub curves across progressively technologies, e.g., 180nm, 130nm, 110nm, and 90nm. This work may lead to more accurate prediction of device life given a range of mission operating conditions, and may become particularly beneficial for predicting device life of progressive technologies outside of normal operating conditions. It is the goal of this work to investigate and validate reliability trends as a function of technology scaling by conducting independent accelerated stress testing at the product level, data analysis of the results,

modeling, and failure analysis of several scaled device technologies. Testing at multiple conditions to quantify the rate processes of different failure mechanisms will be attempted. Memory devices are excellent choices for product reliability experimentation because of their high density of transistors, memory cells, and repetitive layout of memory blocks. Current SDRAM products are available in >512Mb density per semiconductor chip.

Predicting long-term performance of scaled microelectronic memory products can be difficult because ALT involving elevated stresses can often result in either too few or no failures to make realistic predictions or inferences. It is also possible to overstress the part during accelerated stress testing to the point of thermal runaway where the device goes into catastrophic failure. Manufacturers often report product FIT rates based on zero failures over a fixed amount of time. To overcome this problem, ADT can be used as a means to predict performance in such cases. By identifying key performance measures which are expected to degrade over time, product reliability can be inferred by the degradation paths without observing actual physical failures. Using this approach, the engineer defines a failure as the first time a key performance measure exceeds a pre-specified threshold and the degradation path is then correlated to product reliability. Manufacturers will develop specification minimum and maximum limits on key operating parameters for their products and establish acceptable ranges for key characteristics. Through internal process controls and reliability and qualification testing, manufacturers will create acceptable parameter limits to achieve a target reliability FIT. Often times, however, the user does not have access to the actual failure data, failure distribution or confidence level bounds for a given product.

1.4.2 Objectives

The main objectives of the research are to: test, analyze, and model competing intrinsic failure mechanisms of scaled microelectronic products involving both hard catastrophic and soft degradation failures under accelerated conditions; validate existing models and/or propose new models describing wearout and performance degradation of several scaled technologies from the experimental baseline; and develop conclusions and predictions of the expected failure rate of the next product generation.

Chapter 2: Scaling Impact on SDRAM

2.1 Overview

Dynamic RAM is a type of volatile memory that needs to be periodically refreshed to retain its contents. SDRAM has a synchronous interface, meaning that it waits for a clock signal before responding to its control inputs. It is synchronized with the computer's system bus, and thus with the processor. DRAM is the most common kind of random access memory for personal computers, workstations and flight computers, such as the one that will be used in the upcoming NASA JUNO mission. DRAMs use charge storage on a capacitor in each memory cell to represent stored binary data values of a logic "1" or a logic "0". A DRAM cell consists of a transfer device, a MOSFET that acts like a switch and a storage capacitor as is displayed in Figure 10 [99]. The absence of a charge on the capacitor represents a logic "0" and the presence of a charge indicates a logic "1" in each memory cell. Millions of these memory cells are populated in high density arrays.

The clock is used to drive an internal finite state machine that pipelines incoming instructions. This allows the chip to have a more complex pattern of operation than DRAM which does not have synchronizing control circuits. Pipelining means that the chip can accept a new instruction before it has finished processing the previous one. In a pipelined write, the write command can be immediately followed by another instruction without waiting for the data to be written to the memory array. In a pipelined read, the requested data appears after a fixed number of clock

pulses after the read instruction, and then cycles, during which additional instructions can be sent; this delay is called the latency [100].

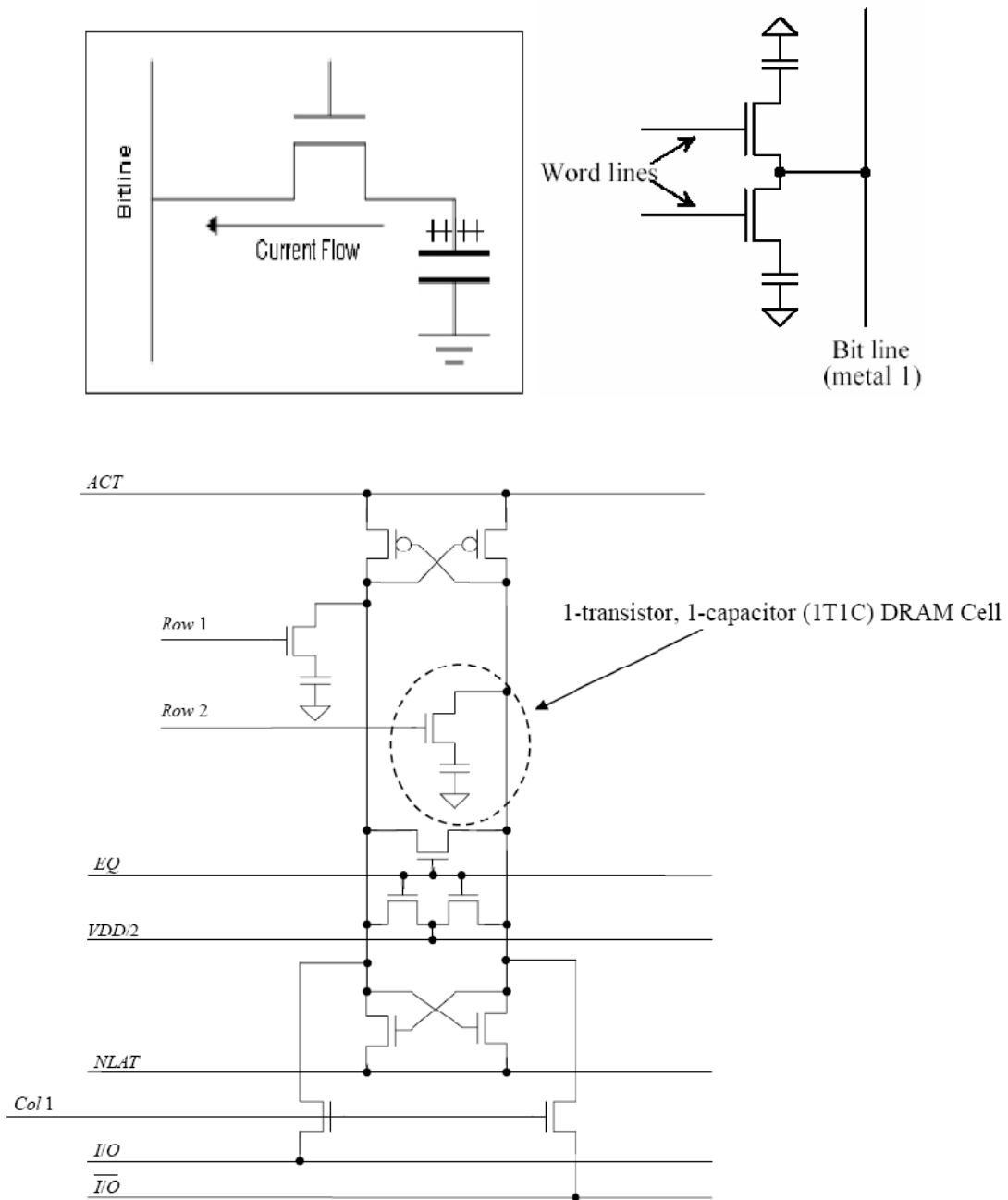


Figure 10. 1T1C DRAM Cell.

While the access latency of DRAM is fundamentally limited by the DRAM array, DRAM has very high potential bandwidth because each internal read is actually a row of many thousands of bits. To make more of this bandwidth available to users, a Double Data Rate (DDR) interface was developed. This uses the same commands, accepted once per cycle, but reads or writes two words of data per clock cycle. Some minor changes to the Single Data Rate (SDR) interface timing were made and the supply voltage was reduced from 3.3 to 2.5 V. DDR SDRAM (also called "DDR1") doubles the minimum read or write unit; every access refers to at least two consecutive words. DDR2 SDRAM was originally seen as a minor enhancement based on the industry standard single-core CPU on DDR1 SDRAM. It mainly allowed higher clock speeds and somewhat deeper pipelining better suited for the rapid acceptance of the multi-core CPU in 2006. With the development and introduction of DDR3 SDRAM in 2007, it is anticipated that DDR3 will quickly replace the more limited DDR and newer DDR2 in cutting edge multi-core CPU architectures. The popularity of DRAM for such applications as PCs, wireless access, MP3 players, digital televisions and DVD video recorders makes this type of memory a leading technology driver, with ever increasing pressure to reduce cost per bit with higher densities. DRAM makes up over 50% of the embedded memory market. Figures 11a-c display current commercial DRAM trends [101].

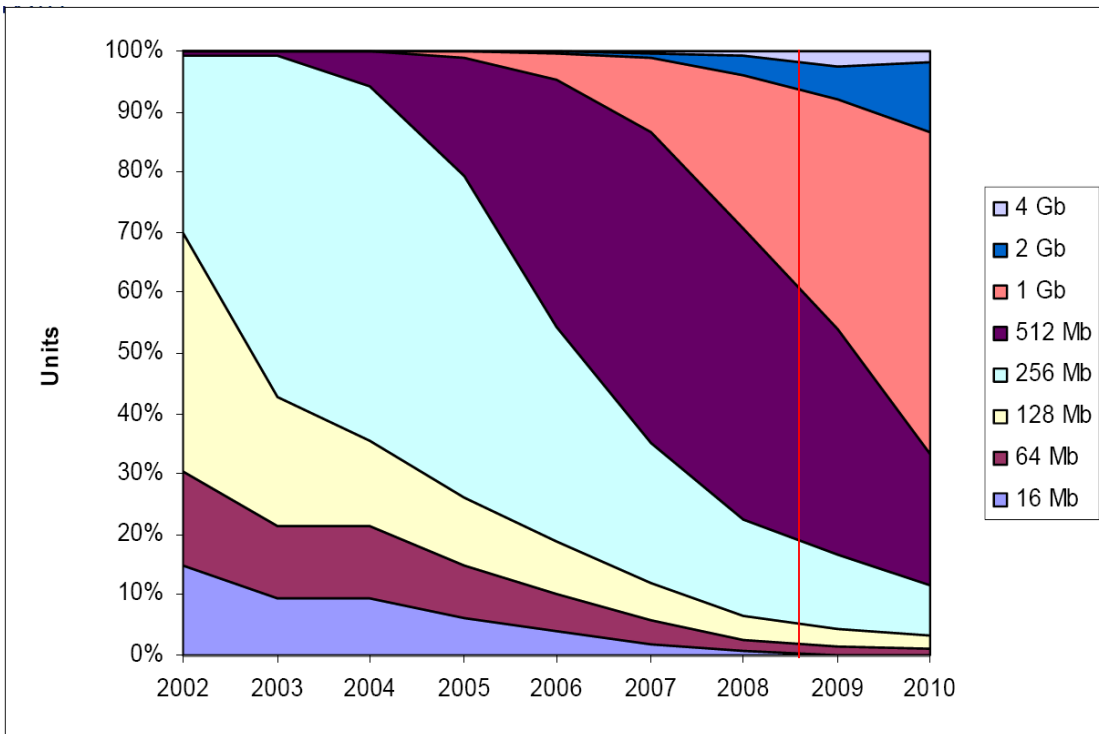
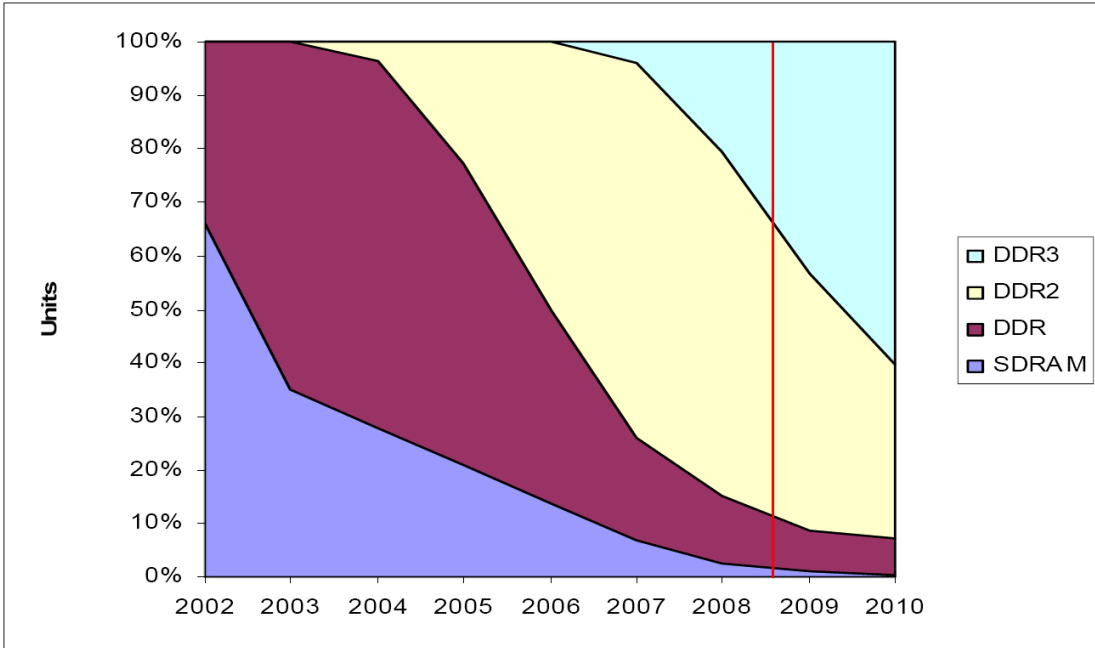


Figure 11a-b. Current DRAM Trends.

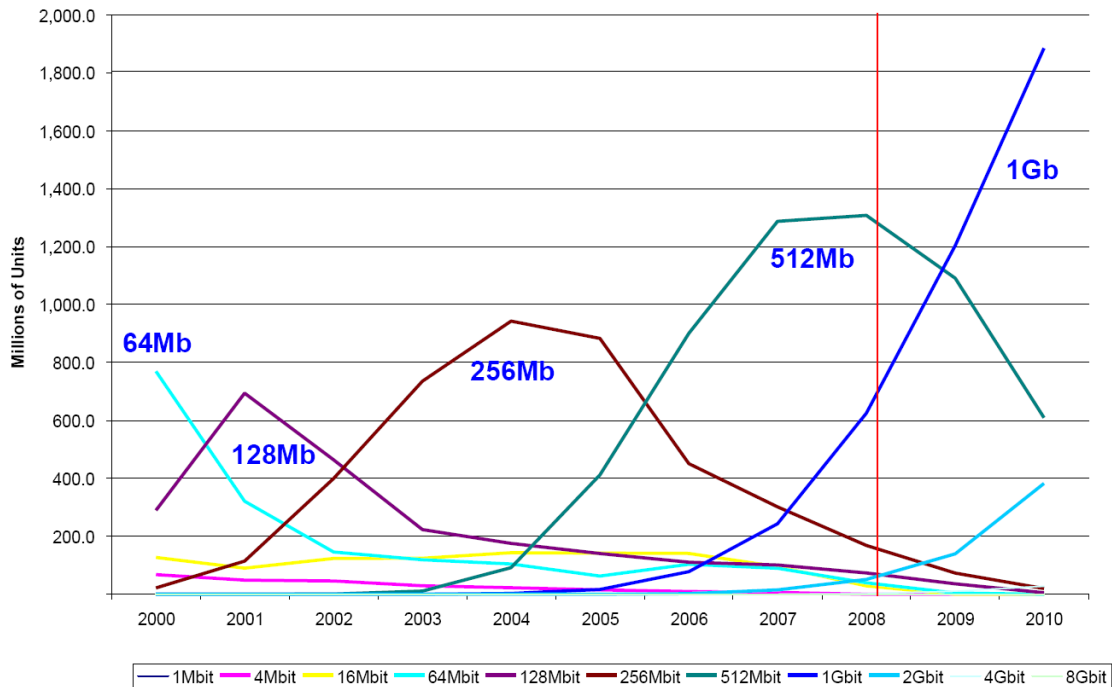


Figure 11c. Current DRAM Trends.

2.2 Design of Experiments

Because manufacturers are generally not willing to share specific design margins, process recipes and steps, and detailed product reliability information with the user, who may use their products in highly reliable applications, the user may use several approaches to assess the reliability the product. These include empirical methodologies or standards-based prediction approach, life or accelerated stress testing approach, and physics-of-failure methodology based on the understanding of the failure mechanism and applying the appropriate physics-of-failure model to the data. Stress testing combined with PoF was used in this study to determine the relative degradation and reliability of three progressive technologies using the same type and size of product for each technology.

Commercial 512Mb DDR SDRAMs (three progressive technologies – 130nm, 110nm and 90nm) were selected for the experimental baseline to investigate failure and degradation trends as a function of scaling. 65nm DRAMs have only recently been released and were not available at the commencement of this study. Furthermore, DDR2 and DDR3 SDRAM architectures become much more costly and timely to evaluate at the product level due to their complexity. Table 2 outlines the experimental baseline. Table 3 explains the stress test matrix approach to stress the parts. The test approach consisted of three experiments; the design of experiments included an accelerated stress test to 1000 hours:

- Experiment 1 forced accelerated stress conditions at different clock frequencies and temperatures, while voltage was kept fixed ($1.5 \times V_{dd}$).
- Experiment 2 forced accelerated stress conditions at different voltages (1.4, 1.5 & 1.6 x V_{dd}), while the clock frequency and temperature were kept fixed (i.e., F_{max} , T_{max}).
- Experiment 3 included evaluation of the retention time performance and degradation of the DRAM array.

Parts were dynamically stimulated with address write/read operations and monitored for fail or degradation during testing. In addition, functional characterization tests, including address write/read/verify and access time measurements were conducted at -70°C , -55°C , $+25^{\circ}\text{C}$ and $+125^{\circ}\text{C}$ at periodic intervals. Data analysis of the performance degradation was conducted from the results of the three technology experiment.

Table 2. Experimental Baseline.

Product	Technology	Memory Capacity	Vnom	Fmin	Fmax	Temp. Range	No. Samples
DDR SDRAM	90nm	512Mb	2.5V	77MHz	133MHz	0 to +70°C	36
DDR SDRAM	110nm	512Mb	2.5V	125MHz	200MHz	0 to +70°C	36
DDR SDRAM	130nm	512Mb	2.5V	84MHz	166MHz	0 to +70°C	36

Table 3. Experimental Stress Test Matrix.

Stress	Temp.		Freq.		Voltage		
	25°C	125°C	Min	Max	3.51V (1.4xVdd)	3.78V (1.5xVdd)	4.05V (1.6xVdd)
S1	X			X			X
S2	X		X				X
S3		X	X				X
S4		X		X	X		
S5		X		X		X	
S6		X		X			X

Experiment 1 allows accelerated stress test conditions at different clock frequencies and temperatures, while the voltage is kept steady.

- (5 pieces) Max Clock Freq @ 25°C and 4.05V
- (5 pieces) Min Clock Freq @ 25°C and 4.05V (5 pieces) Min Clock Freq @ 125°C and 4.0V

Experiment 2 allows accelerated stress test conditions at different voltages, while the clock frequency and temperature is kept steady.

- (5 pieces) Max Clock Freq @ 125°C and 3.51V
- (5 pieces) Max Clock Freq @ 125°C and 3.78V

- (5 pieces) Max Clock Freq @ 125°C and 4.05V

Burn-in boards were developed; each board corresponding to one of the stress test conditions in each experiment. Each board allowed for the testing of fifteen devices (five specimens of each technology per board). Testing was carried out at maximum clock frequencies using Credence Sapphire S automated test equipment (ATE). The Sapphire S features 96 programmable I/Os (400 MHz) and 8 digital power supplies (DPS). See Figure 12.

National Instruments test boards (National Instruments PCI-6542) were used for the low frequency (Fmin) stress tests. See Figure 13. The NI test boards features 100MHz maximum clock rate, programmable input levels, and 64 Mb/channel on-board memory.



Sapphire ATE

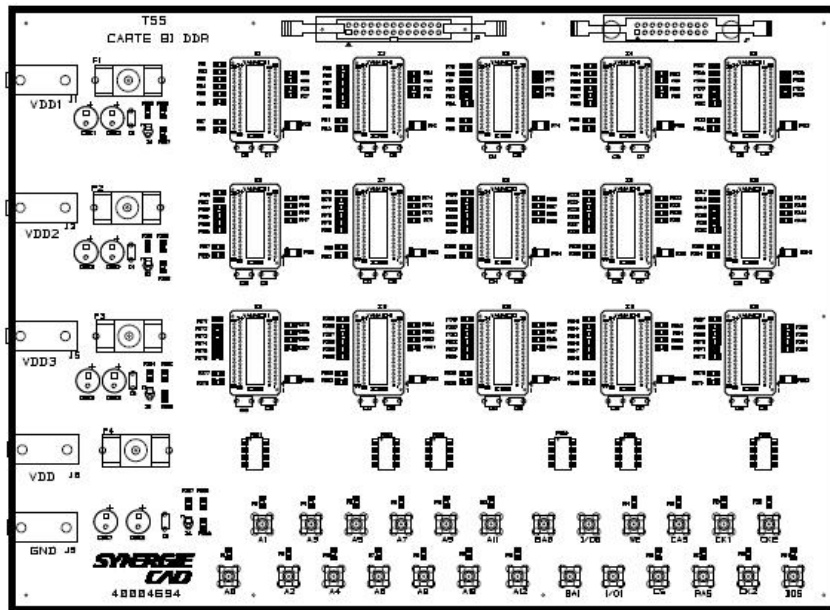
Figure 12. Sapphire S ATE.



NI PCI-6542

Figure 13. National Instruments PCI-6542.

Thirty components of each technology were submitted to the stress matrix test. Six different Burn-In boards with fifteen positions each were designed to accommodate the stress matrix conditions. Refer to Figure 14 and Table 4.



BI-BOARD 15 positions
Figure 14. Stress Burn-in Boards.

Table 4. Test Conditions and BI Board Layout.

Stress	T°C		Freq		Voltage			Serial number (parts)	BI Board
	25°C	125°C	Min	Max	3.51V	3.78V	4.05V		
S1	X			X			X	#21 to #25	#5
S2	X		X				X	#26 to #30	#6
S3		X	X				X	#16 to #20	#4
S4		X		X	X			#11 to #15	#3
S5		X		X		X		#6 to #10	#2
S6		X		X			X	#1 to #5	#1

2.2.1 Electrical Test Flow

For each memory device, electrical test software and hardware were developed. Tests were performed using an EXA 3000 digital tester. At each electrical test step the following tests were conducted:

DC Tests:

- Continuity Tests (Vfwd).
- Input leakage current test (I_{iL}/I_{iH}).
- Output leakage current test (I_{oL}/I_{oH}).
- Low/High output current (I_{oL}/I_{oH}).
- Operating current (ACT-PRE) (Iddo0).
- Operating current (ACT-READ-PRE) (Iddo1).
- Idle power down standby current (Iddo2P).
- Floating idle standby current (Iddo2F).
- Active power down standby current (Iddo3P).
- Active standby current (Iddo3N).
- Operating current (Burst Read Operation) (Iddo4R).
- Operating current (Burst Write Operation) (Iddo4W).
- Auto-Refresh Burst Current (Iddo5).
- Self refresh current (Iddo6).
- Operating current (4 banks interleaving) (Iddo7).

Functional Tests:

- Functional test at 133MHz and nominal V_{dd} .

- Functional test at 133MHz and minimum V_{dd} .
- Functional test at 133MHz and maximum V_{dd} .

Dynamic Tests:

- DQ output access time from CK, CK/ (tAC).

2.2.2 Electrical Test Conditions and Limits

The electrical test conditions, limits and patterns for each parameter are described in Table 5 where:

Device D1 (90nm): 512Mb DDR SDRAM

Device D2 (110nm): 512Mb DDR SDRAM

Device D3 (130nm): 512Mb DDR SDRAM

Table 5. DC Tests, Conditions and Limits.

Test	Name	Test Conditions	Limits	
			Min	Max
Continuity Tests	Vfwd	Iforce : -100uA	-800mV	-200mV
Input leakage current test	IiL/IiH	VDD ≥ Vin ≥ VSS	-2μA	2μA
Output leakage current test	IozL/IozH	VDDQ ≥ VOUT ≥ VSS	-5μA	5μA
Low output current	IoL	VOUT = 0.35V	D1 : 16.8mA D2 : 15.2mA D3 : 15.2mA	-
High output current	IoH	VOUT = 1.95V	D1 : -16.8mA D2 : -15.2mA D3 : -15.2mA	-
Operating current (ACT-PRE)	Iddo0	VDD = 2.5V	-	D1 : 115mA D2 : 160mA D3 : 150mA
Operating current (ACT-READ-PRE)	Iddo1	VDD = 2.5V	-	D1 : 145mA D2 : 220mA D3 : 180mA
Idle power down standby current	Iddo2P	VDD = 2.5V	-	D1 : 5mA D2 : 3mA D3 : 3mA
Floating idle standby current	Iddo2F	VDD = 2.5V	-	D1 : 40mA D2 : 35mA D3 : 40mA
Active power down standby current	Iddo3P	VDD = 2.5V	-	D1 : 30mA D2 : 30mA D3 : 20mA
Active standby current	Iddo3N	VDD = 2.5V	-	D1 : 45mA D2 : 70mA D3 : 70mA
Operating current (Burst Read Operation)	Iddo4R	VDD = 2.5V	-	D1 : 145mA D2 : 310mA D3 : 210mA
Operating current (Burst Write Operation)	Iddo4W	VDD = 2.5V	-	D1 : 135mA D2 : 310mA D3 : 210mA
Auto refresh current	Iddo5	VDD = 2.5V	-	D1 : 280mA D2 : 330mA D3 : 290mA
Self refresh current	Iddo6	VDD = 2.5V	-	D1 : 5mA D2 : 4mA D3 : 4mA
Operating current (4 banks interleaving)	Iddo7	VDD = 2.5V	-	D1 : 350mA D2 : 550mA D3 : 430mA

Functional Tests:

All functional patterns were written in mode:

- CAS LATENCY: 2
- BURST: 8

All test patterns were written and performed in the following sequences:

ZEROS Pattern:

Symbol: ZEROS

addr	0	1	..	1FFF
data	#0000	#0000		#0000

ONES Pattern:

Symbol: ONES

addr	0	1	..	1FFF
data	#FFFF	#FFFF		#FFFF

CHECKERBOARD Pattern

Symbol: CHECK

addr	0	1	..	1FFF
data	#5555	#AAAA		#5555

INVERTED CHECKERBOARD Pattern

Symbol: CHECK/

addr	0	1	..	1FFF
data	#AAAA	#5555		#AAAA

RANDOM Pattern

Symbol: RDM

addr	0	1	..	1FFF
data	#1234	#ABCD		#0A5B

Dynamic Tests:

The dynamic measurements with test conditions and limits are as follows:

Test	Name	Test conditions	Limits	
			Min	Max
DQ output access Time	Tac	Vdd : 2.5V		D1 : 700ps D2 : 700ps D3 :700ps
Data Retention Time	Tret	Vdd: 2.5V		64mSec

Test Capability and Accuracy:

The test capability and accuracy of the SCHLUMBERGER (CREDENCE) Model: EXA3000 is as follows:

- *General overview:*

800 Mbps channel	375
High speed channel (up to 3.2Gbps)	8
High accuracy analog channel	4
± 30V analog channel	4

- *Static characteristics:*

Voltage measurements	Range	Accuracy
	1V	0.2% of measured value ± 622µV
	8V	0.2% of measured value ± 1.4766mV
	30V	0.2% of measured value ± 4.16mV
Current measurements	Range	Accuracy
	1µA	0.2% of measured value ± 5.1nA
	8µA	0.2% of measured value ± 6nA
	64µA	0.2% of measured value ± 13nA
	512µA	0.2% of measured value ± 68.5nA
	4mA	0.2% of measured value ± 513.6nA
	32mA	0.2% of measured value ± 4µA
	256mA	0.2% of measured value ± 32.5µA
	1A	0.2% of measured value ± 588µA

- *Dynamic characteristics:*

Impedance	45Ω ± 5Ω
Maximum capacitive load	60pF
Overall time accuracy	8ps
Drivers accuracy	± (0.2% + 10 mV) of programmed value
Comparators accuracy	± (0.2% +10 mV) of programmed value

Experiment 3 included further memory characterization of the three technologies in Table 2. Data retention testing was performed by maximizing the device refresh commands. Weak bit failures, distributions and failure times were recorded as a function of temperature.

Memory devices from each SDRAM technology (130nm, 110nm, and 90nm) were characterized for data retention under nominal V_{dd} as a function of temperature. Initial data retention characterization was conducted to determine the approximate refresh time range of data retention failures (as defined by 10% of the memory bit fails) by extending the refresh time. Data retention characterization on eight devices of each technology was performed at -55°C , $+25^{\circ}\text{C}$, $+75^{\circ}\text{C}$ and $+125^{\circ}\text{C}$ under nominal V_{dd} , by extending the refresh time. Bit fails and passes were then recorded until all bits failed.

2.3 Technology and Construction Analysis

Each of the 512Mb DRAM parts representing the three progressive technologies in the experiment (130nm, 110nm and 90nm), consist of four memory banks, B_0 - B_3 . Each memory bank contains an array of 128Mb of DRAM. All three technologies run on an external 2.5V V_{dd} . Each part consists of 567 million transistors and each memory cell is configured in a 1-Transistor, 1-Capacitor configuration (Ref. Figure 19). There are 512 million 1T1C memory cells in each part. The rest of the active transistors comprise the periphery, voltage control and regulation, and input-output circuitry. The periphery, voltage control and regulation, input-output interface, control logic, and sense amps are CMOS, and each memory cell consists of an nMOS transistor and a stacked technology capacitor (STC). Earlier trench capacitor configurations were phased out below the 180nm process designs due to scaling limitations. As

DRAM has scaled down, the amount of charge needed for reliable memory operation has basically remained the same. For current generation DRAM, the capacitance is typically 30-40fF/cell. Although the external power supply is 2.5V for each part, internal on-chip voltage regulator circuitry subdivides this voltage as follows:

130nm Technology Parts:

- Peripheral Circuitry Voltage: 2.2V
- Memory Core Voltage: 1.8V

110nm Technology Parts:

- Peripheral Circuitry Voltage: 1.8V
- Memory Core Voltage: 1.4V

90nm Technology Parts:

- Peripheral Circuitry Voltage: 1.4V
- Memory Core Voltage: 1.0V

The memory cell capacitor dielectric material of the parts is Ta₂O₅. The gate oxide thickness for the larger peripheral circuitry transistors is approximately 7nm, and the gate oxide thickness for the nMOS memory cell transistors is approximately 4.2 nm.

A basic functional block diagram of the 512Mb SDRAM is shown in Figure 15 [102].

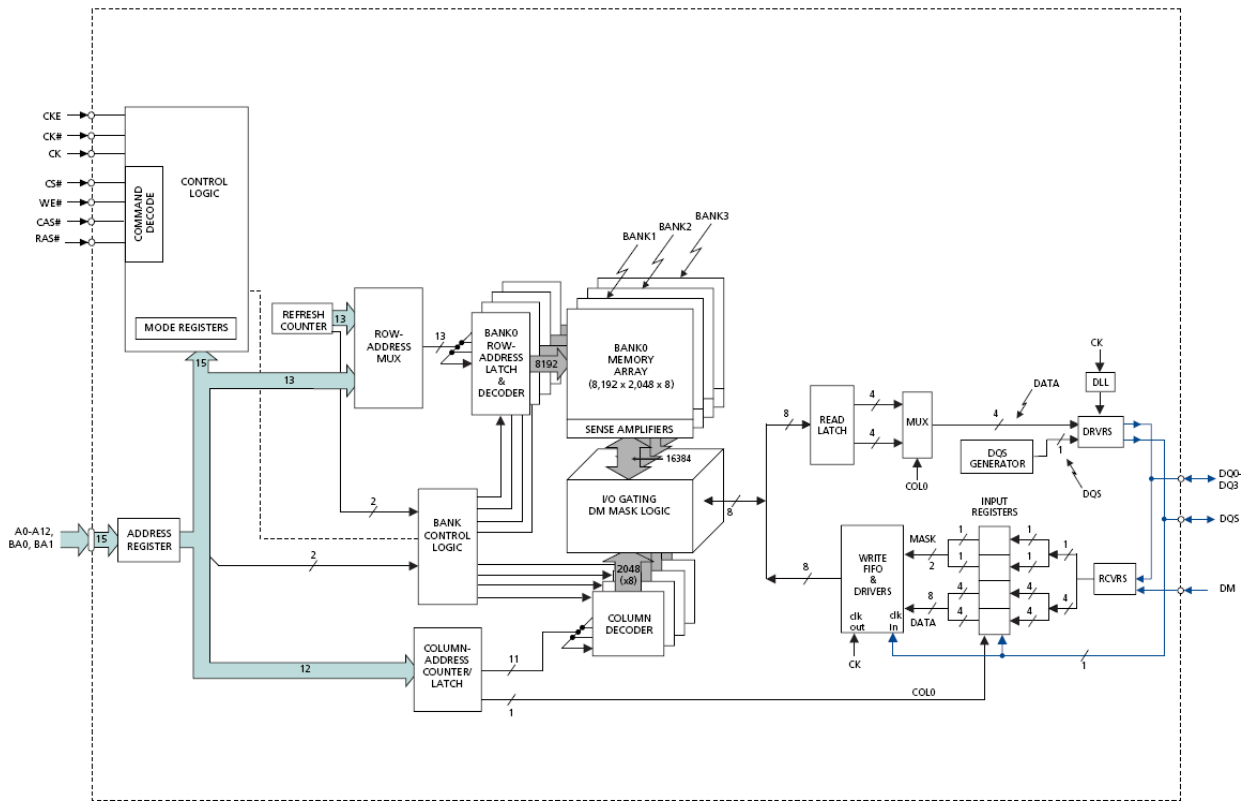


Figure 15. 512Mb SDRAM Functional Block Diagram.

2.4 Device Characterization

2.4.1 Voltage Breakdown

Two devices from each technology were used for voltage breakdown characterization to determine the point of breakdown. The following approach was used to characterize the breakdown voltage:

Ramp V_{dd} from 2.7V to 8V

- Continuity I/O test
- Continuity V_{dd}/V_{ddQ} test
- Measure Standby I_{dd}

For the three technologies, the breakdown voltage was higher than 6V for each of the 2.5V nominal parts (130nm, 110 and 90nm). The 110nm and 130nm samples exhibited breakdown at >7V.

2.4.2 Minimum Frequency Operation Characterization

Two devices from each technology were used to determine the actual minimum operating frequency for each technology. Devices were electrically tested at 125°C to determine the breakdown voltage for each technology (high temperature, ramp voltage to device breakdown). All three technologies remained functional to 50MHz and the 130nm and 110nm parts remained functional to 25MHz, well below the specified minimum operating frequency. The low frequency used for electrical stress in the experimentation, F_{min} , was 50MHz.

2.5 Stress Test Results

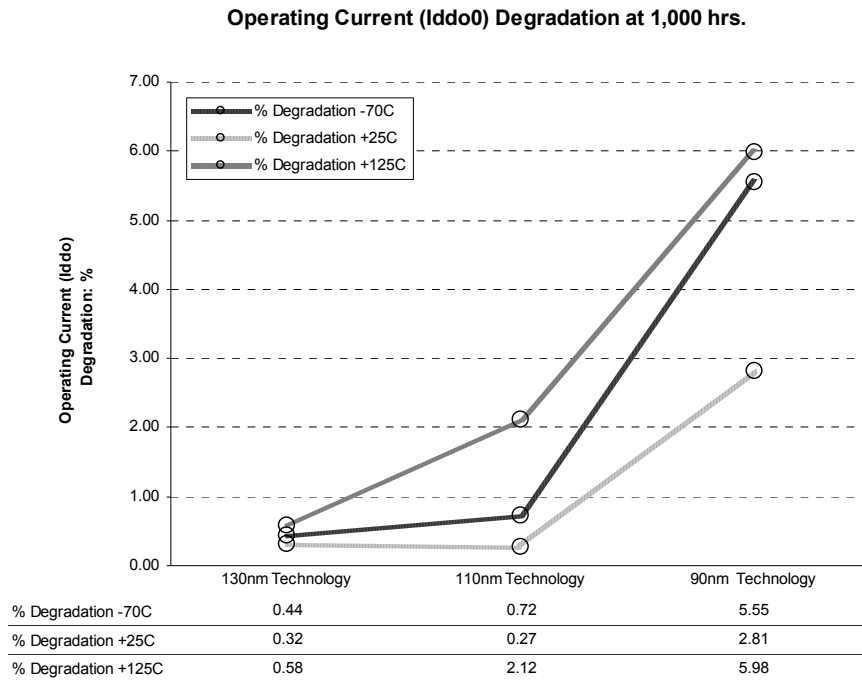
Most importantly, there were no hard functional failures of any of the devices after being subjected to the stress conditions in experiments one and two. Although there were no failures from the stress conditions applied from the stress test matrix, I_{ddo} degradation was observed on some parameters after 1,000 hours. Analyses of the results indicate the following parameters were most affected by the stress conditions:

- Operating current: I_{ddo0}
- Auto refresh current : I_{ddo5}
- Data Retention Time: T_{ret}

A scaling factor was observed; the smaller the technology, the greater the I_{ddo} drifts. The -70°C cold temperature results are misleading and do not represent the actual current measurements. At this cold temperature, the amount of moisture and frost build-up on the parts and test fixture distorts the actual measurements. I_{ddo} drifts are plotted in Figures 16a-b.

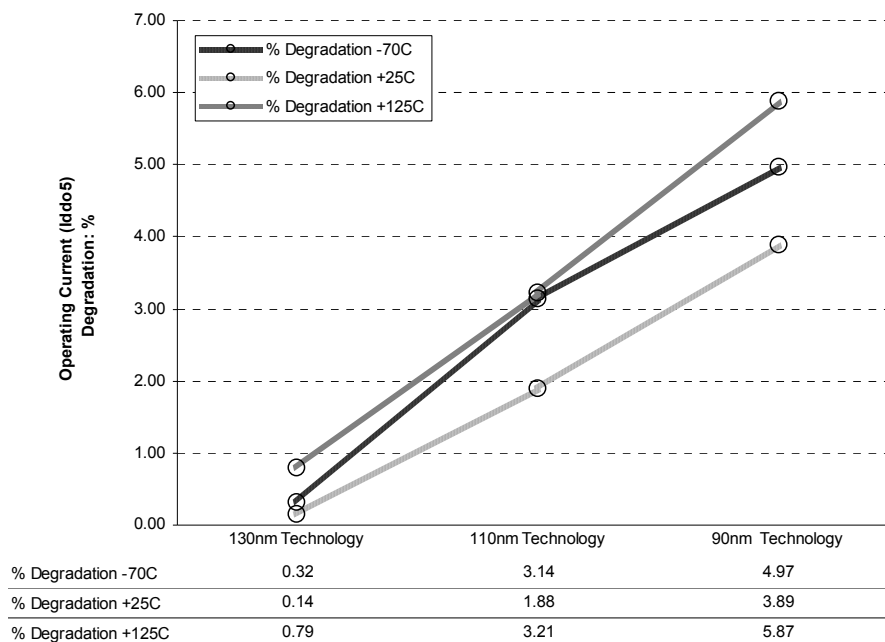
There was no T_{ac} degradation after 1,000 hours. This can be correlated to no F_{max} degradation under the stress conditions.

2.5.1 Stress Test Results (I_{ddo})



(a)

Auto Refresh Current (I_{ddo5}) Degradation at 1,000 hrs.



(b)

Figure 16a-b. Operating Current and Refresh Current Degradation.

The operating current and refresh current degradation (magnitude increase) are noteworthy because they reflect increased leakage through one or multiple points within the complex array of internal circuitry. In both cases (I_{ddo} and I_{ddo5}) the 90nm technology measurements were an order of magnitude higher than the 130nm technology devices. Because leakage current is inversely proportional to retention time, further investigation is warranted.

Tables 6a and 6b summarize the I_{ddo} performance degradation after 1,000 hours.

Table 6a. I_{ddo} Performance Summary.

Stress Condition	Temperature	Frequency	Voltage*	Effect on I _{ddo}
1	High	High	High	Moderate
2	High	High	Medium	Moderate
3	High	High	Low	Moderate
4	High	Low	High	Moderate
5	Low	High	High	Negligible
6	Low	Low	High	Negligible

*HV=1.6 x V_{dd} , MV=1.5 x V_{dd} , LV=1.4 x V_{dd}

Table 6b. Iddo Performance Characterization Drifts.

Stressed at Fmax, 4.05V, 125C								
130nm			110nm			90nm		
		Avg.			Avg.			Avg.
		1,000 hr. Drift			1,000 hr. Drift			1,000 hr. Drift
-70C	Iddo0	0.44%	-70C	Iddo0	0.72%	-70C	Iddo0	5.55%
Measure	Iddo1	0.12%	Measure	Iddo1	1.26%	Measure	Iddo1	4.87%
	Iddo2P	0.19%		Iddo2P	3.98%		Iddo2P	14.23%
	Iddo5	0.32%		Iddo5	3.14%		Iddo5	4.97%
	Iddo6	0.39%		Iddo6	1.86%		Iddo6	10.99%
	Avg.	0.29%		Avg.	2.19%		Avg.	8.12%
+25C	Iddo0	0.32%	+25C	Iddo0	0.27%	+25C	Iddo0	2.81%
Measure	Iddo1	0.06%	Measure	Iddo1	0.34%	Measure	Iddo1	4.22%
	Iddo2P	0.17%		Iddo2P	1.70%		Iddo2P	5.23%
	Iddo5	0.14%		Iddo5	1.88%		Iddo5	3.89%
	Iddo6	0.24%		Iddo6	0.68%		Iddo6	3.08%
	Avg.	0.19%		Avg.	0.97%		Avg.	3.85%
+125C	Iddo0	0.58%	+125C	Iddo0	2.12%	+125C	Iddo0	5.98%
Measure	Iddo1	0.29%	Measure	Iddo1	3.34%	Measure	Iddo1	5.14%
	Iddo2P	1.09%		Iddo2P	4.17%		Iddo2P	17.87%
	Iddo5	0.79%		Iddo5	3.21%		Iddo5	5.87%
	Iddo6	0.83%		Iddo6	3.27%		Iddo6	13.45%
	Avg.	0.72%		Avg.	3.22%		Avg.	9.66%

An unexpected finding was that there were no I_{ddo} degradation differences across the different voltage conditions. Degradation appeared to be strictly temperature dependent and the relative differences in the voltage inputs in this experiment exhibited no difference in performance. Samples from each technology were decapsulated and subjected to construction analysis, e.g. emission microscopy, internal probing, and SEM analysis, to determine why this is. All three technologies had voltage regulator and over-voltage protection circuitry, limiting the actual voltage applied to the internal memory cells. This circuitry is capable of maintaining constant voltage to the memory core up to an externally applied 6V V_{dd} . Thus, there was no voltage acceleration to the memory core as a result of the product level testing. Voltage stress acceleration must be applied to representative memory cell test structures; it cannot be applied at the product level.

2.5.2 Retention Time Degradation (Tret)

There were no functional bit failures observed after comparing the data retention characteristics to the JEDEC specification (maximum 64mSec). In general, the data retention is much better at lower temperatures compared to higher temperature measurements. Data retention time measurements were better than 6 seconds at -55°C, 5 seconds at +25°C, 0.9 second at +75°C, and 100ms at +125°C. Retention time did degrade, however, over the 1,000 hour test.

A scale factor was evident; the more integrated the device, generally the better the retention time across temperature and the tighter the standard deviation. The scale factor may be explained by a difference of the oxide layers used in smaller technologies (advanced high-K processes) and improvements in cell design and geometry, i.e., vertical/horizontal stacked capacitors, materials, dimensions, etc.

Figures 17a-f show the data retention time cumulative failed bits for each technology as a function of temperature. Parts were taken out of the auto refresh mode (refresh every 64mSec), and the cumulative failures for each technology are plotted at the initial time=0, and 1,000 hour points. The plots show how much data retention degrades as a function of temperature at fixed voltage.

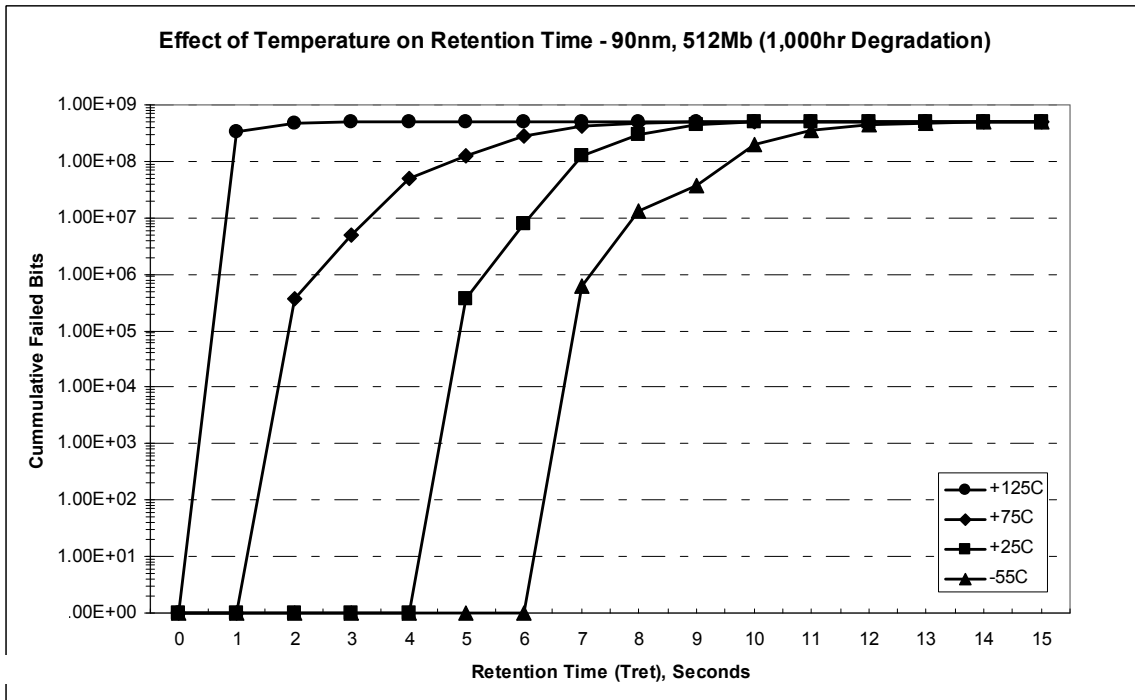
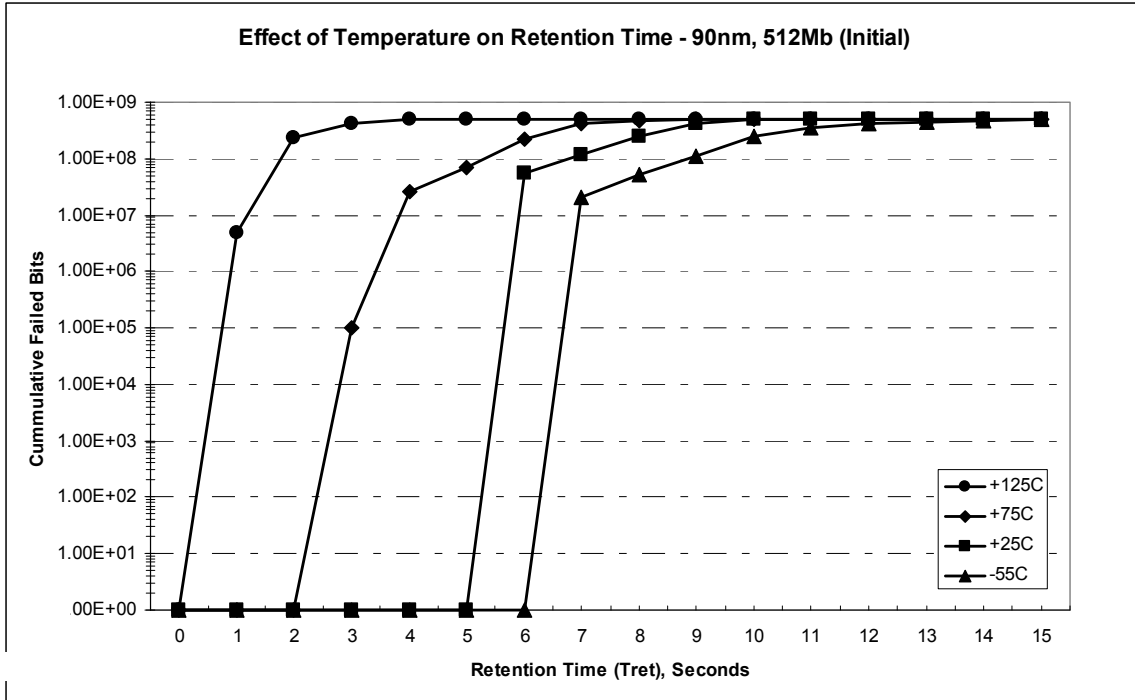


Figure 17a-b. Effect of Temperature on Data Retention for 90nm Technology.

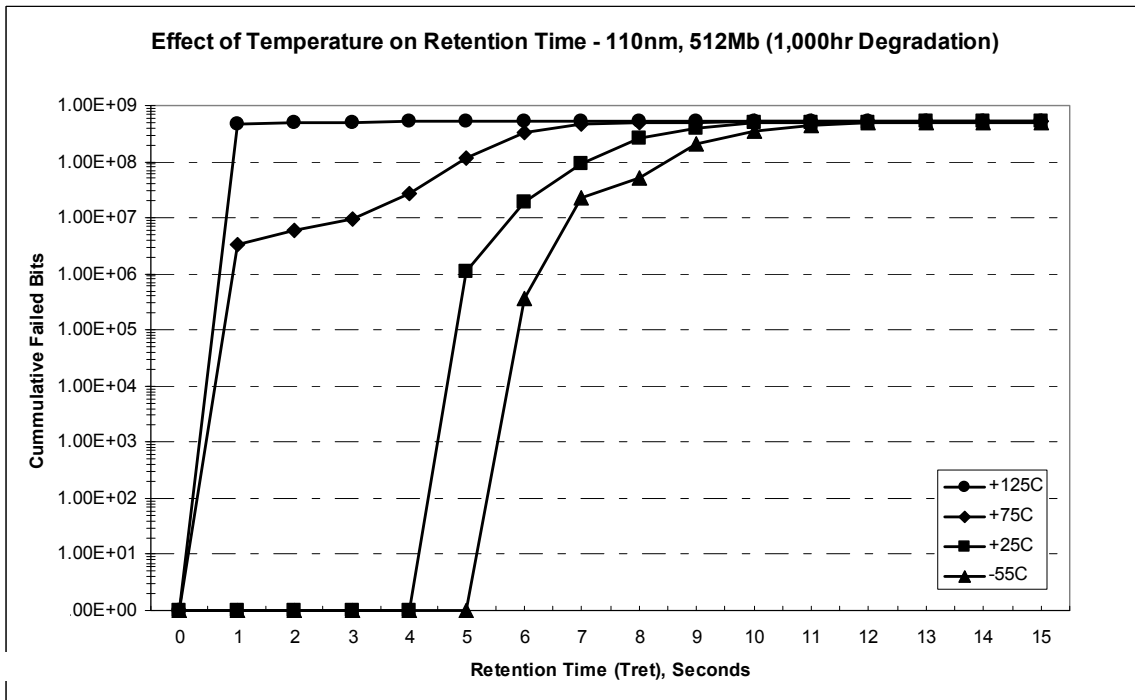
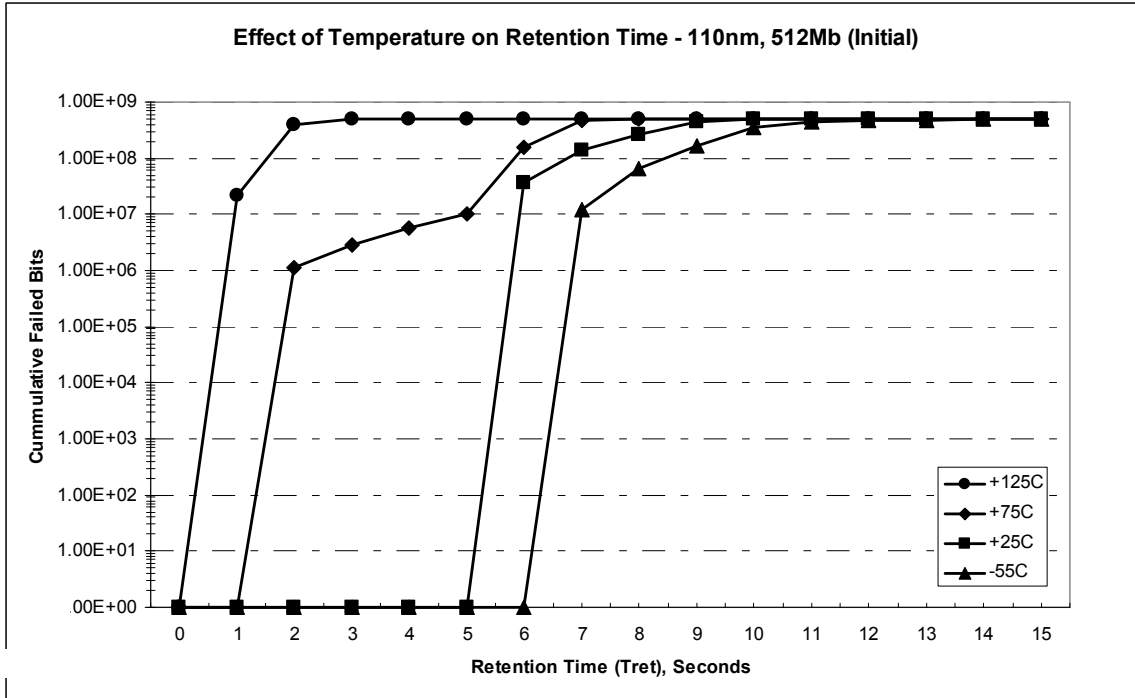


Figure 17c-d. Effect of Temperature on Data Retention for 110nm Technology.

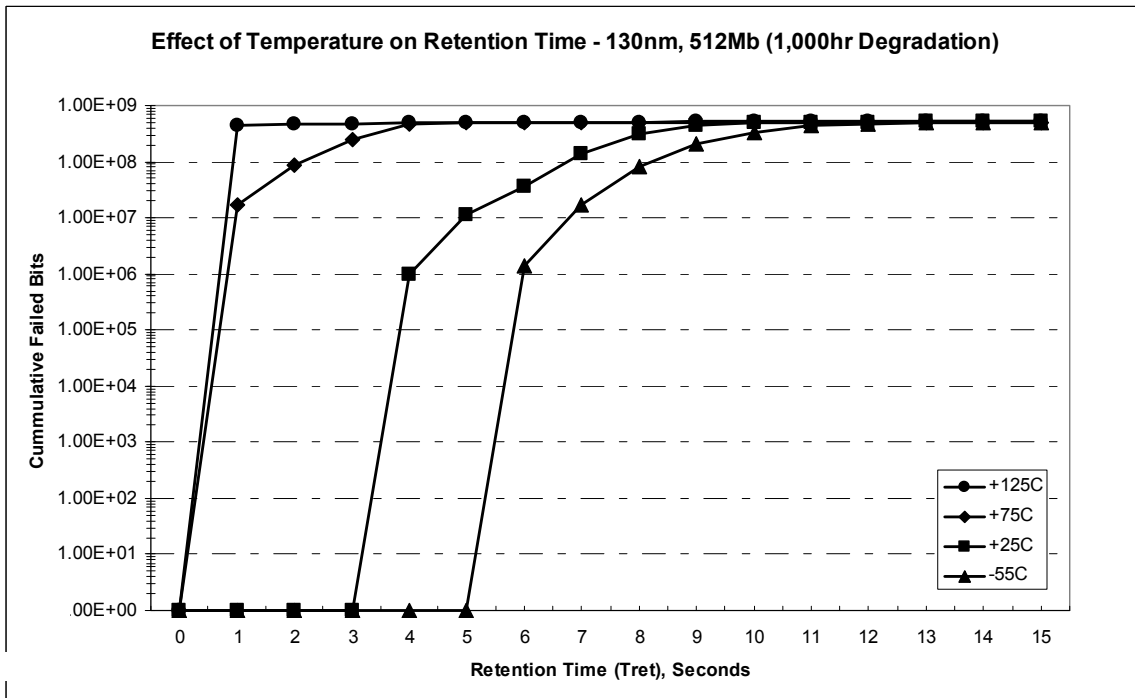
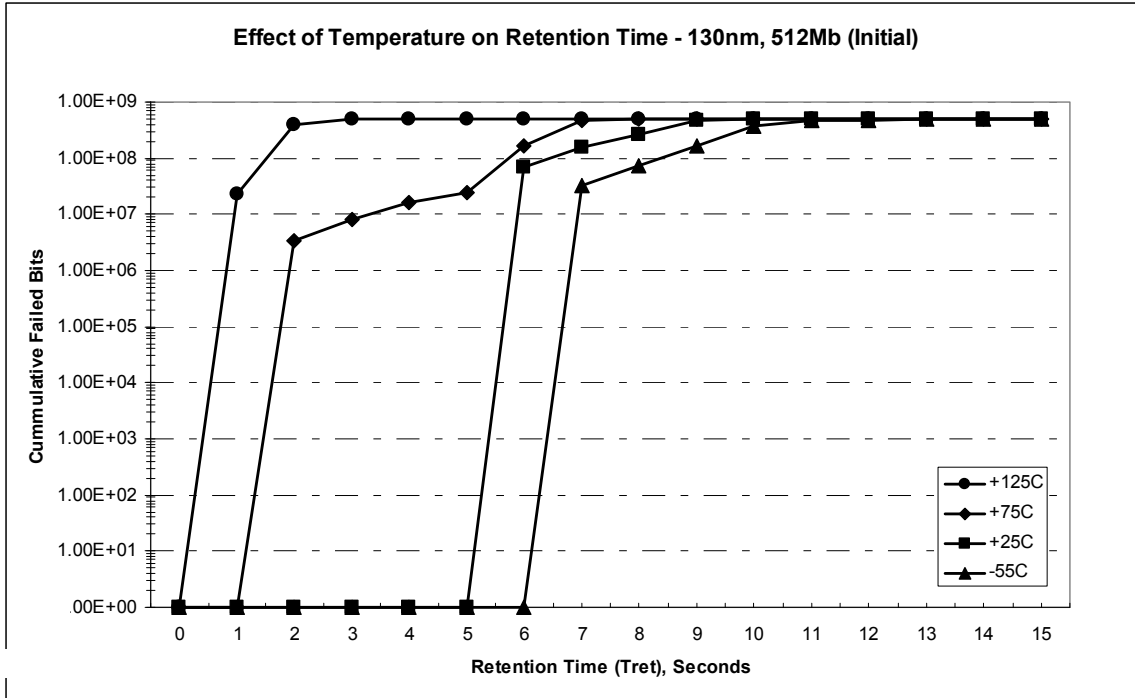


Figure 17e-f. Effect of Temperature on Data Retention for 130nm Technology.

Chapter 3: SDRAM Degradation and Predictive Model

3.1 Acceleration Model

Physical acceleration models based upon the physical or chemical theory that describes the failure causing process over the range of data may be employed for well understood failure mechanisms. Usually, individual test structures are utilized in the DOE to more accurately measure threshold voltage (V_t), drain current (I_{dsat}), and transconductance (g_m) shifts, as well as dielectric breakdown over a range of stress conditions. At the complex product level, such as the 512Mb SDRAM, it is difficult to identify the exact physical mechanism causing minute physical characteristic changes embedded deep within the internal circuitry from product level data. Often we are constrained by the product performance degradation to develop empirical-based acceleration models that fit the observed data.

Data retention (T_{ret}) characteristics were determined to be the best measurable indicator of the performance degradation of the DRAMs, as the storage cell's critical function is to retain a charge representing its state. Each DRAM was tested until each memory cell lost its ability to store a '1' in the memory bit locale. Since all bits were run to failure, the data is said to be complete with no right-censoring. Due to the high number of repetitive bits of information in each memory product, a significant sample size was examined from a limited number of products. Data retention tests at 100 hour increments, up to 1,000 hours, revealed how the retention time degrades over time. The performance data was analyzed by fitting a degradation model to the data showing the relationship between performance, age, stress and technology.

3.1.1 Life Distribution

A likelihood test was conducted at each test interval to determine the appropriate life distribution for each data set. The Weibull distribution had the highest likelihood value, followed by Lognormal and Exponential distributions. The Weibull probability density function is described as:

$$f(t) = \frac{\beta}{\eta} \left(\frac{t}{\eta} \right)^{\beta-1} e^{-\left(\frac{t}{\eta} \right)^\beta}, \quad (3.1)$$

where the parameter Eta (η) or α is the scale parameter which influences the distribution and is equal to the characteristic life, i.e., life at which 63.2% of the population will have failed, and parameter Beta (β) is the shape parameter [103]. Depending on the value of (β), the Weibull function can take the form of the following distributions:

$\beta < 1$: Gamma

$\beta = 1$: Exponential

$\beta = 2$: Lognormal

$\beta = 3.5$: Normal

The Lognormal probability density function is a two-parameter distribution described as:

$$f(t) = \frac{1}{\sigma_t t \sqrt{2\pi}} \left[\frac{-1}{2\sigma_t^2} (\ln t - \mu t)^2 \right], \quad (3.2)$$

where $\mu = E(\ln t)$ and $\sigma_t^2 = \text{var}(\ln t)$. The failure rate initially increases with time and then decreases depending on the values of parameters μ and σ_t [103].

The Exponential probability density function is described as:

$$f(t) = \lambda e^{(-\lambda t)}, \quad (3.3)$$

where the parameter Lambda (λ) is the rate of occurrence in time interval (t).

3.1.2 Multivariable Life-Stress Relationship

In the case where there is more than one accelerating variable, both should be considered in the life-stress relationship. Temperature and voltage are the two stress factors in this experiment, therefore, the Arrhenius and the Inverse Power Law models may be combined to yield the Temperature – Non-Thermal (T-NT) Model [104]:

$$L(U, V) = \frac{C}{U^n e^{\frac{B}{V}}}, \quad (3.4)$$

where,

- L represents a quantifiable life measure, such as mean life, characteristic life, median life or B(x) life, etc.
- U is the non-thermal stress (voltage),
- V is the temperature in absolute units,
- B is one of the model parameters to be determined derived from the relationship:

$$B = \frac{Ea}{K} = \frac{\text{activation energy}}{8.623e^{-5} eVK^{-1}}$$

- C and n are the 2nd and 3rd model parameters to be determined, (C > 0).

This relationship can be linearized by taking the LN of both sides:

$$\ln(L(U, V)) = \ln(C) - n \ln(U) + \frac{B}{V}. \quad (3.5)$$

The acceleration factor for the T-NT relationship is explained by:

$$A_F = \frac{L_{USE}}{L_{Accelerated}} = \frac{\frac{C}{U_u^n} e^{\frac{B}{V_u}}}{\frac{C}{U_A^n} e^{\frac{B}{V_A}}} = \left(\frac{U_A}{U_u} \right)^n e^{B \left(\frac{1}{V_u} - \frac{1}{V_A} \right)}, \quad (3.6)$$

where,

- L_{use} is one life at use stress level,
- $L_{Accelerated}$ is the life at the accelerated stress level,
- V_u is the use temperature,
- V_A is the accelerated temperature,
- U_A is the accelerated voltage,
- U_u is the use voltage,
- B is one of the model parameters to be determined derived from the relationship:

$$B = \frac{Ea}{K} = \frac{\text{activation energy}}{8.623 e^{-5} eVK^{-1}}$$

- C and n are the 2nd and 3rd model parameters to be determined, (C > 0).

Combining the joint distribution of stress and life, the Weibull life pdf becomes:

$$f(t, U, V) = \frac{\beta U^n e^{-\frac{B}{V}}}{C} \left(\frac{t \cdot U^n e^{-\frac{B}{V}}}{C} \right)^{\beta-1} e^{-\left(\frac{t \cdot U^n e^{-\frac{B}{V}}}{C} \right)^\beta} \quad (3.7)$$

by setting η or $\alpha = L(U, V)$ from Equation (4.4).

Expanding upon the statistical properties of the T-NT Weibull Model, the Mean or MTTF is:

$$\bar{T} = \frac{C}{U^n e^{\frac{B}{V}}} * \Gamma\left(\frac{1}{\beta} + 1\right), \quad (3.8)$$

where $\Gamma\left(\frac{1}{\beta} + 1\right)$ is the Gamma function evaluated at the value of $\left(\frac{1}{\beta} + 1\right)$.

The standard deviation, σ_T , is given by:

$$\sigma_T = \frac{C}{U^n e^{\frac{B}{V}}} * \sqrt{\Gamma\left(\frac{2}{\beta} + 1\right) - \left(\Gamma\left(\frac{1}{\beta} + 1\right)\right)^2}. \quad (3.9)$$

The Reliability function of the T-NT Weibull Model is described as:

$$R(T,U,V) = e^{-\left(\frac{TU^n e^{-\frac{B}{V}}}{C}\right)^\beta}, \quad (3.10)$$

and the Conditional Reliability function as specified stress level, t , is given by:

$$R(T,t,U,V) = \frac{R(T+t,U,V)}{R(T,U,V)} = \frac{e^{-\left(\frac{(T+t)U^n e^{-\frac{B}{V}}}{C}\right)^\beta}}{e^{-\left(\frac{TU^n e^{-\frac{B}{V}}}{C}\right)^\beta}}. \quad (3.11)$$

The T-NT Weibull failure rate function, $\lambda(T)$, is described as:

$$\lambda(T,U,V) = \frac{f(T,U,V)}{R(T,U,V)} = \frac{\beta U e^{-\frac{B}{V}}}{C} * \left(\frac{TU^n e^{-\frac{B}{V}}}{C}\right)^{\beta-1}, \quad (3.12)$$

and Reliable Life, T_R , of a unit for a specified reliability starting at age zero is given by:

$$T_R = \frac{C}{U^n e^{\frac{B}{V}}} * \{-\ln[R(T_R, U, V)]\}^{\frac{1}{\beta}}. \quad (3.13)$$

The Maximum Likelihood Estimation for parameter determination is given by substituting the T-NT Model into the Weibull Log-Likelihood function, yielding:

$$\ln(L) = \Lambda = \sum_{i=1}^F N_i \ln \left[\frac{\beta U_i^n e^{-\frac{B}{V_i}}}{C} \left(\frac{U_i^n e^{-\frac{B}{V_i}}}{C} T_i \right)^{\beta-1} e^{-\left(\frac{U_i^n e^{-\frac{B}{V_i}}}{C} T_i \right)^\beta} \right] - \sum_{i=1}^S N_i \left(\frac{U_i^n e^{-\frac{B}{V_i}}}{C} T_i \right)^\beta, \quad (3.14)$$

where,

- F is the number of groups of exact times-to-failure data points,
- N_i is the number of times-to-failure data points in the i^{th} time-to-failure data group,
- β is the Weibull shape parameter (unknown, the 1st of four parameters to be estimated),
- B is the first T-NT parameter (unknown, the 2nd of four parameters to be estimated),
- C is the second T-NT parameter (unknown, the 3rd of four parameters to be estimated),
- n is the third T-NT parameter (unknown, the 4th of four parameters to be estimated),
- V_i is the temperature stress level of the i^{th} group,
- U_i is the voltage stress level of the i^{th} group,

- T_i is the exact failure time of the i^{th} group,
- S is the number of groups of suspension data points,
- N'_i is the number of suspensions in the i^{th} group of suspension data points, and
- T'_i is the running time of the i^{th} suspension data group.

The parameter estimate solutions are found by solving for the parameters B , C , n and β so that:

$$\frac{\partial \Lambda}{\partial B} = 0, \quad \frac{\partial \Lambda}{\partial C} = 0, \quad \frac{\partial \Lambda}{\partial n} = 0, \quad \text{and} \quad \frac{\partial \Lambda}{\partial \beta} = 0.$$

Finally, the Maximum Likelihood Estimation for standard deviation parameter determination is given by:

$$\ln(L) = \Lambda = \sum_{i=1}^F N_i \ln \left[\frac{1}{\sigma_{T'} T_i} \phi_{pdf} \left(\frac{\ln(T_i) - \ln(C) + n \ln(U_i) - \frac{B}{V_i}}{\sigma_{T'}} \right) \right] + \sum_{i=1}^S N'_i \ln \left[1 - \Phi \left(\frac{\ln(T_i) - \ln(C) + n \ln(U_i) - \frac{B}{V_i}}{\sigma_{T'}} \right) \right], \quad (3.15)$$

where,

- F is the number of groups of exact times-to-failure data points,
- N_i is the number of times-to-failure data points in the i^{th} time-to-failure data group,
- $\sigma_{T'}$ is the standard deviation of the natural logarithm of the time-to-failure (unknown, the 1st of four parameters to be estimated),
- B is the first T-NT parameter (unknown, the 2nd of four parameters to be estimated),

- C is the second T-NT parameter (unknown, the 3rd of four parameters to be estimated),
- n is the third T-NT parameter (unknown, the 4th of four parameters to be estimated),
- V_i is the temperature stress level of the i^{th} group,
- U_i is the voltage stress level of the i^{th} group,
- T_i is the exact failure time of the i^{th} group,
- S is the number of groups of suspension data points,
- N_i is the number of suspensions in the i^{th} group of suspension data points, and
- T_i is the running time of the i^{th} suspension data group.

and,

$$\phi(x) = \frac{1}{\sqrt{2\pi}} * e^{-\frac{1}{2}(x)^2},$$

$$\Phi(x) = \frac{1}{\sqrt{2\pi}} * \int_{-\infty}^x e^{-\frac{t^2}{2}} dt.$$
(3.16)

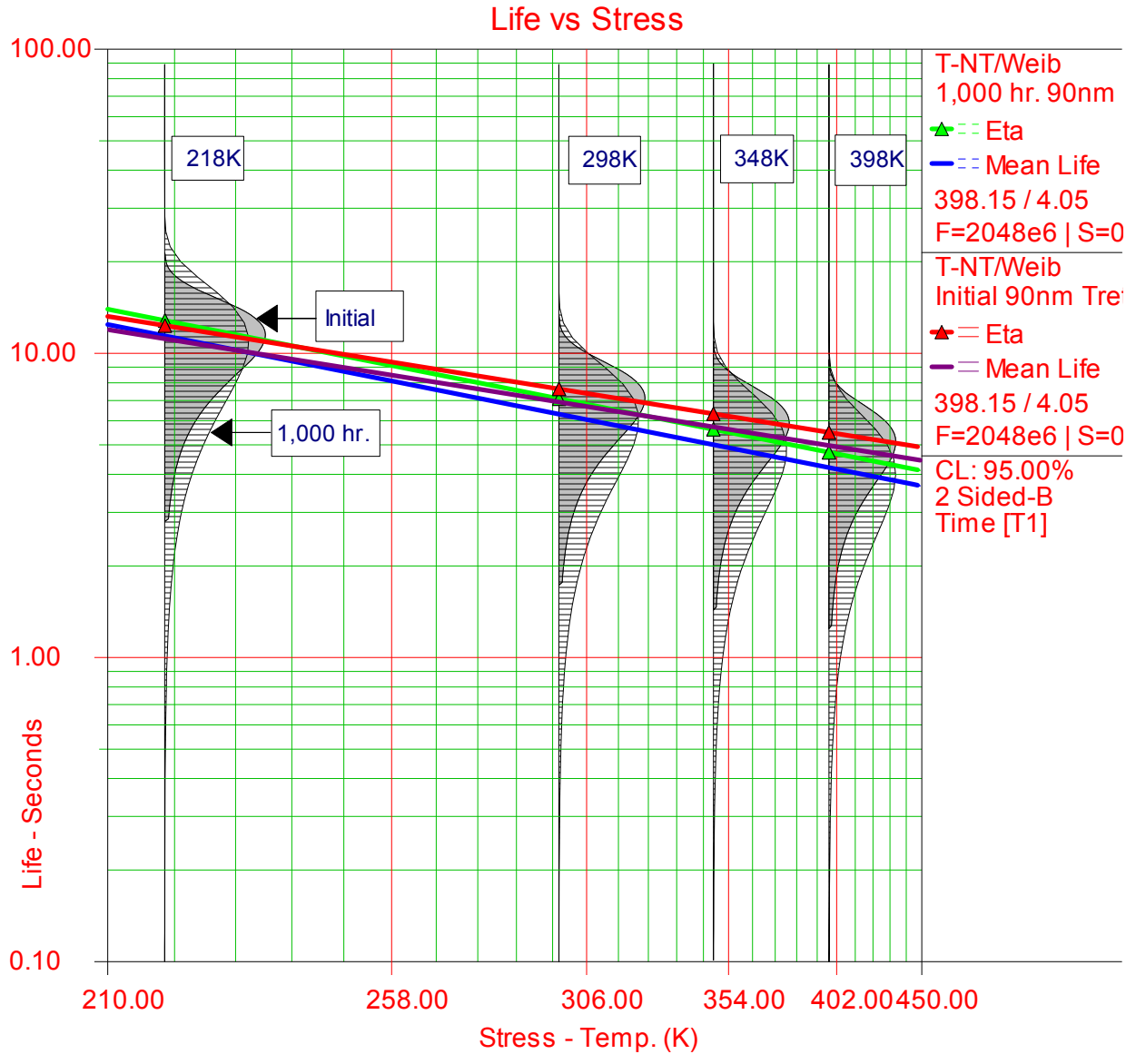
The parameter estimate solutions are found by solving for the parameters $\hat{\sigma}_T$, \hat{B} , \hat{C} , \hat{n} so that:

$$\frac{\partial \Lambda}{\partial \hat{\sigma}_T} = 0, \quad \frac{\partial \Lambda}{\partial \hat{B}} = 0, \quad \frac{\partial \Lambda}{\partial \hat{C}} = 0, \quad \text{and} \quad \frac{\partial \Lambda}{\partial \hat{n}} = 0.$$

3.2 Data Analysis

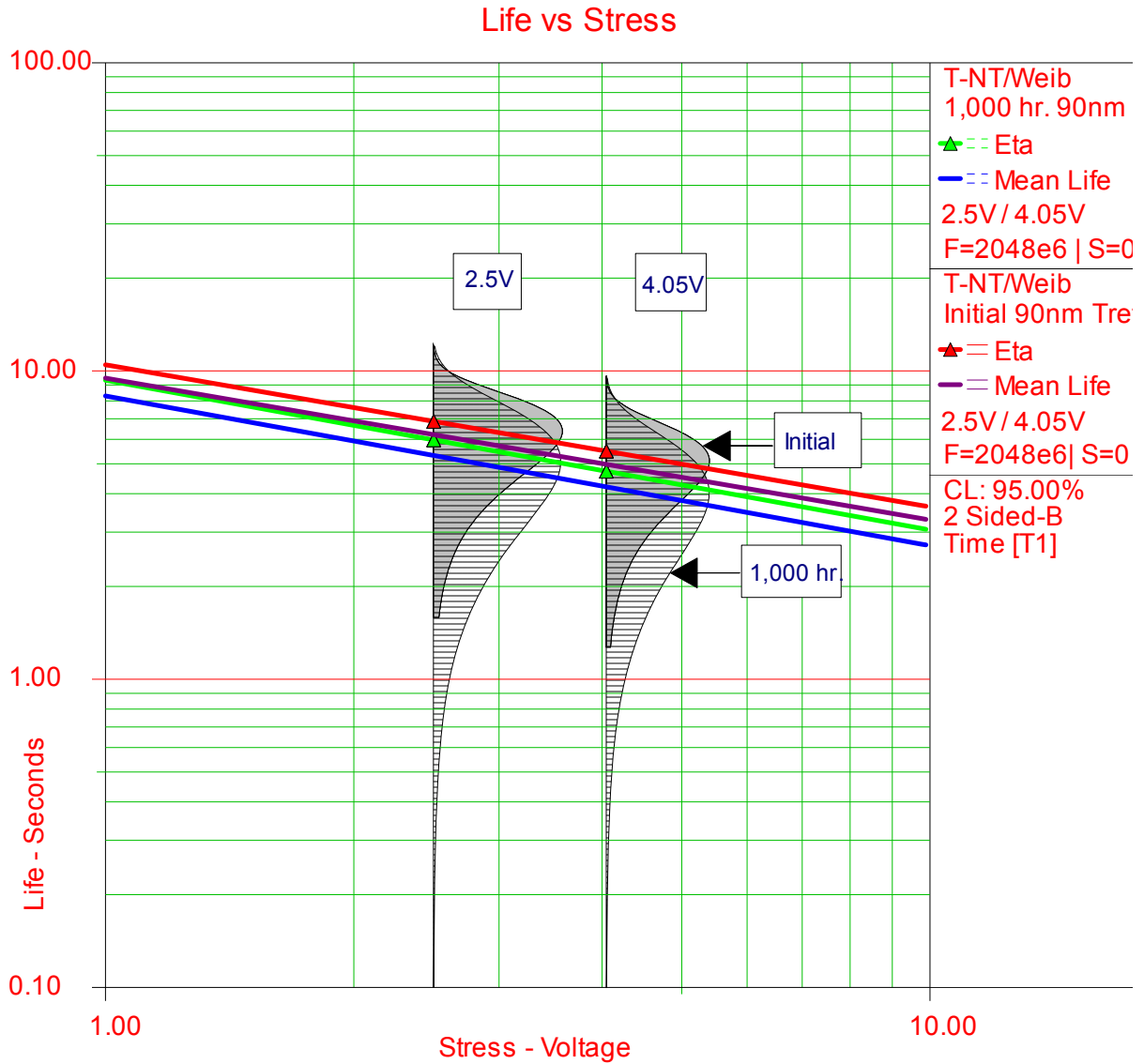
Data from the accelerated test of each of the three technologies were analyzed and plotted using Reliasoft's Alta 6.5 and Weibull ++7. First, combining the joint distribution of life with temperature and voltage stresses, the Weibull life pdf (Eq. 4.7) was used to model the behavior

and relative degradation over 1,000 hours. Comparative multi-plots showing both the initial and 1,000 hour data retention degradation properties using the T-NT Model are displayed in the following Figures. Figures 18a and 18b show comparative multi-plots of how the failure distribution changes over time. Figure 18a shows the 90nm Life vs. Stress relationship across temperature at the worst-case voltage stress condition, 4.05V ($1.6 \times V_{dd}$) and the 95% confidence level. Figure 18b shows the 90nm Life vs. Stress relationship across voltage at the worst-case temperature stress condition, 398.15K, and at the 95% confidence level. By analyzing both stress factors, varying temperature while keeping voltage fixed, and varying voltage while keeping temperature fixed, the relative contribution of each stress on the overall AF can be determined for each technology bit-cell. Similarly, the modeling approach was applied to the 110nm technology data - refer to Figures 19a and 19b, and the 130nm technology data - refer to Figures 20a and 20b. For the modeling, data from four 512Mb SDRAMs (2048×10^6 bits of information) from each technology (90nm, 110nm, and 130nm) were analyzed.



1,000 hr. Beta1=2.7609, B1=481.3743, C1=2.7830, n1=0.4859
 Initial Beta2=3.9654, B2=390.4031, C2=3.9247, n2=0.4607

Figure 18a. 90nm T-NT/Weibull Initial and 1,000 hr. Tret Stress Plots at Fixed Voltage.



1,000 hr. Beta1=2.7609, B1=481.3743, C1=2.7830, n1=0.4859
 Initial Beta2=3.9654, B2=390.4031, C2=3.9247, n2=0.4607

Figure 18b. 90nm T-NT/Weibull Initial and 1,000 hr. Tret Stress Plots at Fixed Temp.

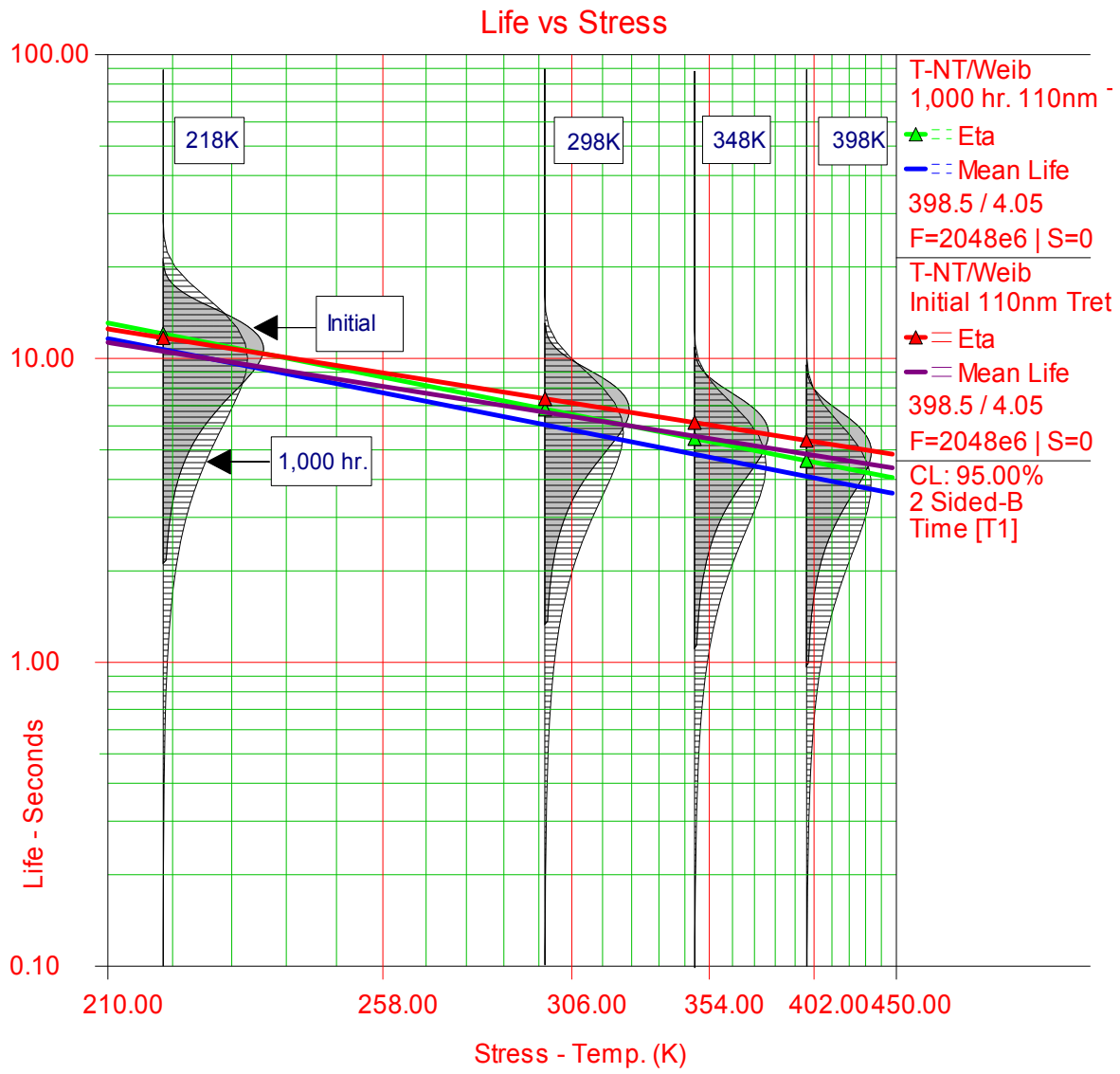
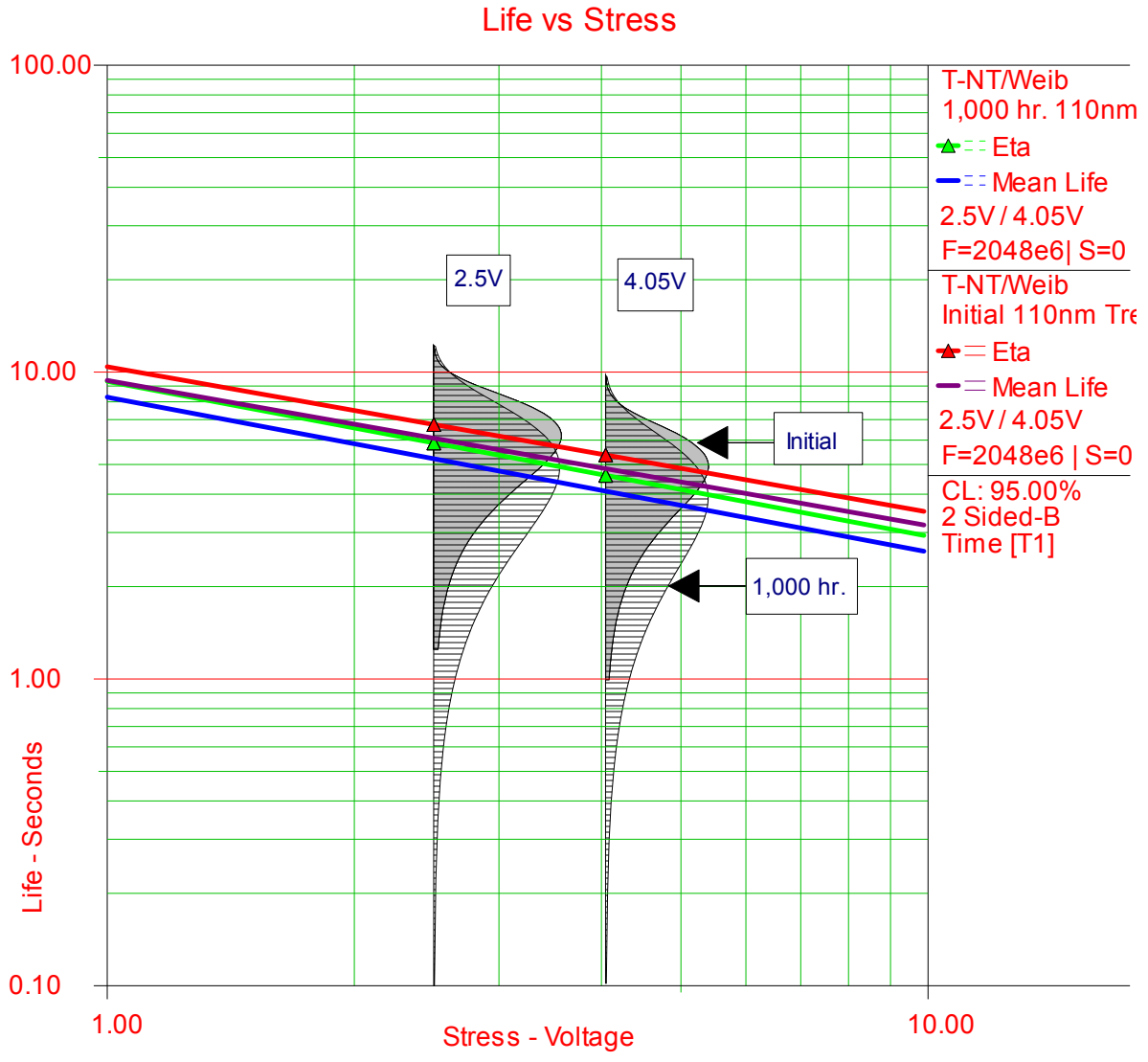
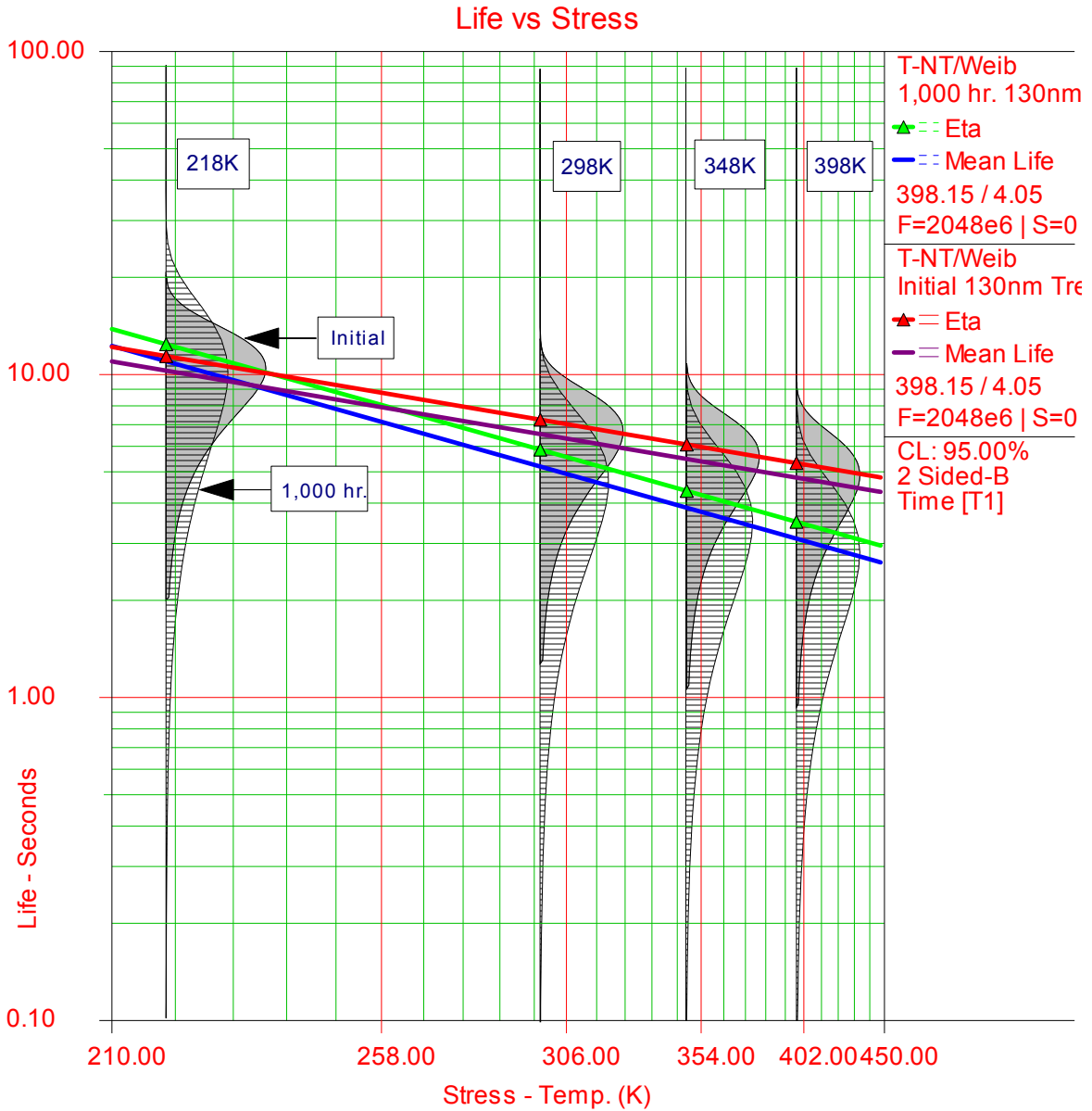


Figure 19a. 110nm T-NT/Weibull Initial and 1,000 hr. Tret Stress Plots at Fixed Voltage.



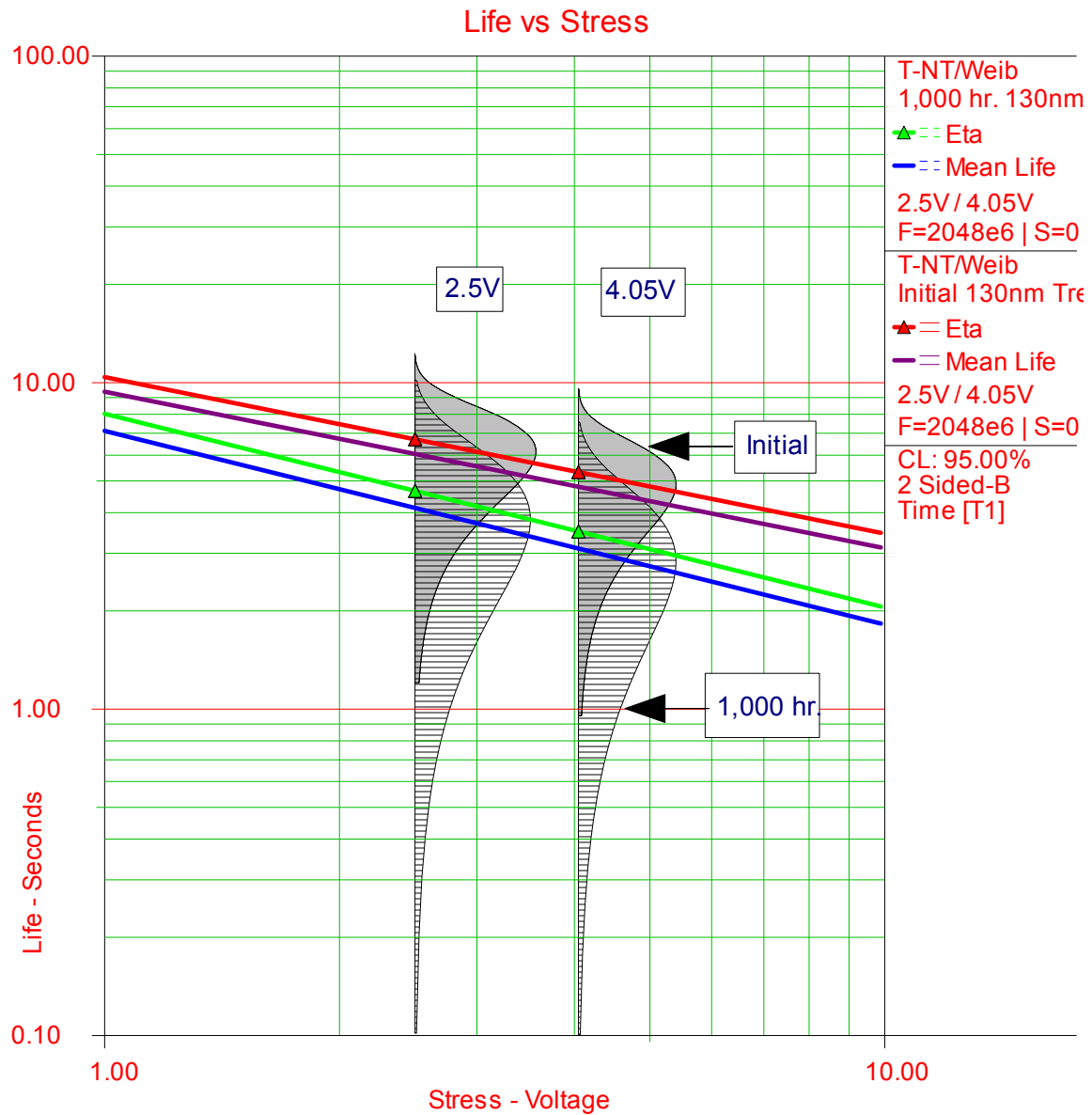
1,000 hr. Beta1=2.5998, B1=463.7186, C1=2.9125, n1=0.5048
 Initial Beta2=3.7014, B2=375.6892, C2=4.0526, n2=0.4736

Figure 19b. 110nm T-NT/Weibull Initial and 1,000 hr. Tret Stress Plots at Fixed Temp.



1,000 hr. Beta1=2.4152, B1=610.6267, C1=1.7314, n1=0.5934
 Initial Beta2=3.6716, B2=367.7282, C2=4.1288, n2=0.4795

Figure 20a. 130nm T-NT/Weibull Initial and 1,000 hr. Tret Stress Plots at Fixed Voltage.



1,000 hr. $\beta_1=2.4152$, $B_1=610.6267$, $C_1=1.7314$, $n_1=0.5934$
 Initial $\beta_2=3.6716$, $B_2=367.7282$, $C_2=4.1288$, $n_2=0.4795$

Figure 20b. 130nm T-NT/Weibull Initial and 1,000 hr. Tret Stress Plots at Fixed Temp.

Model parameters for the T-NT Weibull Model were calculated for each technology up to the end of the time terminated stress test, 1,000 hour point. Model parameters and statistics for each technology and stress condition are summarized in Tables 7 and 8. The retention time Mean (Eq. 3.8) and Std. Deviation (Eq. 3.9) were calculated for each technology at both stress voltages and at four temperatures. Other temperature and voltage stress combinations may also be calculated for the desired use condition.

A Use-Level Weibull Probability plot showing the changing Beta slope of the 90nm technology parts at worst-case test conditions, 398.15K and 4.05V, is shown in Figure 21. Likewise, equivalent plots may be created for any of the combinations of stress temperatures and voltages. The plot shows a decreasing Beta slope over time. The Beta slopes of the 110nm and 130nm technology parts exhibit similar characteristics. Figure 21 shows a decreasing β over time, 3.9654 initially vs. 2.7609 at the 1,000 hr. point. All three regions of the bath-tub curve are represented by the Weibull distribution as determined by the value of the shape-parameter, β . The Weibull distribution is appropriate for complex components or systems composed of a number of constituent components whose failure is governed by the most severe defect or weakest link. For $0 < \beta < 1$, the distribution indicates an early or infant mortality behavior with a decreasing failure rate. For $\beta = 1$, the distribution reduces to the exponential distribution reflecting CFR region of the bath-tub curve. For $\beta > 1$, the distribution reflects an increasing failure rate and models the wearout region of the bath-tub curve [105].

Figure 22 shows the changing reliability vs. time of the data retention time degradation after 1,000 hours at worst-case test conditions, 398.15K and 4.05V. The Reliability vs. Time plots using Eq. 3.10 for the 110nm and 130nm technology parts reveal a comparable shift over time.

The impact of stress on data retention failure rate over time is shown in Figure 23 for the 90nm technology parts. Eq. 3.12 was used for this calculation. The impact on FR over time from the changing Beta is evident in this figure. Comparable shifts were revealed for the 110nm and 130nm technology parts.

Figure 24 shows the Standard Deviation Plot for the 90nm technology parts across temperature at worst-case voltage conditions, 4.05V, at initial and 1,000 hr. points. Using Eq. 3.9, one can see in Figure 24 the increase in standard deviation over time. Comparable shifts were observed for the 110nm and 130nm technology parts.

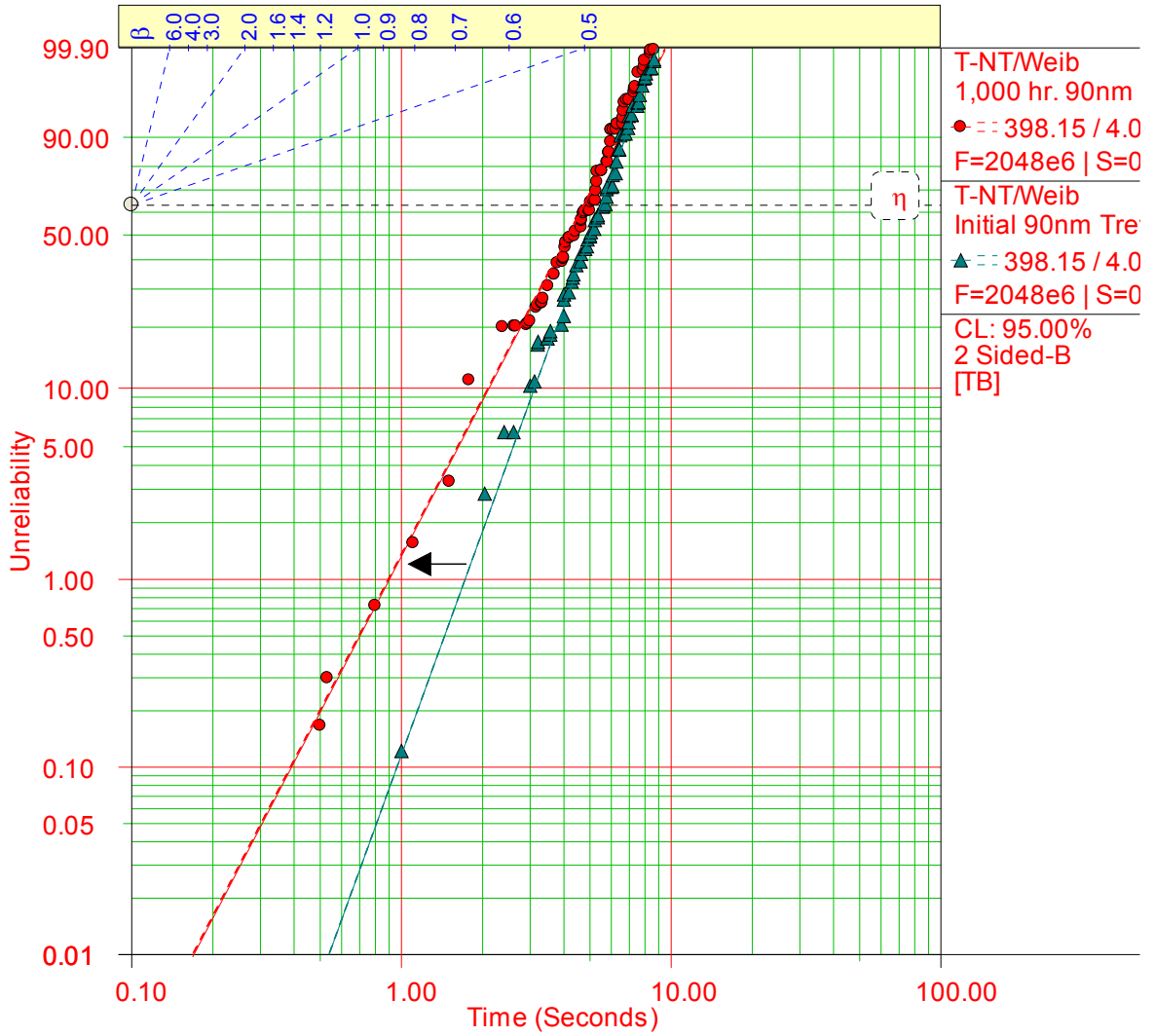
Table 7. Thermal – Non-Thermal Weibull Model Distribution Parameters (4.05V).

Thermal - Non-Thermal Weibull Model Distributions				110nm-Initial Parameters				130nm-Initial Parameters			
90nm-Initial Parameters				110nm-Initial Parameters				130nm-Initial Parameters			
Parameter Bounds Lower = 3.9624 Beta = 3.9654 Upper = 3.9685 Lower = 389.9964 B = 390.4031 Upper = 390.8098 Lower = 3.9179 C = 3.9247 Upper = 3.9315 Lower = 0.4597 n = 0.4607 Upper = 0.4617 Eta = 5.4930 Ea = 0.0336				Parameter Bounds Lower = 3.6984 Beta = 3.7014 Upper = 3.7044 Lower = 375.2421 B = 375.6892 Upper = 376.1363 Lower = 4.0449 C = 4.0526 Upper = 4.0603 Lower = 0.4725 n = 0.4736 Upper = 0.4747 Eta = 5.3639 Ea = 0.0324				Parameter Bounds Lower = 3.6687 Beta = 3.6716 Upper = 3.6746 Lower = 367.2766 B = 367.7282 Upper = 368.1797 Lower = 4.1209 C = 4.1288 Upper = 4.1367 Lower = 0.4784 n = 0.4795 Upper = 0.4806 Eta = 5.3168 Ea = 0.0317			
Temperature (K) = 398.15 Voltage (V) = 4.05 Confidence Bounds = 2-Sided @ 95% CL Std Dev Upper Limit = 4.979 Mean Life (Secs.) = 4.9764 1.42 Lower Limit = 4.9737				Temperature (K) = 398.15 Voltage (V) = 4.05 Confidence Bounds = 2-Sided @ 95% CL Std Dev Upper Limit = 4.8436 Mean Life (Secs.) = 4.8408 1.46 Lower Limit = 4.8379				Temperature (K) = 398.15 Voltage (V) = 4.05 Confidence Bounds = 2-Sided @ 95% CL Std Dev Upper Limit = 4.7989 Mean Life (Secs.) = 4.7961 1.49 Lower Limit = 4.7933			
Temperature (K) = 348.15 Voltage (V) = 4.05 Confidence Bounds = 2-Sided @ 95% CL Upper Limit = 5.7315 Mean Life (Secs.) = 5.7289 1.63 Lower Limit = 5.7263				Temperature (K) = 348.15 Voltage (V) = 4.05 Confidence Bounds = 2-Sided @ 95% CL Upper Limit = 5.5445 Mean Life (Secs.) = 5.5419 1.65 Lower Limit = 5.5392				Temperature (K) = 348.15 Voltage (V) = 4.05 Confidence Bounds = 2-Sided @ 95% CL Upper Limit = 5.4791 Mean Life (Secs.) = 5.4764 1.67 Lower Limit = 5.4738			
Temperature (K) = 298.15 Voltage (V) = 4.05 Confidence Bounds = 2-Sided @ 95% CL Upper Limit = 6.9169 Mean Life (Secs.) = 6.9142 1.95 Lower Limit = 6.9115				Temperature (K) = 298.15 Voltage (V) = 4.05 Confidence Bounds = 2-Sided @ 95% CL Upper Limit = 6.6413 Mean Life (Secs.) = 6.6386 2.01 Lower Limit = 6.6359				Temperature (K) = 298.15 Voltage (V) = 4.05 Confidence Bounds = 2-Sided @ 95% CL Upper Limit = 6.5404 Mean Life (Secs.) = 6.5377 1.98 Lower Limit = 6.535			
Temperature (K) = 218.15 Voltage (V) = 4.05 Confidence Bounds = 2-Sided @ 95% CL Upper Limit = 11.1827 Mean Life (Secs.) = 11.176 3.24 Lower Limit = 11.1692				Temperature (K) = 218.15 Voltage (V) = 4.05 Confidence Bounds = 2-Sided @ 95% CL Upper Limit = 10.5315 Mean Life (Secs.) = 10.5246 3.27 Lower Limit = 10.5177				Temperature (K) = 218.15 Voltage (V) = 4.05 Confidence Bounds = 2-Sided @ 95% CL Upper Limit = 10.2836 Mean Life (Secs.) = 10.2767 3.15 Lower Limit = 10.2699			
Fisher Var/Cov Matrix VarBeta CovBetaB CovBetaC CovBetaD 2.45E-06 -4.03E-05 5.40E-07 -5.22E-08 CovBetaB VarB CovBC CovBn -4.03E-05 4.30E-02 -5.21E-04 1.02E-05 CovBetaC CovBC VarC CovCn 5.40E-07 -5.21E-04 1.20E-05 1.09E-06 CovBetaD CovBn CovCn Varn -5.22E-08 1.02E-05 1.09E-06 2.70E-07				Fisher Var/Cov Matrix VarBeta CovBetaB CovBetaC CovBetaD 2.33E-06 -4.79E-05 6.82E-07 -4.76E-08 CovBetaB VarB CovBC CovBn -4.79E-05 5.20E-02 -6.58E-04 1.05E-05 CovBetaC CovBC VarC CovCn 6.82E-07 -6.58E-04 1.54E-05 1.30E-06 CovBetaD CovBn CovCn Varn -4.76E-08 1.05E-05 1.30E-06 3.09E-07				Fisher Var/Cov Matrix VarBeta CovBetaB CovBetaC CovBetaD 2.31E-06 -5.28E-05 7.58E-07 -4.90E-08 CovBetaB VarB CovBC CovBn -5.28E-05 5.30E-02 -6.85E-04 1.05E-05 CovBetaC CovBC VarC CovCn 7.58E-07 -6.85E-04 1.63E-05 1.35E-06 CovBetaD CovBn CovCn Varn -4.90E-08 1.05E-05 1.35E-06 3.14E-07			
Thermal - Non-Thermal Weibull Model Distributions				110nm-Final Parameters				130nm-Final Parameters			
90nm-Final Parameters				110nm-Final Parameters				130nm-Final Parameters			
Parameter Bounds Lower = 2.7586 Beta = 2.7609 Upper = 2.7632 Lower = 480.7776 B = 481.3743 Upper = 481.9710 Lower = 2.7759 C = 2.7830 Upper = 2.7901 Lower = 0.4844 n = 0.4859 Upper = 0.4873 Eta = 4.7255 Ea = 0.0415				Parameter Bounds Lower = 2.5976 Beta = 2.5998 Upper = 2.6019 Lower = 463.0570 B = 463.7186 Upper = 464.3802 Lower = 2.9045 C = 2.9125 Upper = 2.9206 Lower = 0.5032 n = 0.5048 Upper = 0.5063 Eta = 4.6027 Ea = 0.0400				Parameter Bounds Lower = 2.4134 Beta = 2.4152 Upper = 2.4171 Lower = 609.9189 B = 610.6267 Upper = 611.3345 Lower = 1.7264 C = 1.7314 Upper = 1.7364 Lower = 0.5917 n = 0.5934 Upper = 0.5951 Eta = 3.4993 Ea = 0.0526			
Temperature (K) = 398.15 Voltage (V) = 4.05 Confidence Bounds = 2-Sided @ 95% CL Std Dev Upper Limit = 4.2089 Mean Life (Secs.) = 4.2056 1.59 Lower Limit = 4.2024				Temperature (K) = 398.15 Voltage (V) = 4.05 Confidence Bounds = 2-Sided @ 95% CL Std Dev Upper Limit = 4.0915 Mean Life (Secs.) = 4.0881 1.63 Lower Limit = 4.0847				Temperature (K) = 398.15 Voltage (V) = 4.05 Confidence Bounds = 2-Sided @ 95% CL Std Dev Upper Limit = 3.1053 Mean Life (Secs.) = 3.1024 1.42 Lower Limit = 3.0996			
Temperature (K) = 348.15 Voltage (V) = 4.05 Confidence Bounds = 2-Sided @ 95% CL Upper Limit = 5.0063 Mean Life (Secs.) = 5.0031 2.01 Lower Limit = 4.9999				Temperature (K) = 348.15 Voltage (V) = 4.05 Confidence Bounds = 2-Sided @ 95% CL Upper Limit = 4.8342 Mean Life (Secs.) = 4.8309 1.98 Lower Limit = 4.8276				Temperature (K) = 348.15 Voltage (V) = 4.05 Confidence Bounds = 2-Sided @ 95% CL Upper Limit = 3.8698 Mean Life (Secs.) = 3.8669 1.72 Lower Limit = 3.864			
Temperature (K) = 298.15 Voltage (V) = 4.05 Confidence Bounds = 2-Sided @ 95% CL Upper Limit = 6.3122 Mean Life (Secs.) = 6.3087 2.49 Lower Limit = 6.3053				Temperature (K) = 298.15 Voltage (V) = 4.05 Confidence Bounds = 2-Sided @ 95% CL Upper Limit = 6.0406 Mean Life (Secs.) = 6.0371 2.52 Lower Limit = 6.0336				Temperature (K) = 298.15 Voltage (V) = 4.05 Confidence Bounds = 2-Sided @ 95% CL Upper Limit = 5.1925 Mean Life (Secs.) = 5.1892 2.35 Lower Limit = 5.1859			
Temperature (K) = 218.15 Voltage (V) = 4.05 Confidence Bounds = 2-Sided @ 95% CL Upper Limit = 11.4145 Mean Life (Secs.) = 11.4046 4.39 Lower Limit = 11.3947				Temperature (K) = 218.15 Voltage (V) = 4.05 Confidence Bounds = 2-Sided @ 95% CL Upper Limit = 10.6723 Mean Life (Secs.) = 10.6622 4.42 Lower Limit = 10.6521				Temperature (K) = 218.15 Voltage (V) = 4.05 Confidence Bounds = 2-Sided @ 95% CL Upper Limit = 11.0083 Mean Life (Secs.) = 10.9972 4.82 Lower Limit = 10.986			
Fisher Var/Cov Matrix VarBeta CovBetaB CovBetaC CovBetaD 1.35E-06 -7.06E-05 6.73E-07 -4.90E-08 CovBetaB VarB CovBC CovBn -7.06E-05 9.27E-02 -8.10E-04 1.80E-05 CovBetaC CovBC VarC CovCn 6.73E-07 -8.10E-04 1.30E-05 1.61E-06 CovBetaD CovBn CovCn Varn -4.90E-08 1.80E-05 1.61E-06 5.55E-07				Fisher Var/Cov Matrix VarBeta CovBetaB CovBetaC CovBetaD 1.23E-06 -6.76E-05 6.41E-07 -5.92E-08 CovBetaB VarB CovBC CovBn -6.76E-05 1.14E-01 -1.04E-03 2.16E-05 CovBetaC CovBC VarC CovCn 6.41E-07 -1.04E-03 1.69E-05 1.89E-06 CovBetaD CovBn CovCn Varn -5.92E-08 2.16E-05 1.89E-06 6.27E-07				Fisher Var/Cov Matrix VarBeta CovBetaB CovBetaC CovBetaD 8.90E-07 -5.14E-05 2.24E-07 -9.17E-08 CovBetaB VarB CovBC CovBn -5.14E-05 1.30E-01 -6.75E-04 4.13E-05 CovBetaC CovBC VarC CovCn 2.24E-07 -6.75E-04 6.52E-06 1.23E-06 CovBetaD CovBn CovCn Varn -9.17E-08 4.13E-05 1.23E-06 7.39E-07			

Table 8. Thermal – Non-Thermal Weibull Model Distribution Paramaters (2.5V).

Thermal - Non-Thermal/Weibull Model Distributions				110nm-Initial Parameters				130nm-Initial Parameters			
90nm-Initial Parameters				110nm-Initial Parameters				130nm-Initial Parameters			
Parameter Bounds Lower = 3.9624 Beta = 3.9654 Upper = 3.9685 Lower = 389.9964 B = 390.4031 Upper = 390.8098 Lower = 3.9179 C = 3.9247 Upper = 3.9315 Lower = 0.4597 n = 0.4607 Upper = 0.4617 Eta = 6.86 Ea = 0.0336 Temperature (K) = 398.15 Voltage (V) = 2.5 Confidence Bounds = 2-Sided @ 95% CL Std Dev Upper Limit = 6.218 Mean Life (Secs.) = 6.2149 1.75 Lower Limit = 6.2118				Parameter Bounds Lower = 3.6984 Beta = 3.7014 Upper = 3.7044 Lower = 375.2421 B = 375.6892 Upper = 376.1363 Lower = 4.0449 C = 4.0526 Upper = 4.0603 Lower = 0.4725 n = 0.4736 Upper = 0.4747 Eta = 6.7407 Ea = 0.0324 Temperature (K) = 398.15 Voltage (V) = 2.5 Confidence Bounds = 2-Sided @ 95% CL Std Dev Upper Limit = 6.0866 Mean Life (Secs.) = 6.0833 1.81 Lower Limit = 6.08				Parameter Bounds Lower = 3.6687 Beta = 3.6716 Upper = 3.6746 Lower = 367.2766 B = 367.7282 Upper = 368.1797 Lower = 4.1209 C = 4.1288 Upper = 4.1367 Lower = 0.4784 n = 0.4795 Upper = 0.4806 Eta = 6.7006 Ea = 0.0317 Temperature (K) = 398.15 Voltage (V) = 2.5 Confidence Bounds = 2-Sided @ 95% CL Std Dev Upper Limit = 6.0478 Mean Life (Secs.) = 6.0444 1.81 Lower Limit = 6.0411			
Temperature (K) = 348.15 Voltage (V) = 2.5 Confidence Bounds = 2-Sided @ 95% CL Std Dev Upper Limit = 7.1576 Mean Life (Secs.) = 7.1547 2.06 Lower Limit = 7.1517				Temperature (K) = 348.15 Voltage (V) = 2.5 Confidence Bounds = 2-Sided @ 95% CL Std Dev Upper Limit = 6.9675 Mean Life (Secs.) = 6.9644 2.23 Lower Limit = 6.9612				Temperature (K) = 348.15 Voltage (V) = 2.5 Confidence Bounds = 2-Sided @ 95% CL Std Dev Upper Limit = 6.9049 Mean Life (Secs.) = 6.9018 2.18 Lower Limit = 6.8987			
Temperature (K) = 298.15 Voltage (V) = 2.5 Confidence Bounds = 2-Sided @ 95% CL Std Dev Upper Limit = 8.6382 Mean Life (Secs.) = 8.635 2.41 Lower Limit = 8.6317				Temperature (K) = 298.15 Voltage (V) = 2.5 Confidence Bounds = 2-Sided @ 95% CL Std Dev Upper Limit = 8.346 Mean Life (Secs.) = 8.3426 2.5 Lower Limit = 8.3393				Temperature (K) = 298.15 Voltage (V) = 2.5 Confidence Bounds = 2-Sided @ 95% CL Std Dev Upper Limit = 8.2426 Mean Life (Secs.) = 8.2393 2.48 Lower Limit = 8.236			
Temperature (K) = 218.15 Voltage (V) = 2.5 Confidence Bounds = 2-Sided @ 95% CL Std Dev Upper Limit = 13.9663 Mean Life (Secs.) = 13.9574 3.9 Lower Limit = 13.9485				Temperature (K) = 218.15 Voltage (V) = 2.5 Confidence Bounds = 2-Sided @ 95% CL Std Dev Upper Limit = 13.2351 Mean Life (Secs.) = 13.2261 4.01 Lower Limit = 13.217				Temperature (K) = 218.15 Voltage (V) = 2.5 Confidence Bounds = 2-Sided @ 95% CL Std Dev Upper Limit = 12.9605 Mean Life (Secs.) = 12.9515 3.96 Lower Limit = 12.9426			
Fisher Var/Cov Matrix VarBeta CovBetaB CovBetaC CovBetaD 2.45E-06 -4.03E-05 5.40E-07 -5.22E-08 CovBetaB VarB CovBC CovBn -4.03E-05 4.30E-02 -5.21E-04 1.02E-05 CovBetaC CovBC VarC CovCn 5.40E-07 -5.21E-04 1.20E-05 1.09E-06 CovBetaD CovBn CovCn Varn -5.22E-08 1.02E-05 1.09E-06 2.70E-07				Fisher Var/Cov Matrix VarBeta CovBetaB CovBetaC CovBetaD 2.33E-06 -4.79E-05 6.82E-07 -4.76E-08 CovBetaB VarB CovBC CovBn -4.79E-05 5.20E-02 -6.58E-04 1.05E-05 CovBetaC CovBC VarC CovCn 6.82E-07 -6.58E-04 1.54E-05 1.30E-06 CovBetaD CovBn CovCn Varn -4.76E-08 1.05E-05 1.30E-06 3.09E-07				Fisher Var/Cov Matrix VarBeta CovBetaB CovBetaC CovBetaD 2.31E-06 -5.28E-05 7.58E-07 -4.90E-08 CovBetaB VarB CovBC CovBn -5.28E-05 5.30E-02 -6.85E-04 1.05E-05 CovBetaC CovBC VarC CovCn 7.58E-07 -6.85E-04 1.63E-05 1.35E-06 CovBetaD CovBn CovCn Varn -4.90E-08 1.05E-05 1.35E-06 3.14E-07			
Thermal - Non-Thermal/Weibull Model Distributions				110nm-Final Parameters				130nm-Final Parameters			
90nm-Final Parameters				110nm-Final Parameters				130nm-Final Parameters			
Parameter Bounds Lower = 2.7596 Beta = 2.7609 Upper = 2.7632 Lower = 480.7776 B = 481.3743 Upper = 481.9710 Lower = 2.7759 C = 2.7830 Upper = 2.7901 Lower = 0.4844 n = 0.4859 Upper = 0.4873 Eta = 5.9737 Ea = 0.0415 Temperature (K) = 398.15 Voltage (V) = 2.5 Confidence Bounds = 2-Sided @ 95% CL Std Dev Upper Limit = 5.3204 Mean Life (Secs.) = 5.3165 2.08 Lower Limit = 5.3126				Parameter Bounds Lower = 2.5976 Beta = 2.5998 Upper = 2.6019 Lower = 463.0570 B = 463.7186 Upper = 464.3802 Lower = 2.9045 C = 2.9125 Upper = 2.9206 Lower = 0.5032 n = 0.5048 Upper = 0.5063 Eta = 5.8778 Ea = 0.0400 Temperature (K) = 398.15 Voltage (V) = 2.5 Confidence Bounds = 2-Sided @ 95% CL Std Dev Upper Limit = 5.2248 Mean Life (Secs.) = 5.2207 2.18 Lower Limit = 5.2166				Parameter Bounds Lower = 2.4134 Beta = 2.4152 Upper = 2.4171 Lower = 609.9189 B = 610.6267 Upper = 611.3345 Lower = 1.7264 C = 1.7314 Upper = 1.7364 Lower = 0.5917 n = 0.5934 Upper = 0.5951 Eta = 5.8072 Ea = 0.0526 Temperature (K) = 398.15 Voltage (V) = 2.5 Confidence Bounds = 2-Sided @ 95% CL Std Dev Upper Limit = 4.1342 Mean Life (Secs.) = 4.1308 1.81 Lower Limit = 4.1274			
Temperature (K) = 348.15 Voltage (V) = 2.5 Confidence Bounds = 2-Sided @ 95% CL Std Dev Upper Limit = 6.3284 Mean Life (Secs.) = 6.3246 2.5 Lower Limit = 6.3208				Temperature (K) = 348.15 Voltage (V) = 2.5 Confidence Bounds = 2-Sided @ 95% CL Std Dev Upper Limit = 6.1752 Mean Life (Secs.) = 6.1712 2.57 Lower Limit = 6.1673				Temperature (K) = 348.15 Voltage (V) = 2.5 Confidence Bounds = 2-Sided @ 95% CL Std Dev Upper Limit = 5.1521 Mean Life (Secs.) = 5.1486 2.37 Lower Limit = 5.1452			
Temperature (K) = 298.15 Voltage (V) = 2.5 Confidence Bounds = 2-Sided @ 95% CL Std Dev Upper Limit = 7.9793 Mean Life (Secs.) = 7.9751 3.12 Lower Limit = 7.9709				Temperature (K) = 298.15 Voltage (V) = 2.5 Confidence Bounds = 2-Sided @ 95% CL Std Dev Upper Limit = 7.7201 Mean Life (Secs.) = 7.7158 3.34 Lower Limit = 7.7114				Temperature (K) = 298.15 Voltage (V) = 2.5 Confidence Bounds = 2-Sided @ 95% CL Std Dev Upper Limit = 6.9134 Mean Life (Secs.) = 6.9092 3 Lower Limit = 6.9051			
Temperature (K) = 218.15 Voltage (V) = 2.5 Confidence Bounds = 2-Sided @ 95% CL Std Dev Upper Limit = 14.4301 Mean Life (Secs.) = 14.417 5.61 Lower Limit = 14.404				Temperature (K) = 218.15 Voltage (V) = 2.5 Confidence Bounds = 2-Sided @ 95% CL Std Dev Upper Limit = 13.6621 Mean Life (Secs.) = 13.6485 5.67 Lower Limit = 13.635				Temperature (K) = 218.15 Voltage (V) = 2.5 Confidence Bounds = 2-Sided @ 95% CL Std Dev Upper Limit = 14.6583 Mean Life (Secs.) = 14.6424 6.5 Lower Limit = 14.6265			
Fisher Var/Cov Matrix VarBeta CovBetaB CovBetaC CovBetaD 1.35E-06 -7.06E-05 6.73E-07 -4.90E-08 CovBetaB VarB CovBC CovBn -7.06E-05 9.27E-02 -8.10E-04 1.80E-05 CovBetaC CovBC VarC CovCn 6.73E-07 -8.10E-04 1.30E-05 1.61E-06 CovBetaD CovBn CovCn Varn -4.90E-08 1.80E-05 1.61E-06 5.55E-07				Fisher Var/Cov Matrix VarBeta CovBetaB CovBetaC CovBetaD 1.23E-06 -6.76E-05 6.41E-07 -5.92E-08 CovBetaB VarB CovBC CovBn -6.76E-05 1.14E-01 -1.04E-03 2.16E-05 CovBetaC CovBC VarC CovCn 6.41E-07 -1.04E-03 1.69E-05 1.89E-06 CovBetaD CovBn CovCn Varn -5.92E-08 2.16E-05 1.89E-06 6.27E-07				Fisher Var/Cov Matrix VarBeta CovBetaB CovBetaC CovBetaD 8.90E-07 -5.14E-05 2.24E-07 -9.17E-08 CovBetaB VarB CovBC CovBn -5.14E-05 1.30E-01 -6.75E-04 4.13E-05 CovBetaC CovBC VarC CovCn 2.24E-07 -6.75E-04 6.52E-06 1.23E-06 CovBetaD CovBn CovCn Varn -9.17E-08 4.13E-05 1.23E-06 7.39E-07			

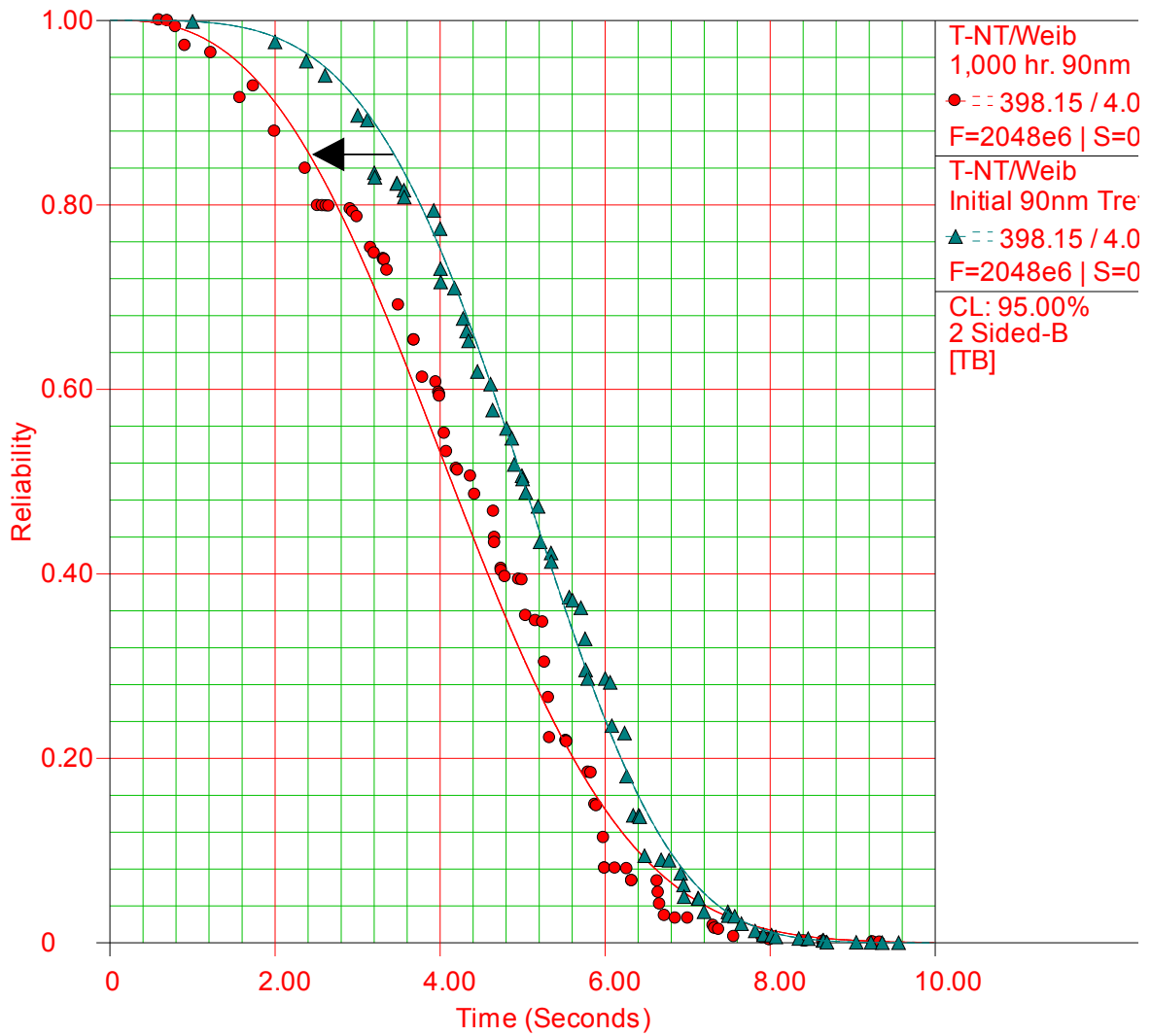
Use Level Probability Weibull



1,000 hr. Beta1=2.7609, B1=481.3743, C1=2.7830, n1=0.4859
 Initial Beta2=3.9654, B2=390.4031, C2=3.9247, n2=0.4607

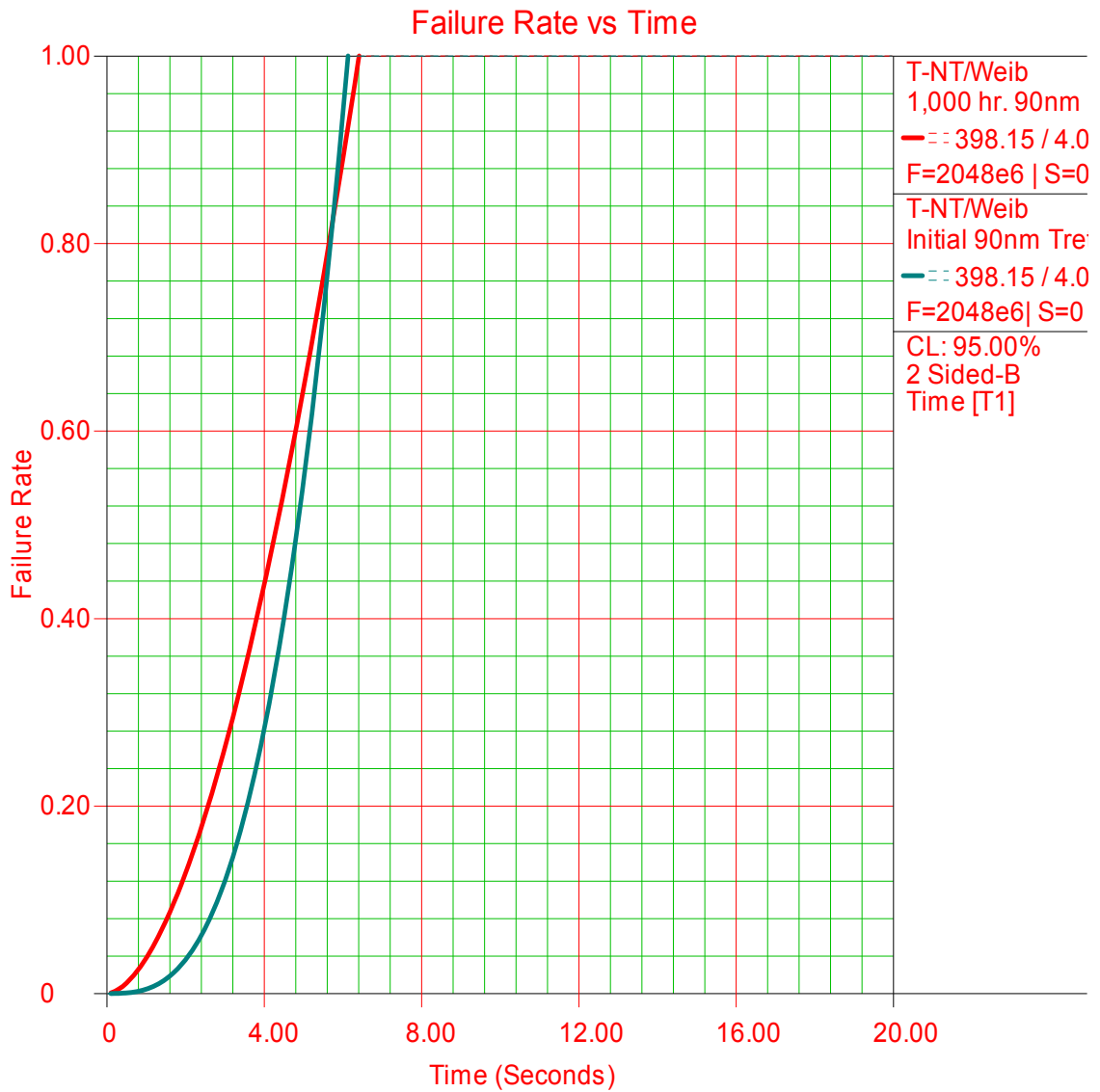
Figure 21. 90nm T-NT/Weibull Initial and 1,000 hr. Use Level Plots at Fixed 398.15K and 4.05V.

Reliability vs Time



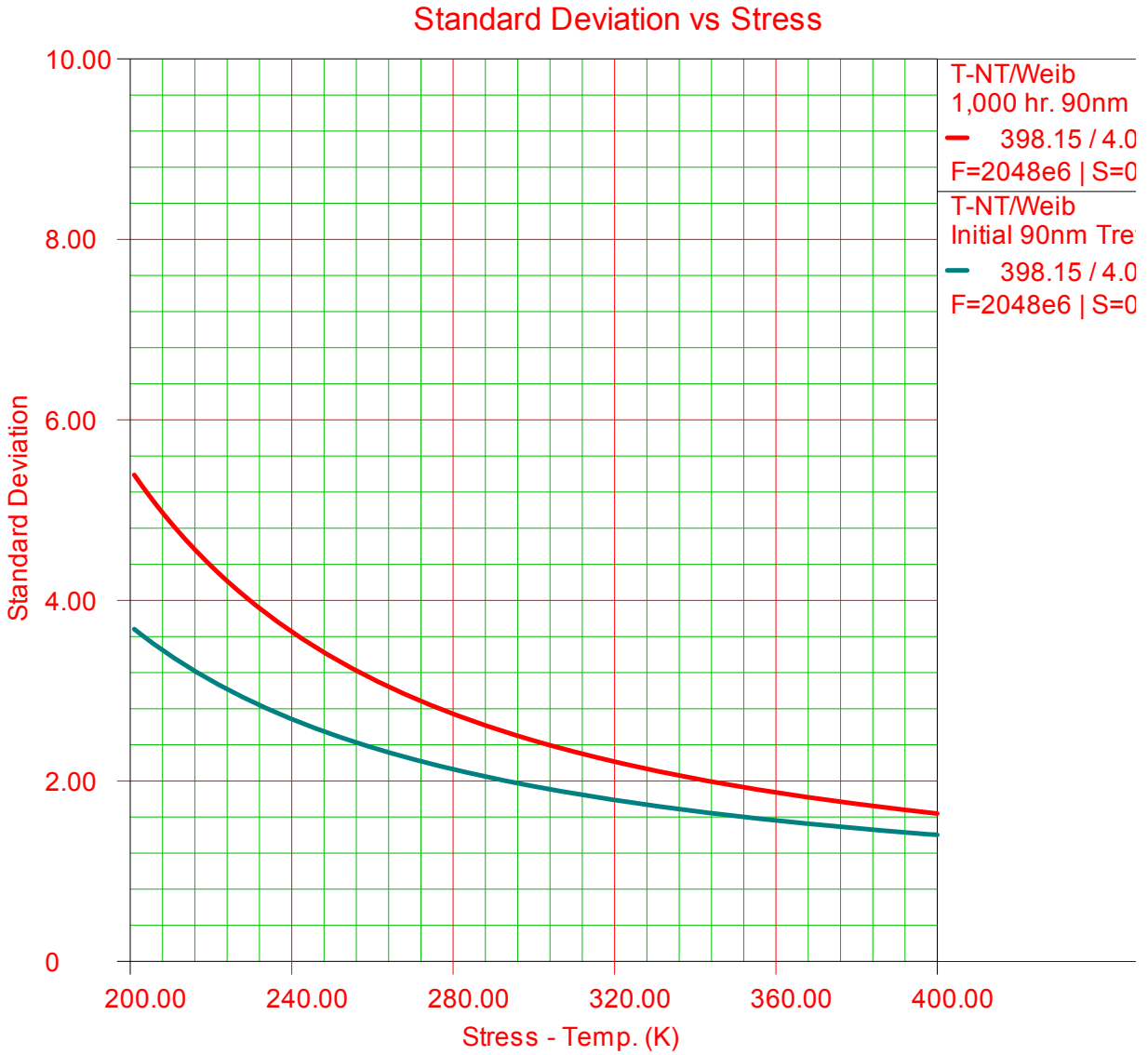
1,000 hr. Beta1=2.7609, B1=481.3743, C1=2.7830, n1=0.4859
 Initial Beta2=3.9654, B2=390.4031, C2=3.9247, n2=0.4607

Figure 22. 90nm T-NT/Weibull Initial and 1,000 hr. Reliability Plots at at Fixed 398.15K and 4.05V.



1,000 hr. Beta1=2.7609, B1=481.3743, C1=2.7830, n1=0.4859
 Initial Beta2=3.9654, B2=390.4031, C2=3.9247, n2=0.4607

Figure 23. 90nm T-NT/Weibull Initial and 1,000 hr. FR Plots at Fixed 398.15K and 4.05V.



1,000 hr. Beta1=2.7609, B1=481.3743, C1=2.7830, n1=0.4859
 Initial Beta2=3.9654, B2=390.4031, C2=3.9247, n2=0.4607

Figure 24. 90nm T-NT/Weibull Initial and 1,000 hr. SD Plots at Fixed 4.05V.

3.3 Degradation Model

Given that the data retention measurements were recorded at 100 hour increments up to 1,000 hours, degradation analysis is implemented to predict how data retention degrades over time under different stress conditions. Retention time degradation was analyzed by fitting the appropriate degradation model to the data using the Mean Square Error (MSE) method. This model describes the relationship between data retention properties over time for several stress conditions and technologies. As with conventional reliability data, the amount of uncertainty in the results is directly related to the number of units or bits of information tested and one must be cautious of extrapolation error. The following models were analyzed and ranked for the best fit to the observed degradation: Linear, Exponential, Power, Logarithmic, Gompertz and Lloyd-Lipow. The Exponential relationship was the highest ranked model for the observed data:

$$y = a * e^{(-bx)}, \quad (3.17)$$

where y represents the performance stress condition, x represents time-to-fail, and a and b are the unknown model parameters to be calculated for different stress conditions. Model parameters for t 0.1 (99.9% Reliability) are calculated in Table 9 using non-linear regression analysis for each of the three technologies. The cold temperature (218K) data retention properties over time do not follow any degradation model over the tested period. Therefore, the degradation model can only be applied at $\geq 298\text{K}$. Statistical nonlinear regression analysis, results and 95% Confidence Levels at each condition are summarized in Appendix A.

Table 9. Exponential Model Parameters.

Data ID	Parameter a	Parameter b
90nm: 298.15K, 2.5V	8.5506	8.331E-05
90nm: 348.15K, 2.5V	7.1762	1.354E-04
<u>90nm: 398.15K, 2.5V</u>	<u>6.1696</u>	<u>1.625E-04</u>
90nm: 298.15K, 4.05V	6.8529	9.116E-05
90nm: 348.15K, 4.05V	5.4943	7.289E-05
<u>90nm: 398.15K, 4.05V</u>	<u>4.8682</u>	<u>1.567E-04</u>
110nm: 298.15K, 2.5V	8.3135	8.168E-05
110nm: 348.15K, 2.5V	6.8425	1.203E-04
<u>110nm: 398.15K, 2.5V</u>	<u>6.0345</u>	<u>1.540E-04</u>
110nm: 298.15K, 4.05V	6.6194	9.737E-05
110nm: 348.15K, 4.05V	5.5363	1.322E-04
<u>110nm: 398.15K, 4.05V</u>	<u>4.8036</u>	<u>1.639E-04</u>
130nm: 298.15K, 2.5V	8.3441	1.929E-04
130nm: 348.15K, 2.5V	6.7430	3.071E-04
<u>130nm: 398.15K, 2.5V</u>	<u>5.4443</u>	<u>3.194E-04</u>
130nm: 298.15K, 4.05V	6.5241	2.498E-04
130nm: 348.15K, 4.05V	5.4715	3.727E-04
<u>130nm: 398.15K, 4.05V</u>	<u>4.7582</u>	<u>4.386E-04</u>

The critical degradation value of data retention time for the devices is 64 milliseconds, the point at which bit-cells are automatically refreshed in auto-refresh mode. Once cell retention time degrades below this threshold, data is likely to be lost, i.e., a logic-1 changes states to logic-0 as data retention capability falls below the auto-refresh time of the devices. Figure 25 shows the Tret degradation prediction of the three technologies at accelerated conditions. The 130nm technology is the worst performer compared to both the 110nm and 90nm technology parts. As was initially noted in Chapter Three, a scale factor is evident; the more integrated the device, generally the better the retention time across temperature and the tighter the standard deviation. The scale factor is most likely explained by a difference of the oxide layers used in smaller

technologies (advanced high-K processes) and improvements in cell design, processing and geometry, i.e., vertical/horizontal staked capacitors, materials, dimensions, etc.

Based on the 64 milliseconds critical threshold and substituting the parameter values into the Exponential degradation model and solving for x, the t 0.1 time when data retention drops to 99.9% reliability at different stress levels are summarized in Table 10. Times were calculated at the 95% CL.

Table 10. Data Retention TTF (t 0.1 Point).

Data ID	t 0.1 Time-to-Fail (Hours)
90nm: 298.15K, 2.5V	67920.4
90nm: 348.15K, 2.5V	40067.5
<u>90nm: 398.15K, 2.5V</u>	<u>32852.2</u>
90nm: 298.15K, 4.05V	51730.2
90nm: 348.15K, 4.05V	42329.7
<u>90nm: 398.15K, 4.05V</u>	<u>28027.1</u>
110nm: 298.15K, 2.5V	68404.7
110nm: 348.15K, 2.5V	45485.3
<u>110nm: 398.15K, 2.5V</u>	<u>34222.4</u>
110nm: 298.15K, 4.05V	47881.2
110nm: 348.15K, 4.05V	33500.9
<u>110nm: 398.15K, 4.05V</u>	<u>26417.9</u>
130nm: 298.15K, 2.5V	28425.5
130nm: 348.15K, 2.5V	17977.6
<u>130nm: 398.15K, 2.5V</u>	<u>17161.8</u>
130nm: 298.15K, 4.05V	18716.5
130nm: 348.15K, 4.05V	12044.3
<u>130nm: 398.15K, 4.05V</u>	<u>9912.3</u>

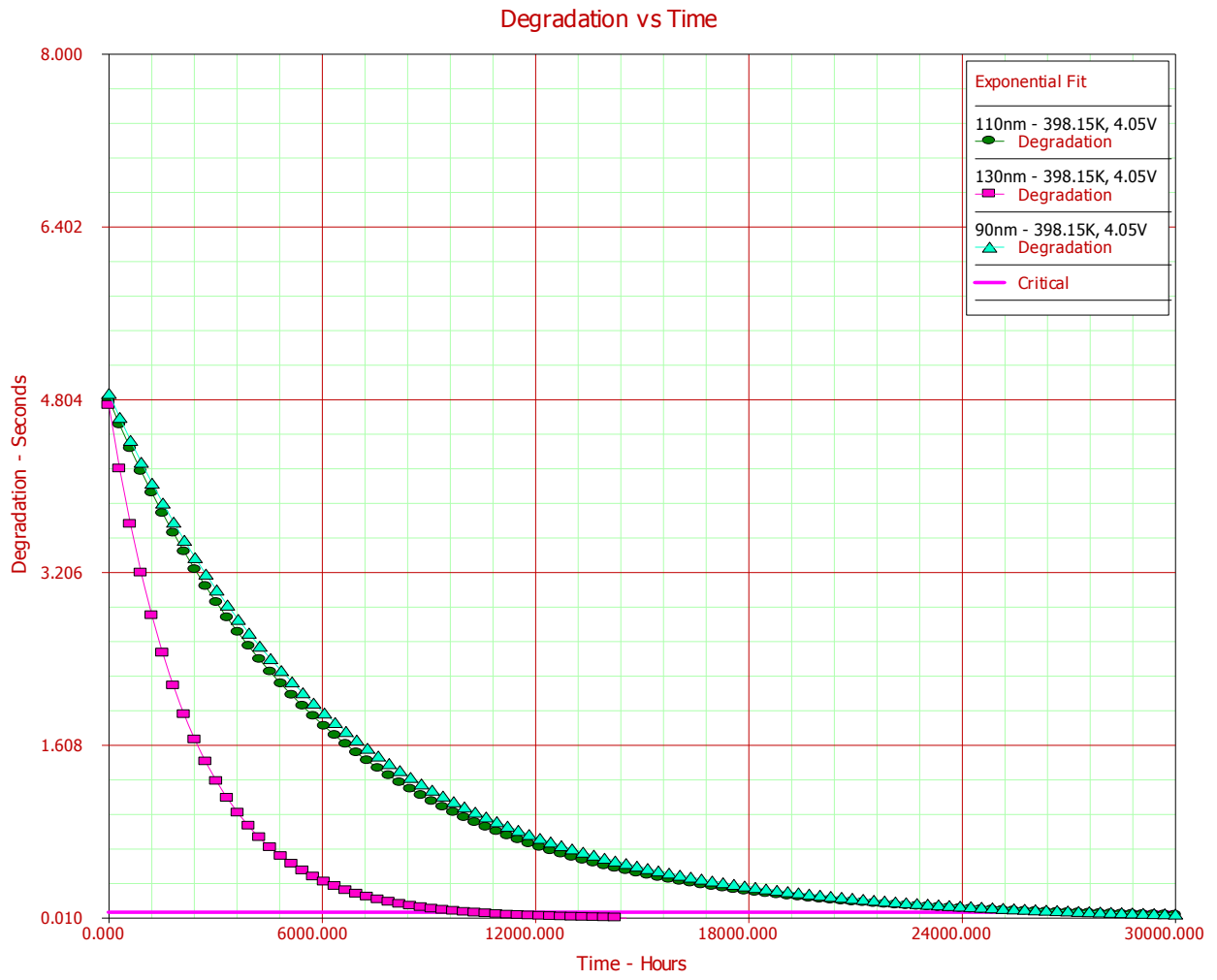


Figure 25. Tret Degradation Prediction at Accelerated Conditions.

Chapter 4: Physics-of-Failure & Systems Approach

4.1 Overview

Retention time margin may also be measured using a Q-ratio of the time-to-first-failure distribution (t_I) to the maximum specified refresh time, (t_M). This ratio provides insight into the tolerance of each technology generation to degradation with respect to voltage and temperature stresses. The ratio also provides a quality factor demonstrating the amount of margin between actual soft breakdown and the manufacturer's specified refresh time. Table 11 shows the $(t_I)/(t_M)$ Q-ratios for each technology and stress condition. A high Q-ratio number represents a high operating margin; a low number represents low margin.

Data retention characteristics are most robust at low temperature, 218K, and nominal operating voltage, 2.5V. The Q-ratio also reveals that 90nm devices are more robust across the full stress profile range than the 110nm and 130nm devices. While all three technologies reveal diminishing margin with increasing temperature and voltage stresses, Table 11 shows that the temperature component of the stress profile has a greater effect on data retention margin.

Table 11. Q-Ratio $(t_I)/(t_M)$ at Initial Test Point.

Test Conditions	90nm $(t_I)/(t_M)$ Q-Ratio	110nm $(t_I)/(t_M)$ Q-Ratio	130nm $(t_I)/(t_M)$ Q-Ratio
218K, 2.5V	140.6	140.6	140.6
298K, 2.5V	125.0	125.0	125.0
348K, 2.5V	78.1	62.5	62.5
398K, 2.5V	46.9	31.3	31.3
218K, 4.0V	109.4	109.4	109.4
298K, 4.0V	93.8	93.8	93.8
348K, 4.0V	46.9	31.3	31.3
398K, 4.0V	15.6	4.7	3.1

After passing of a memory cell's retention time, a charged cell has lost a certain threshold charge such that the remaining charge is detected as a logic zero. This fixed threshold charge equals the average leakage current times the retention time. Therefore, the retention time is inversely proportional to the average leakage current, and the distribution of cell leakage currents may be determined by measuring the distribution of retention times. Three leakage paths should be considered: first, sub-threshold leakage through the access transistors; second, leakage from the storage node of the transistor to the substrate; and third, leakage through the dielectric of the storage capacitor. Newer DRAM designs generally bias the cell plate at $V_{dd}/2$ in order to reduce the electric field in the thin dielectric of the storage capacitor. The leakage of the dielectric of the storage capacitors should be increased by charge injection under stress before breakdown of the dielectric. Low temperature testing, 218K, was included in the stress profile in an attempt to identify this effect. Thermal carrier generation is based on tunneling through the dielectric, from leakage to the substrate and through the access transistor.

4.2 Failure Mechanisms

The data retention time breakdown failure distributions are similar to the time-to-failure distributions of the breakdown of thin dielectrics. Therefore, dielectric leakage may be a precursor to breakdown, and increased through electrical and thermal stresses before breakdown or other loss of functionality occurs. This effect would show up as a shift in the retention time distribution measured after stressing the devices. This will be shown graphically later.

The three paths for storage capacitor charge to leak out are through the capacitor dielectric, through the substrate, and through the transistor channel. The two latter effects on the time to first-bit failure can be magnified by either increasing or decreasing the substrate bias as was shown by Shaw et al [106]. For an n-channel transistor, negative substrate biasing decreases the sub-threshold current exponentially. However, at a very large negative bias, substantial current may be generated in the depletion region of the storage node's p-n junction. This current may be generated by thermal activation of electrons through near mid-gap centers and is proportional to the depletion width. At temperatures high enough to overcome the full bandgap of silicon, diffusion of minority carriers may also be a factor. Earlier work shows that a small negative substrate bias may be generated on-chip, which in effect suppresses both the sub-threshold and the substrate current [106].

4.3 Discussion

Model distributions were fitted to the failure distributions for each of the technologies studied. The data supports and fits the Thermal – Non-Thermal (T-NT) Model comprised of the Arrhenius relationship for the thermal stress, and the Inverse Power Law for the voltage stress.

Using this model and the Weibull distribution for plotting, it is shown that the β slope decreases over time for each stress condition. There are two distinct breakdown failure modes as are shown in the Weibull distributions in Figures 26 and 27. The first observed breakdown failures in each distribution appear to be caused by random defects, considered to be extrinsic in nature, and generally process induced. These failures may be caused by weak areas or defects in the oxide film, contaminants, fine cracks, or pin holes. Such defects can cause increases in leakage within the memory cell and early breakdown. The randomness of the defect related first failures lends itself well for further statistical analysis.

Figure 26 shows that for the 130nm products initial readings at elevated stress conditions, approximately 0.34% of the early retention time failures are attributable to randomly distributed weak bits. Similarly, after 1,000 hour stress, Figure 27 shows that at elevated stress conditions a higher percentage, approximately 0.58% of the early retention time failures, is attributable to randomly distributed weak bits. At the other end of the spectrum, colder temperature and nominal operating voltage, the data retention characteristics are much better.

Figure 28 shows that for the 110nm products initial readings at elevated stress conditions, approximately 0.052% of the early retention time failures are attributable to randomly distributed weak bits. Similarly, after 1,000 hour stress, Figure 29 shows that at elevated stress conditions a higher percentage, approximately 0.5% of the early retention time failures, is attributable to randomly distributed weak bits. Likewise with the 130nm products, at colder temperature and nominal operating voltage, the data retention characteristics are much better.

Figures 30 and 31 show that for the 90nm products, initial and 1,000 readings at elevated stress conditions correlate much better, demonstrating that approximately 0.32% of the early retention time failures are attributable to randomly distributed weak bits.

The second distinct failure breakdown mode consists of the main population of the distribution. The soft breakdown related failure mechanism may be related to the robustness of the oxide processing. Although data retention soft errors are plotted, a hard degradation is observed over time. Similar distributions with two distinct populations, randomly distributed weak bits with $\beta = 1$, and a main population with increasing failure rate with $\beta > 1$ were also observed with the 110nm and 90nm and product technologies. Refer to Figures 28 – 31.

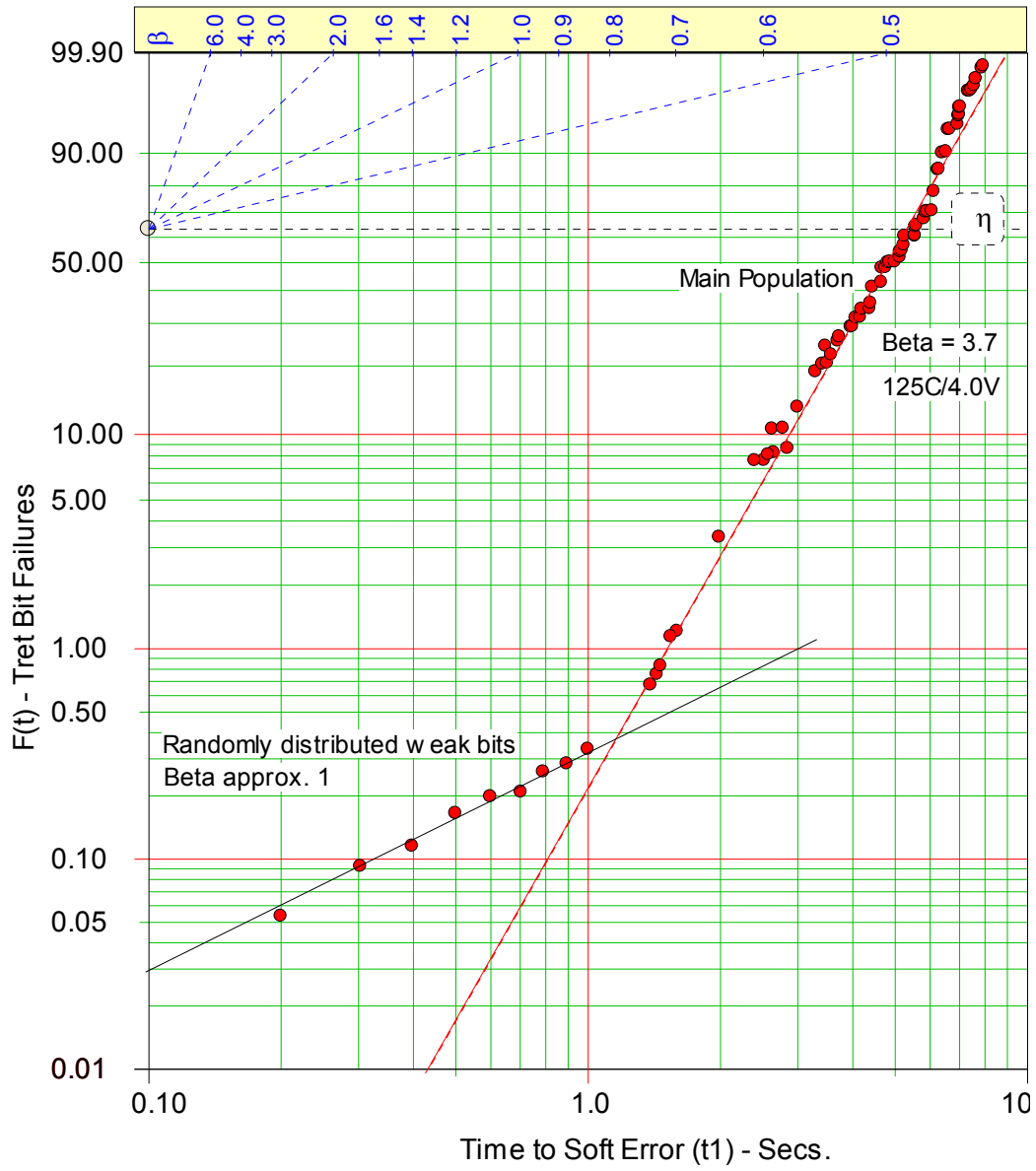


Figure 26. 130nm Bit Failure Distribution at Initial Time (t_1), 125°C/4.0V.

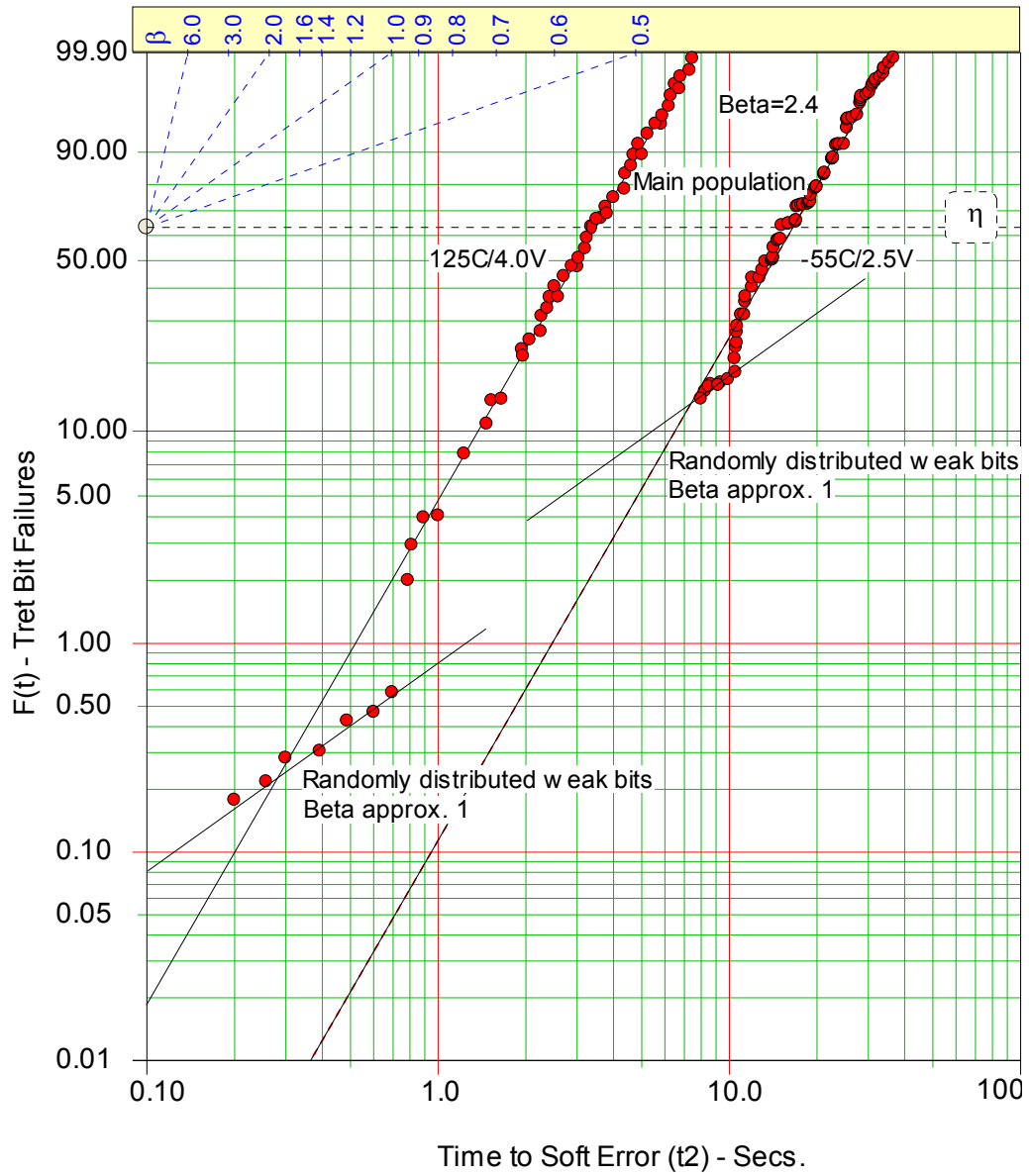


Figure 27. 130nm Bit Failure Distribution at Time (t_2).

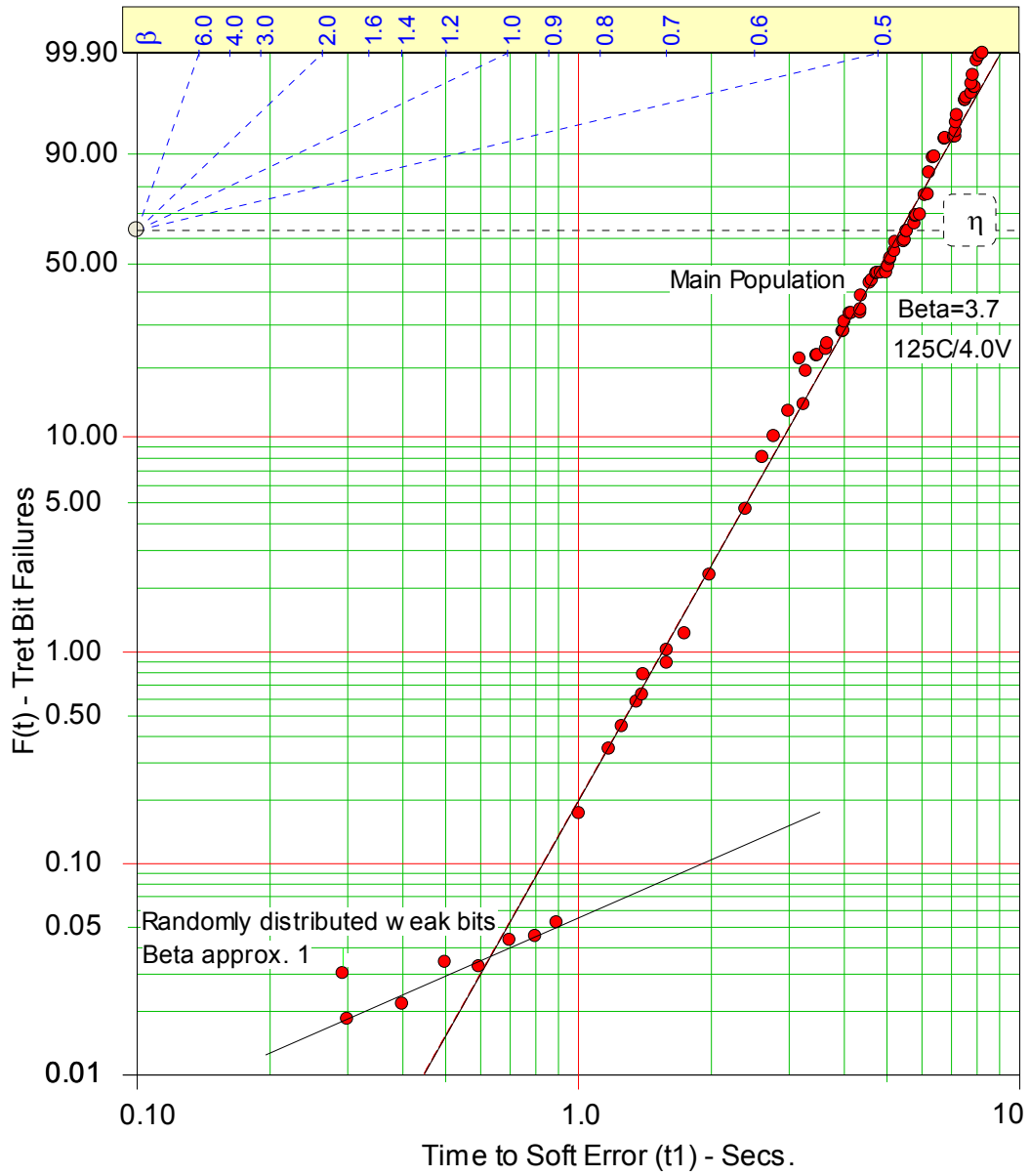


Figure 28. 110nm Bit Failure Distribution at Initial Time (t_1), $125^\circ\text{C}/4.0\text{V}$.

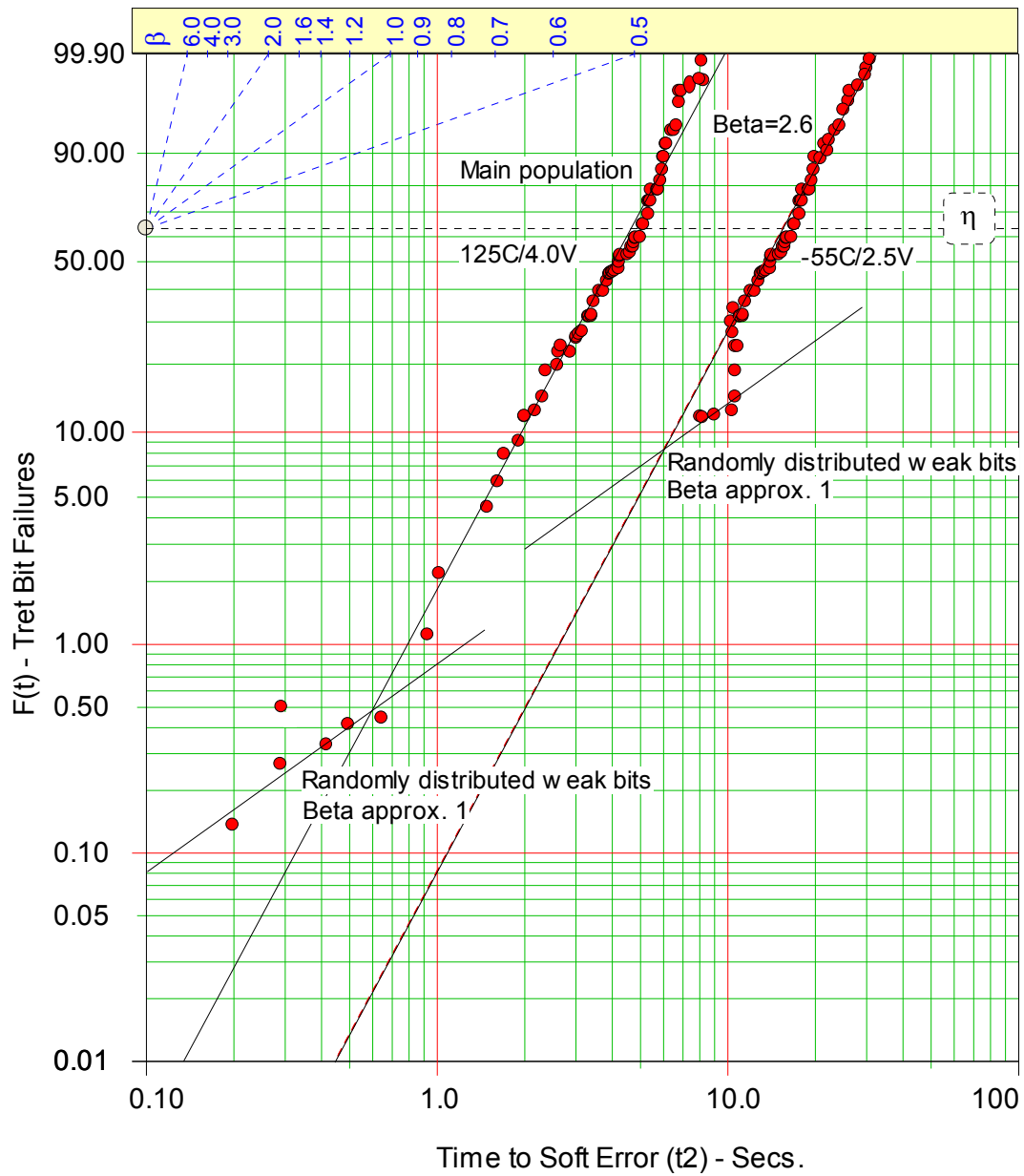


Figure 29. 110nm Bit Failure Distribution at Time (t_2).

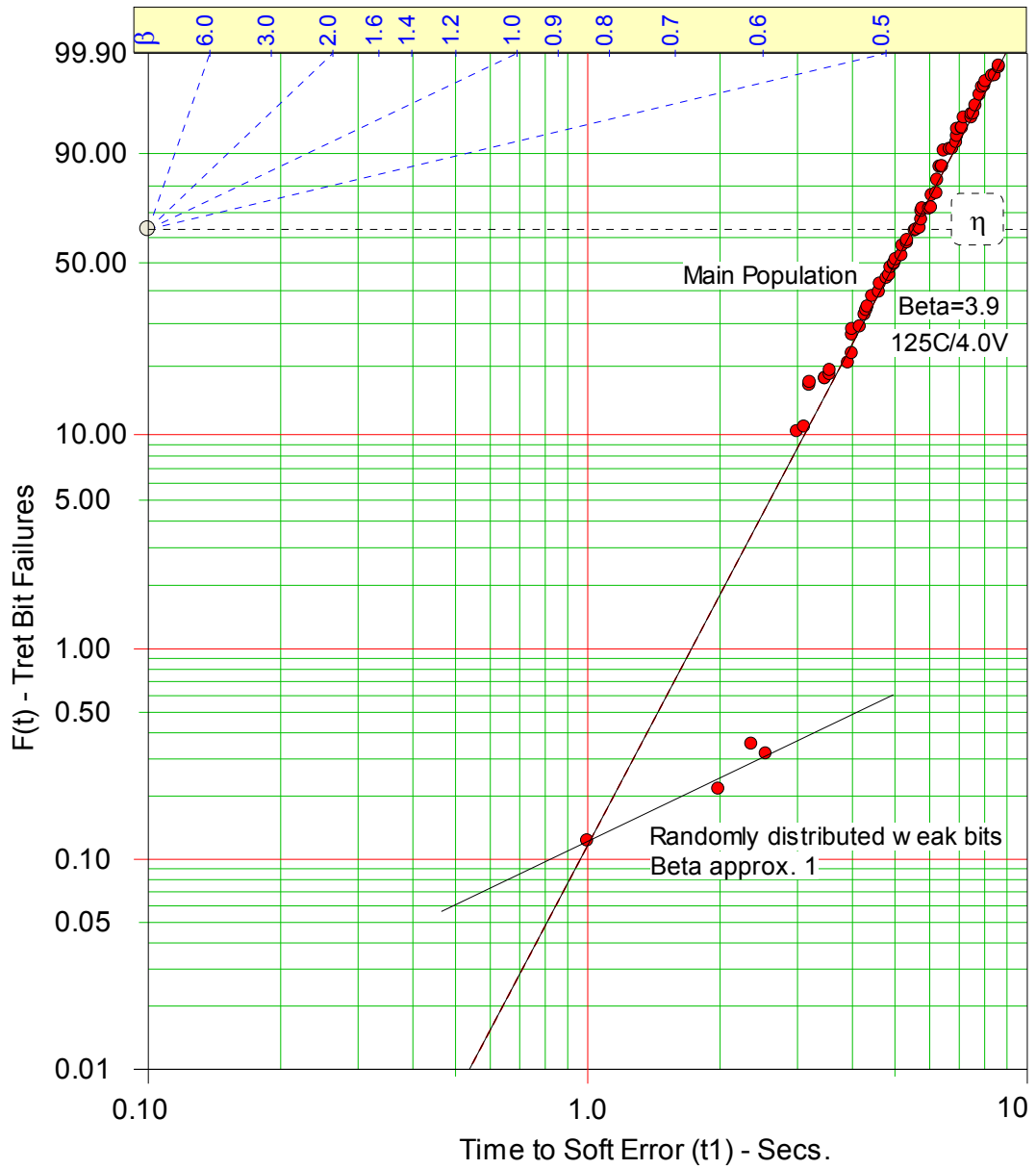


Figure 30. 90nm Bit Failure Distribution at Initial Time (t_1), 125°C/4.0V.

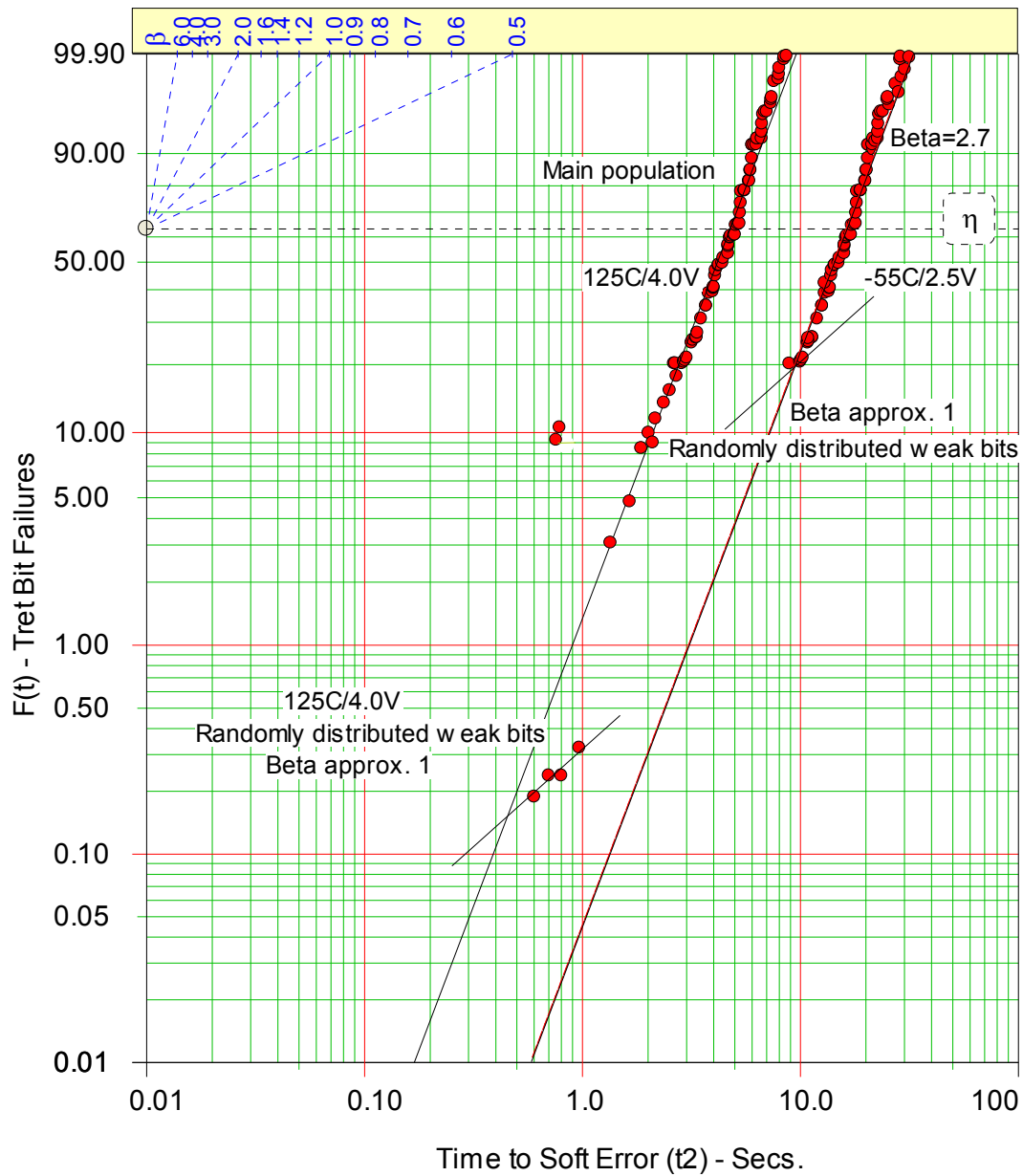


Figure 31. 90nm Bit Failure Distribution at Time (t_2).

4.3.1 Randomness

The early failures were confirmed to be random by comparing the address locations to the physical memory block locations; clustering or systemic patterns of the failure locales were not observed. The first early failures are identified by yellow blocks in 90nm SN 2 memory layout map in Figure 32.

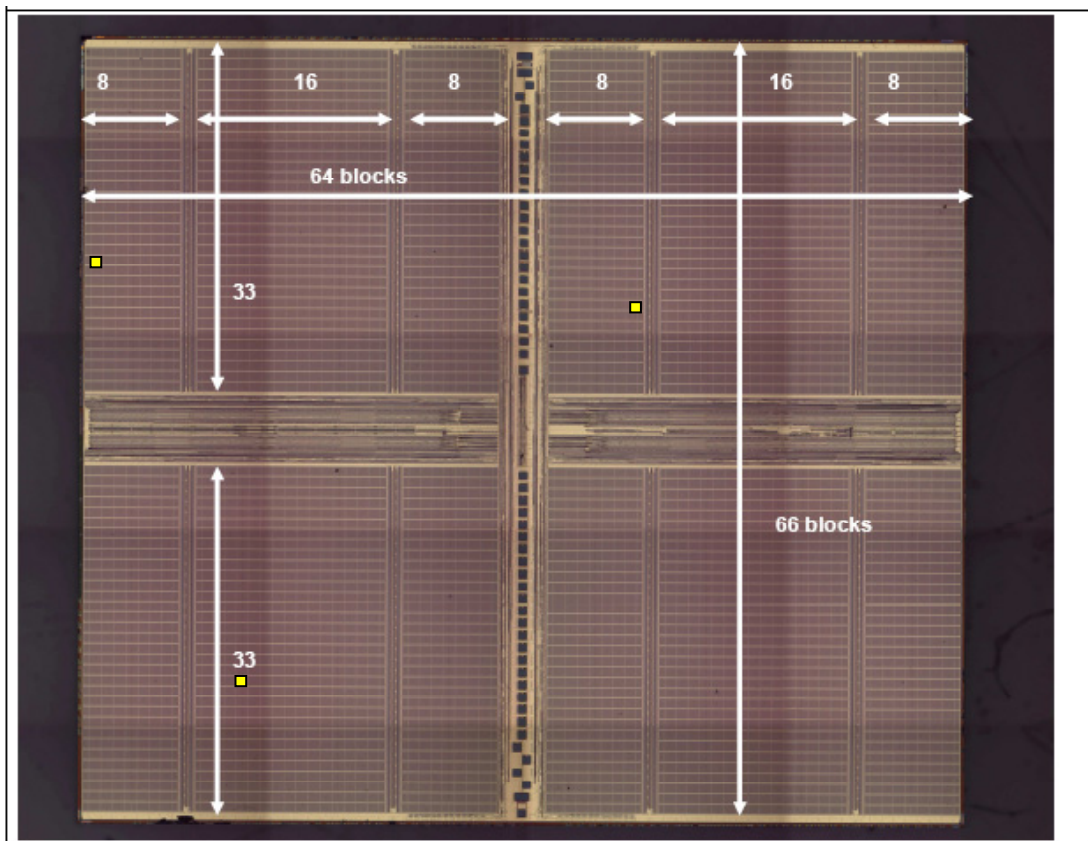


Figure 32. Optical Overview of Memory Block Layout.

4.4 Retention Time Early Breakdown

The Weibull distribution takes the form of the Exponential distribution at $\beta = 1$. This greatly simplifies the predictive model, and enables a more straightforward approach in predicting the behavior and TTF of the next technology generation. Table 12 shows the retention time soft error rates, calculated at 95% CL, of the randomly distributed weak bits at the 512Mb product (system) level at each stress condition.

It is important to note that these calculations reflect the soft error rate of the early retention time breakdown at the 1,000 hour test point, and do not reflect the hard failure breakdown of the memory product. Up to the 1,000 hour test point, even the first retention time breakdowns for all three product technologies are above the specified 64mSec refresh rate, the time one would see data loss in an actual application. Refer to Figures 26-31. The results in Table 12 reveal that a combination of high voltage and high temperature stress yields the largest SER and is the best way to identify weak bits in DRAM devices. It is shown that for each of the three memory technologies studied, there is a trend of increasing reliability (decreasing FR) for the same density of memory under equivalent stress conditions as the size of the memory cell and feature size decreases.

Table 12. 512Mb Product Level Retention Time Soft Error Rate Calculations.

Stress Conditions	90nm CFR (λ) %/1Khrs	90nm Equiv. FIT/512Mb	110nm CFR (λ) %/1Khrs	110nm Equiv. FIT/512Mb	130nm CFR (λ) %/1Khrs	130nm Equiv. FIT/512Mb
218K, 2.5V	0.0287	287	0.03025	302.5	0.02895	289.5
298K, 2.5V	0.06065	606.5	0.06215	621.5	0.06865	686.5
348K, 2.5V	0.08135	813.5	0.08245	824.5	0.09625	962.5
398K, 2.5V	0.1013	1013	0.10185	1018.5	0.1240	1240
218K, 4.0V	0.03865	386.5	0.0420	420	0.0429	429
298K, 4.0V	0.08175	817.5	0.0863	863	0.1017	1017
348K, 4.0V	0.1096	1096	0.11445	1144.5	0.1426	1426
398K, 4.0V	0.13645	1364.5	0.1414	1414	0.1837	1837

We can approximate a complex integrated circuit by a competing failure or series failure system. It is shown that the early failures, the most important failures, are random and that they are well approximated by an exponential distribution with a constant failure rate at different stress levels. For a constant failure rate system, the FIT is interchangeable with MTTF according to its definition such that:

$$FIT_s = \frac{10^9}{MTTF_s} \quad (4.1)$$

Furthermore, the FIT or CFR may be broken down into a temperature stress element and a voltage stress element. Figures 33a-c show the relative impact of the voltage and temperature stresses on product (system) level early retention time soft error rates, calculated at 95% CL, of the randomly distributed weak bits. There is a clear trend of decreasing FR with each product technology generation for the same density memory under equivalent stress conditions.

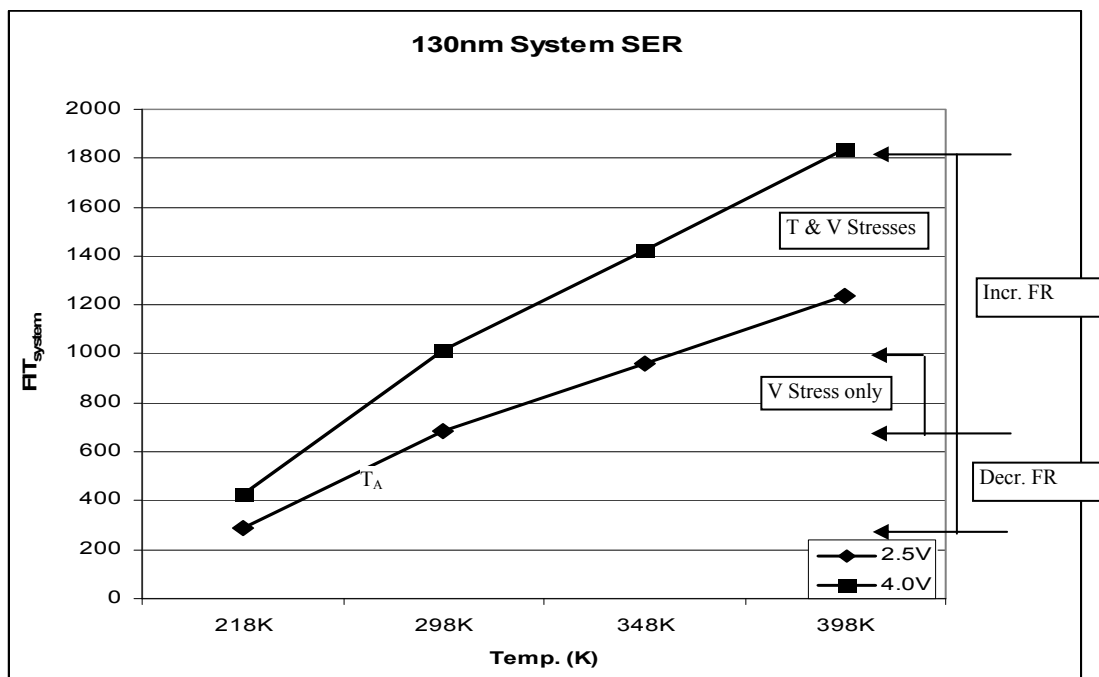


Figure 33a. 130nm System Retention Time Soft Error Rates (95% CL, 1,000hrs)

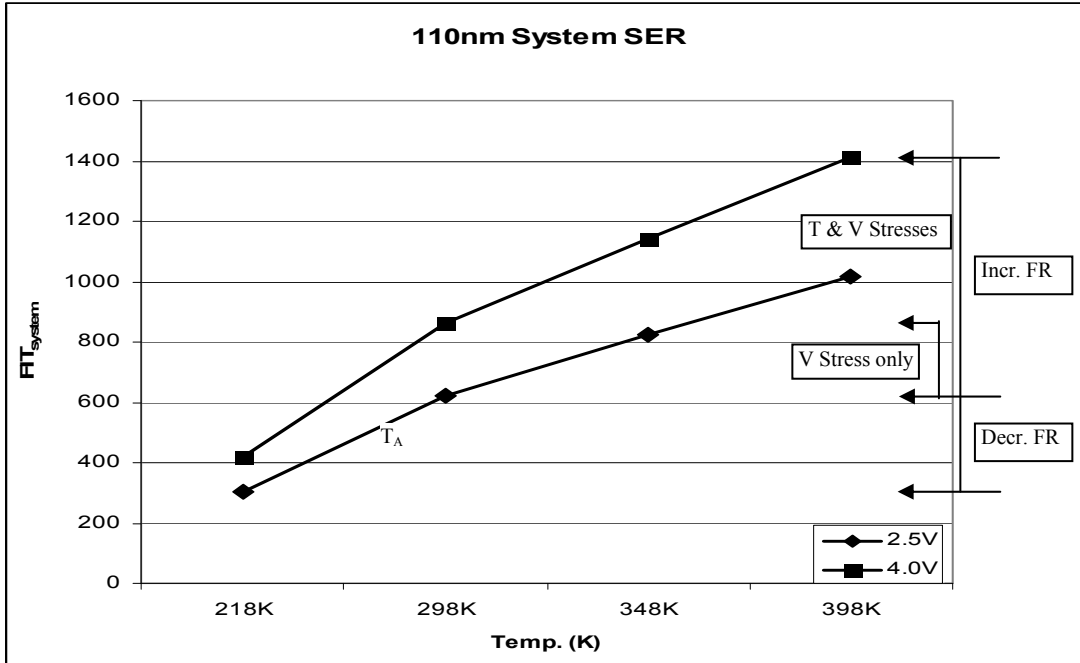


Figure 33b. 110nm System Retention Time Soft Error Rates (95% CL, 1,000hrs)

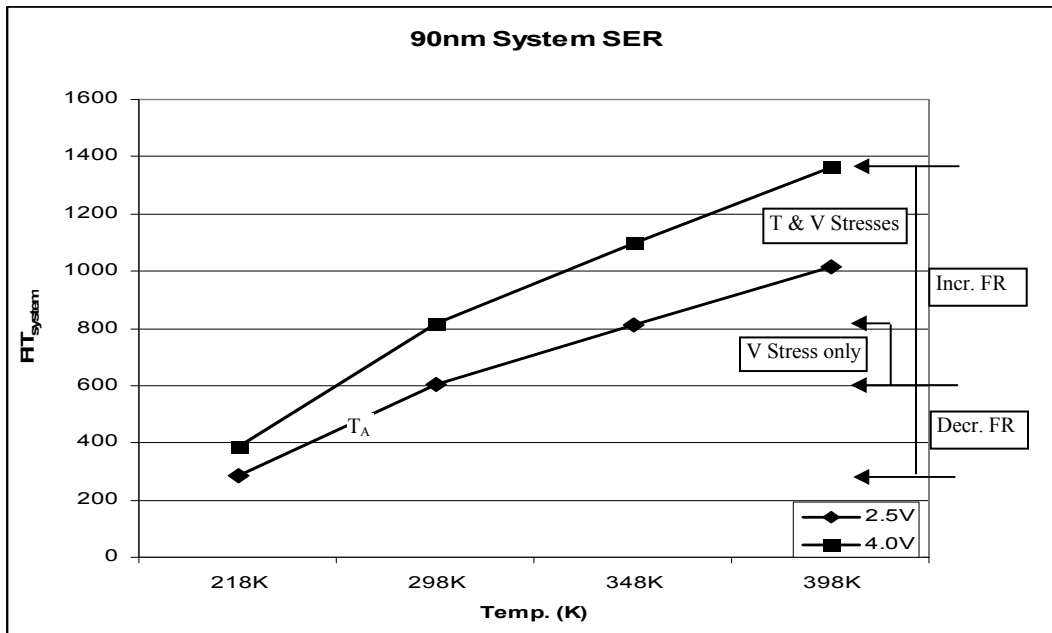


Figure 33c. 90nm System Retention Time Soft Error Rates (95% CL, 1,000hrs)

The product or system level FR results yield the impact of temperature and voltage on the acceleration factor for each of the product technologies. A test matrix with the corresponding influences of both temperature and voltage follows for each product technology follow in Tables 13a-c. The test matrices show the actual Acceleration Factor or Derating Factor for each stress condition to yield the early failures or defects.

Table 13a. 130nm Retention Time Soft Error Rate Test Matrix for Early Failures.

130nm CFR (λ) %/1Khrs	218K	298K	348K	398K
2.5V	0.02895	0.06865	0.09625	0.1240
4.0V	0.0429	0.1017	0.1426	0.1837
130nm AF_{sys}	218K	298K	348K	398K
2.5V	0.42	1	1.40	1.81
4.0V	0.62	1.48	2.1	2.68

Table 13b. 110nm Retention Time Soft Error Rate Test Matrix for Early Failures.

110nm CFR (λ) %/1Khrs	218K	298K	348K	398K
2.5V	0.03025	0.06215	0.08245	0.10185
4.0V	0.0420	0.0863	0.11445	0.1414
110nm AF_{sys}	218K	298K	348K	398K
2.5V	0.49	1	1.33	1.64
4.0V	0.67	1.39	1.84	2.28

Table 13c. 90nm Retention Time Soft Error Rate Test Matrix for Early Failures.

90nm CFR (λ) %/1Khrs	218K	298K	348K	398K
2.5V	0.0287	0.06065	0.08135	0.1013
4.0V	0.03865	0.08175	0.1096	0.13645
90nm AF_{sys}	218K	298K	348K	398K
2.5V	0.47	1	1.34	1.67
4.0V	0.64	1.34	1.81	2.25

4.5 Power Relationship as a Function of Scaling

As was described earlier in Section 1.1.2, a semiconductor device's lifetime is affected by changing its operating parameters, specifically junction temperature, because of heat activated mechanisms as well as supply voltage. The device's operating voltage (V_{dd}) directly affects many of its parameters, including current density (j_e) and the electric field (E_{ox}) across the gate dielectric. Supply voltage also has a significant effect on junction temperature (T_j) which is dependent on the power dissipated from the device (P_D), the ambient operating temperature (T_a), and the sum of the thermal impedances between the die and ambient environment (θ_{ja}). The power dissipated of the device is the sum of both dynamic and static power dissipation, such that:

$$P_D = Cl * V_{dd}^2 * f + i_l V_{dd} \quad (4.2)$$

where Cl is the total capacitance load, V_{dd} is the supply voltage, f is the frequency, and i_l is the load current in the static mode. The dissipated power of the device is then used to calculate the junction temperature such that:

$$T_j = \theta_{ja} * P_D + T_a \quad (4.3)$$

where θ_{ja} is the junction-to-ambient thermal resistance and T_a is the ambient temperature.

An analysis and comparison of the P_D and T_j for the products in this data retention study follows:

90nm product P_D and T_j calculations:

$$P_D = (Cl * Vdd^2 * f) + \text{Max}(I_{oh} DC_{max} * (Vdd - V_{oh}), I_{ol} DC_{max} * V_{ol})$$

$$P_{D(2.5V)} = (5 \times 10^{-12} * 6.25 * 133 \times 10^6) + (16.8 \text{mA} (2.5V - 1.927V)) = 13.78 \text{mW}$$

$$T_{j(-55C)} = 48.4 \text{ } ^\circ\text{C/W} * 13.78 \text{mW} + -55 \text{ } ^\circ\text{C} = -54.3 \text{ } ^\circ\text{C}$$

$$T_{j(+25C)} = 48.4 \text{ } ^\circ\text{C/W} * 13.78 \text{mW} + 25 \text{ } ^\circ\text{C} = +25.67 \text{ } ^\circ\text{C}$$

$$T_{j(+75C)} = 48.4 \text{ } ^\circ\text{C/W} * 13.78 \text{mW} + 75 \text{ } ^\circ\text{C} = +75.67 \text{ } ^\circ\text{C}$$

$$T_{j(+125C)} = 48.4 \text{ } ^\circ\text{C/W} * 13.78 \text{mW} + 125 \text{ } ^\circ\text{C} = +125.67 \text{ } ^\circ\text{C}$$

$$P_{D(4.0V)} = (5 \times 10^{-12} * 16 * 133 \times 10^6) + (16.8 \text{mA} (4.0V - 1.927V)) = 45.47 \text{mW}$$

$$T_{j(-55C)} = 48.4 \text{ } ^\circ\text{C/W} * 45.47 \text{mW} + -55 \text{ } ^\circ\text{C} = -52.8 \text{ } ^\circ\text{C}$$

$$T_{j(+25C)} = 48.4 \text{ } ^\circ\text{C/W} * 45.47 \text{mW} + 25 \text{ } ^\circ\text{C} = +27.2 \text{ } ^\circ\text{C}$$

$$T_{j(+75C)} = 48.4 \text{ } ^\circ\text{C/W} * 45.47 \text{mW} + 75 \text{ } ^\circ\text{C} = +77.2 \text{ } ^\circ\text{C}$$

$$T_{j(+125C)} = 48.4 \text{ } ^\circ\text{C/W} * 45.47 \text{mW} + 125 \text{ } ^\circ\text{C} = +127.2 \text{ } ^\circ\text{C}$$

110nm product P_D and T_j calculations:

$$P_D = (Cl * Vdd^2 * f) + \text{Max}(I_{oh} DC_{max} * (Vdd - V_{oh}), I_{ol} DC_{max} * V_{ol})$$

$$P_{D(2.5V)} = (5 \times 10^{-12} * 6.25 * 200 \times 10^6) + (15.2 \text{mA} (2.5V - 1.95V)) = 14.61 \text{mW}$$

$$T_{j(-55C)} = 48.4 \text{ } ^\circ\text{C/W} * 14.61 \text{mW} + -55 \text{ } ^\circ\text{C} = -54.3 \text{ } ^\circ\text{C}$$

$$T_{j(+25C)} = 48.4 \text{ } ^\circ\text{C/W} * 14.61 \text{mW} + 25 \text{ } ^\circ\text{C} = +25.7 \text{ } ^\circ\text{C}$$

$$T_{j(+75C)} = 48.4 \text{ } ^\circ\text{C/W} * 14.61 \text{mW} + 75 \text{ } ^\circ\text{C} = +75.7 \text{ } ^\circ\text{C}$$

$$T_{j(+125C)} = 48.4 \text{ } ^\circ\text{C/W} * 14.61 \text{mW} + 125 \text{ } ^\circ\text{C} = +125.7 \text{ } ^\circ\text{C}$$

$$P_{D(4.0V)} = (5 \times 10^{-12} * 16 * 200 \times 10^6) + (15.2 \text{mA} (4.0V - 1.95V)) = 41.16 \text{mW}$$

$$T_{j(-55C)} = 48.4 \text{ } ^\circ\text{C/W} * 41.16 \text{mW} + -55 \text{ } ^\circ\text{C} = -53.0 \text{ } ^\circ\text{C}$$

$$T_{j(+25C)} = 48.4 \text{ } ^\circ\text{C/W} * 41.16 \text{mW} + 25 \text{ } ^\circ\text{C} = +27.0 \text{ } ^\circ\text{C}$$

$$T_{j(+75C)} = 48.4^{\circ}\text{C/W} * 41.16\text{mW} + 75^{\circ}\text{C} = +77.0^{\circ}\text{C}$$

$$T_{j(+125C)} = 48.4^{\circ}\text{C/W} * 41.16\text{mW} + 125^{\circ}\text{C} = +127.0^{\circ}\text{C}$$

130nm product P_D and T_j calculations:

$$P_{D(2.5V)} = (5 \times 10^{-12} * 6.25 * 166 \times 10^6) + (15.2\text{mA}(2.5\text{V}-1.95\text{V})) = 13.55\text{mW}$$

$$T_{j(-55C)} = 48.4^{\circ}\text{C/W} * 13.55\text{mW} + -55^{\circ}\text{C} = -54.3^{\circ}\text{C}$$

$$T_{j(+25C)} = 48.4^{\circ}\text{C/W} * 13.55\text{mW} + 25^{\circ}\text{C} = +25.6^{\circ}\text{C}$$

$$T_{j(+75C)} = 48.4^{\circ}\text{C/W} * 13.55\text{mW} + 75^{\circ}\text{C} = +75.6^{\circ}\text{C}$$

$$T_{j(+125C)} = 48.4^{\circ}\text{C/W} * 13.55\text{mW} + 125^{\circ}\text{C} = +125.6^{\circ}\text{C}$$

$$P_{D(4.0V)} = (5 \times 10^{-12} * 16 * 166 \times 10^6) + (15.2\text{mA}(4.0\text{V}-1.95\text{V})) = 44.44\text{mW}$$

$$T_{j(-55C)} = 48.4^{\circ}\text{C/W} * 44.44\text{mW} + -55^{\circ}\text{C} = -52.8^{\circ}\text{C}$$

$$T_{j(+25C)} = 48.4^{\circ}\text{C/W} * 44.44\text{mW} + 25^{\circ}\text{C} = +27.2^{\circ}\text{C}$$

$$T_{j(+75C)} = 48.4^{\circ}\text{C/W} * 44.44\text{mW} + 75^{\circ}\text{C} = +75.2^{\circ}\text{C}$$

$$T_{j(+125C)} = 48.4^{\circ}\text{C/W} * 44.44\text{mW} + 125^{\circ}\text{C} = +125.2^{\circ}\text{C}$$

It is important to note that with these product technologies, the power dissipation is rather low as SDRAM is not considered to be a power device. Because of this, the junction temperature remains close to the ambient temperature and in this study, comparable stress conditions closely correlate to comparable junction temperatures across the product technologies. This is not the case with leading edge power processors where the power density is increasing exponentially and junction temperature is increasing ~1.45x with each new product generation.

4.6 Physical Failure Model

The soft errors and acceleration factors from each of the different temperature and voltage conditions were analyzed against existing competing and multiple mechanism physical failure models, e.g. Arrhenius, Inverse Power, Exponential. The models were described earlier in Equations 2.4-2.7 and are summarized again here. First, two multiple failure mechanism models were applied: Multiplication of AF's (temperature and voltage) using both Exponential and Power Law Models: $AF_1 = AF_T \cdot AF_V(e)$ (Eq. 4.4) and $AF_2 = AF_T \cdot AF_V(p)$ (Eq. 4.5) ; secondly, two competing failure mechanism models were applied: A weighted sum model of the AF's where $AF_3 = (AF_T + AF_V(e))/2$ (Eq. 4.6) and $AF_4 = (AF_T + AF_V(p))/2$ (Eq. 4.7). The data was analyzed and the model parameters were calculated for each of the models. The model equations are expanded as follows:

$$AF_1 = \frac{\lambda(T_2, V_2)}{\lambda(T_1, V_1)} = AF_T \cdot AF_V = \exp\left(\frac{E_a}{k} \left(\frac{1}{T_1} - \frac{1}{T_2}\right)\right) \exp(\gamma_1(V_2 - V_1)) \quad (4.4)$$

$$AF_2 = \frac{\lambda(T_2, V_2)}{\lambda(T_1, V_1)} = AF_T \cdot AF_V = \exp\left(\frac{E_a}{k} \left(\frac{1}{T_1} - \frac{1}{T_2}\right)\right) (V_2 / V_1)^k \quad (4.5)$$

$$AF_3 = \frac{\lambda(T_2, V_2)}{\lambda(T_1, V_1)} = (AF_T + AF_V) / 2 = \left(\exp\left(\frac{E_a}{k} \left(\frac{1}{T_1} - \frac{1}{T_2}\right)\right) + \exp(\gamma_1(V_2 - V_1))\right) / 2 \quad (4.6)$$

$$AF_4 = \frac{\lambda(T_2, V_2)}{\lambda(T_1, V_1)} = (AF_T + AF_V) / 2 = \left(\exp\left(\frac{E_a}{k} \left(\frac{1}{T_1} - \frac{1}{T_2}\right)\right) + (V_2 / V_1)^k\right) / 2 \quad (4.7)$$

The calculated E_a , γ , and k parameters are as follows:

$$E_a \text{ for 130nm} = 0.06$$

$$E_a \text{ for 110nm} = 0.05$$

$$E_a \text{ for 90nm} = 0.052$$

Applying the Power Law model for AFv, the derived k for each technology node is:

$$k \text{ for 130nm: } 0.84$$

$$k \text{ for 110nm: } 0.693$$

$$k \text{ for 90nm: } 0.637$$

Applying the Exponential model for AFv, the derived γ for each technology node is:

$$\gamma \text{ for 130nm: } 0.263$$

$$\gamma \text{ for 110nm: } 0.216$$

$$\gamma \text{ for 130nm: } 0.1997$$

The multiple failure mechanism acceleration model, refer to Equation 4.5 (product of AF's using the Power Law for AFv) best fits the DRAM retention time data and suggests a single temperature and voltage activated breakdown mechanism. The relative contribution of T and V on the system level FR is shown pictorially in Figures 33a-c. The thermal element is the main contributor to Tret breakdown degradation, the voltage element contributes to the thermally activated mechanism by slightly increasing the junction temperature.

As was discussed earlier, for current generation DRAM, the capacitance is typically 30-40fF/cell and although the external power supply V_{dd} is 2.5V for each part, internal on-chip voltage regulator circuitry subdivides this voltage as follows:

130nm Technology Parts:

- Peripheral Circuitry Voltage: 2.2V
- Memory Core Voltage: 1.8V

110nm Technology Parts:

- Peripheral Circuitry Voltage: 1.8V
- Memory Core Voltage: 1.4V

90nm Technology Parts:

- Peripheral Circuitry Voltage: 1.4V
- Memory Core Voltage: 1.0V

The memory cell capacitor dielectric material is Ta₂O₅. The gate oxide thickness for the larger peripheral circuitry transistors is approximately 7nm, and the gate oxide thickness for the nMOS memory cell transistors is approximately 4.2 nm.

Due to the over-voltage protection circuitry in each of the products, higher V_{dd} stress is not applied directly to the memory cores and this voltage is maintained at the specified amount. Therefore, the impact of higher V_{dd} stress corresponds to an increase in power dissipation for each of the products; these are summarized Section 5.5. There is no feasible method of bypassing the over-voltage protection at the product level for product level testing; however, it is

important to see the overall impact has on the overall product level power dissipation and contribution to the product, or system level FR.

The activation energies are very small for the early retention time breakdown errors, up to the 1,000 hour test measurement. As for the entire population of Tret breakdown, the activation energies are in the same range. Refer to Tables 13a and 13b. The slow degradation of Tret over time and the low activation energies suggest that hot carrier injection may be the intrinsic wearout mechanism at work.

The switching characteristics of a MOSFET can degrade and exhibit instabilities due to the charge that is injected into the gate oxide. The typical effect of hot carrier, or hot electron degradation, is an increase in the off-state current of a p-channel MOSFET, and a reduction in the on-state current of an n-channel MOSFET, e.g., those that comprise each memory cell. The rate of hot carrier degradation is directly related to the length of the channel, the oxide thickness, and the voltage of the device. A measure of transistor degradation or lifetime is commonly defined in terms of percentage shift of threshold voltage, change in transconductance, or variation in drive or saturation current [71]. These parameter shifts, however, were not confirmed in this experiment.

Gradual time-dependent dielectric breakdown of the DRAM stacked storage capacitor cell is another possible intrinsic wearout mechanism explanation. The stacked capacitor cell (STC) relies heavily on the quality and the storage capacity of the dielectric film between two heavily doped polysilicon electrodes. Silicon nitride (Si_3N_4) films have a high dielectric constant and are

known to contain many trap levels which may cause leakage current shifts. An increase in memory capacitor cell leakage current over time as a result of trapped charge, or lacking or inconsistent quality of the capacitor dielectric film, could explain the degradation in critical charge threshold levels.

4.7 DRAM Scaling and Defect Density

For DRAM, the product technology represents the half pitch of metal 1 (M1). See Figure 34 [107]. As the half pitch of M1 decreases with each technology generation, so does the physical transistor gate length (L_g). The gate length is driven by the necessity to improve transistor speed and is generally $\leq 0.5x$ the DRAM half pitch. With a 0.7x reduction each technology generation, a 0.5x linear scaling reduction is realized every two generations.

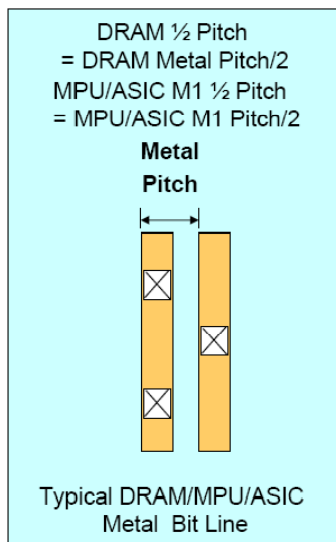


Figure 34. DRAM Metal Bit Line.

Table 14. DRAM Chip and Cell Characteristics.

DRAM Half Pitch Product Generation	130nm	110nm (1/2 node)	90nm	65nm
Physical Gate Length	65nm	50nm	37nm	25nm
Cell Area Factor (<i>a</i>)	8	8	6	6
Cell Area (CA = <i>a</i> ²) μm ²	0.130	0.90	.049	0.024
Cell Array Area (% of chip size)	71.3%	72%	72.6%	73.5%
Chip Size (mm ²)	390/2Gbits	312/2Gbits	287/4Gbits	568/16Gbits
Gbits/cm ²	0.55	0.90	1.49	3.03

The DRAM product technology scaling trend of M1 and the transistor gate length has historically been 0.7x/3 year cycle. However, since 2007, DRAM function size, function density, and chip size scaling rate have increased to a 2.5-year cycle with both geometric and equivalent scaling design enhancements. Table 14 shows chip and cell characteristics for 130nm to 65nm DRAMs [107].

If defects are randomly distributed over surface area, *A*, and a Poisson distribution is assumed given the random distribution of the first few time-to-fails, the defect density *D* (number of weak defective bits/cm²) can be calculated for each product generation, and extrapolated to the next generation, in this case 65nm.

The probability of *n* defects (*D*) in cell array area (*A*) is described as:

$$P = \frac{DA^n}{n!} * \exp[-DA] \quad (4.8)$$

and the probability of a cell array area without defects ($n=0$) is:

$$P = \exp[-DA] \quad (4.9)$$

The yield defect density is measured before stress is applied; defect density at $t = 0$. The reliability defect density is the latent defect density and is measured at some time $t > 0$. These defects may pass the manufacturer's internal screening and then fail in the field at a later time, $t > 0$, at some given stress level. Approximately 99.5% of the retention time failures of each product technology made up the main population with Weibull β slope ranging from 2.4 to 3.9, while the first approximately 0.5% retention failures were attributed to random defects. Figure 35 shows the percentage of manufacturing defects causing the early retention time bit failures for each stressed memory product at the 95% CL.

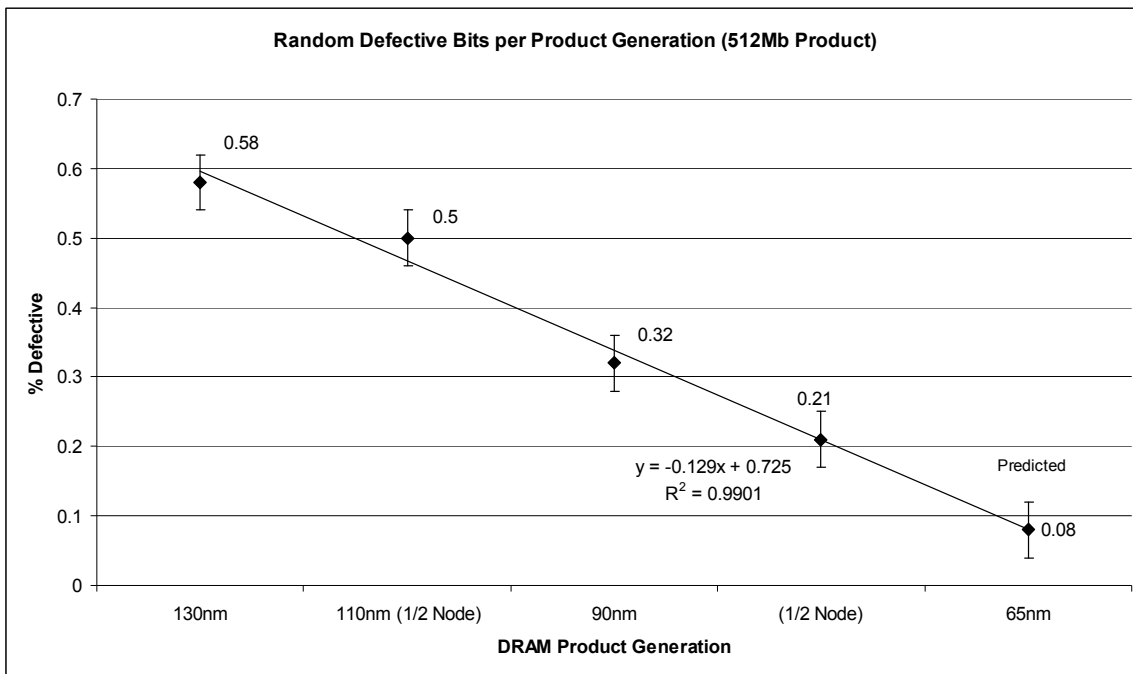


Figure 35. Random Defective Bits per Product Generation.

Observed 512Mb, 130nm product technology: 0.58% random defective bits

Observed 512Mb, 110nm product technology: 0.50% random defective bits

Observed 512Mb, 90nm product technology: 0.32% random defective bits

Predicted 512Mb, 65nm product technology: 0.08% random defective bits

Each smaller technology generation exhibited fewer random defects than the previous generation. Trend analysis predicts the next technology generation, 65nm, to exhibit 0.08% random defective bits assuming the trend continues. Given the option between a 512Mb 130nm product and a 512Mb 65nm product under equivalent stress conditions, the data suggests the 512Mb 65nm product will have fewer defects. This trend is likely to continue due to tighter process controls needed for smaller geometries, and the desire to maintain constant product level failure rates for ever increasing Gb size memory products.

In actuality, with each new product generation and a 2x bit factor for each progressive full node, the standard DRAM product size at the 65nm node is no longer 512 Mbits, but 8 Gbits. Given this trend, the random number of defective bits per cm^2 must also be considered.

By incorporating the defect rates for each representative technology and the cell characteristics in Table 14, the defect density per cm^2 of DRAM memory is calculated as follows:

130nm product generation: $DD = 3.19 \times 10^6$ bits/ cm^2 (0.55 Gb)

110nm product generation: $DD = 4.5 \times 10^6$ bits/ cm^2 (0.90 Gb)

90nm product generation: $DD = 4.768 \times 10^6$ bits/ cm^2 (1.49 Gb)

Using the predicted random defective bits with the cell characteristics of the 65nm DRAM, the defect density per Gbit of DRAM for the next product generation is:

Predicted 65nm product generation: $DD = 2.424 \times 10^6$ bits/cm² (3.03 Gb)

Note that while there is only a marginal increase in defect density per cm² per DRAM generation (130nm to 90nm), the number of Gbits of memory per cm² per DRAM generation is increasing significantly. The 65nm DRAM standard product contains 8 Gbits of memory. Therefore, normalizing the defect density to the standard products, the 512Mb 130nm standard product had 2.9696×10^6 weak bits and an 8 Gbit 65nm product is expected to have 6.5536×10^6 weak bits. A 16x increase in memory size from a 130nm 512Mb standard product to an 8 Gbit 65nm product, corresponds to a disproportional 2.2x increase in defective weak bits, a much better product in terms of proportion of weak bits.

4.8 Soft Error Failure Rate

The defect density and the soft error failure rate of the random bits must be considered in tandem to effectively assess the quality and the reliability of the scaled products. Data was normalized to FIT/Gb of memory and analyses of the soft error failure rate of the random bits are presented in Figure 36 and Table 15. The graph shows how the soft error failure rate of retention time behaves for scaled DRAM at multiple stress conditions. Curves were fit to the data which reveal a power relationship as a function of scaling for the higher stresses, $\geq 348\text{K}$ and 2.5V, or $\geq 298\text{K}$ and 4.0V; a linear relationship exists for lower stress levels across product generations, e.g., $\leq 298\text{K}$ and 2.5V, or $\leq 218\text{K}$ and 4.0V. The lowest failure rates across product generations is

observed at standard operating $V_{dd} = 2.5V$ and 218K. The linear and power functions showing the rate of change at each stress condition for each of the three scaled DRAMs and a prediction is extrapolated to the 65nm node.

Given the normalized curves, one can derive the expected soft error failure rate per Gb of memory from Figure 36 and Table 15.

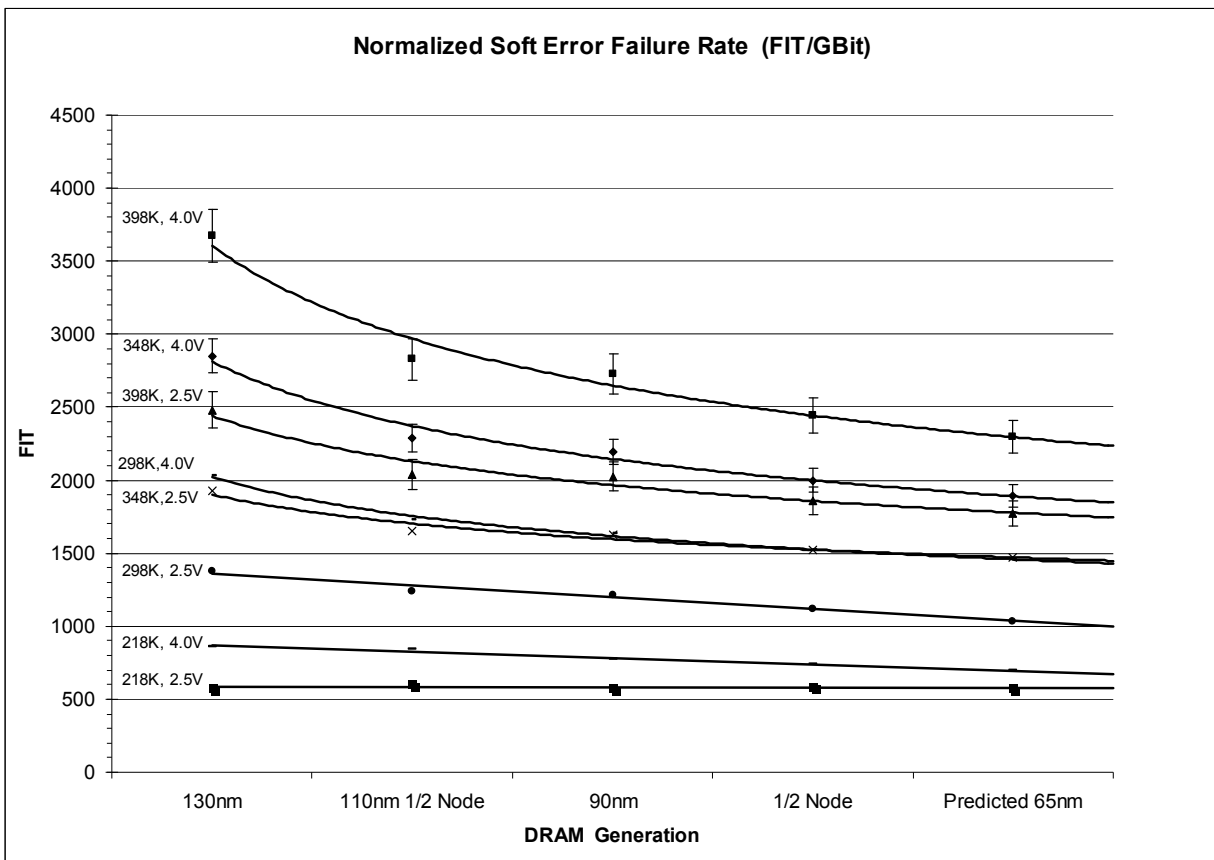


Figure 36. Normalized Soft Error Failure Rate for Scaled DRAM (FIT/Gb).

Table 15. Normalized Soft Error Failure Rate for Scaled DRAM (FIT/Gb).

Stress Condition	130nm	110nm 1/2 Node	90nm	1/2 Node	Predicted 65nm	Relation	Function	R ²
218K, 2.5V	579	605	574	581	579	Linear	y = -2.5x + 591	0.9456
298K, 2.5V	1373	1243	1213	1116	1036	Linear	y = -80x + 1436.3	0.8848
348K, 2.5V	1925	1649	1627	1526	1470	Pwr	y = 1902.6x ^{-0.1606}	0.9117
398K, 2.5V	2480	2037	2026	1860	1774	Pwr	y = 2439.1x ^{-0.1948}	0.8824
218K, 4.0V	858	840	773	739	696	Linear	y = -42.5x + 908.6	0.9003
298K, 4.0V	2034	1726	1635	1525	1458	Pwr	y = 2021.1x ^{-0.2029}	0.9824
348K, 4.0V	2852	2289	2192	1998	1892	Pwr	y = 2815.3x ^{-0.2479}	0.9526
398K, 4.0V	3674	2828	2729	2442	2297	Pwr	y = 3609.1x ^{-0.2822}	0.9321

A generalized model of the scaling effect relationship on the SER of scaled DRAM product may be expressed as a power function:

$$y = 121.79 d (x^{0.5693}) \tag{4.10}$$

where d is the density factor (product density in Gb) and x is the technology node. Reference Figure 37.

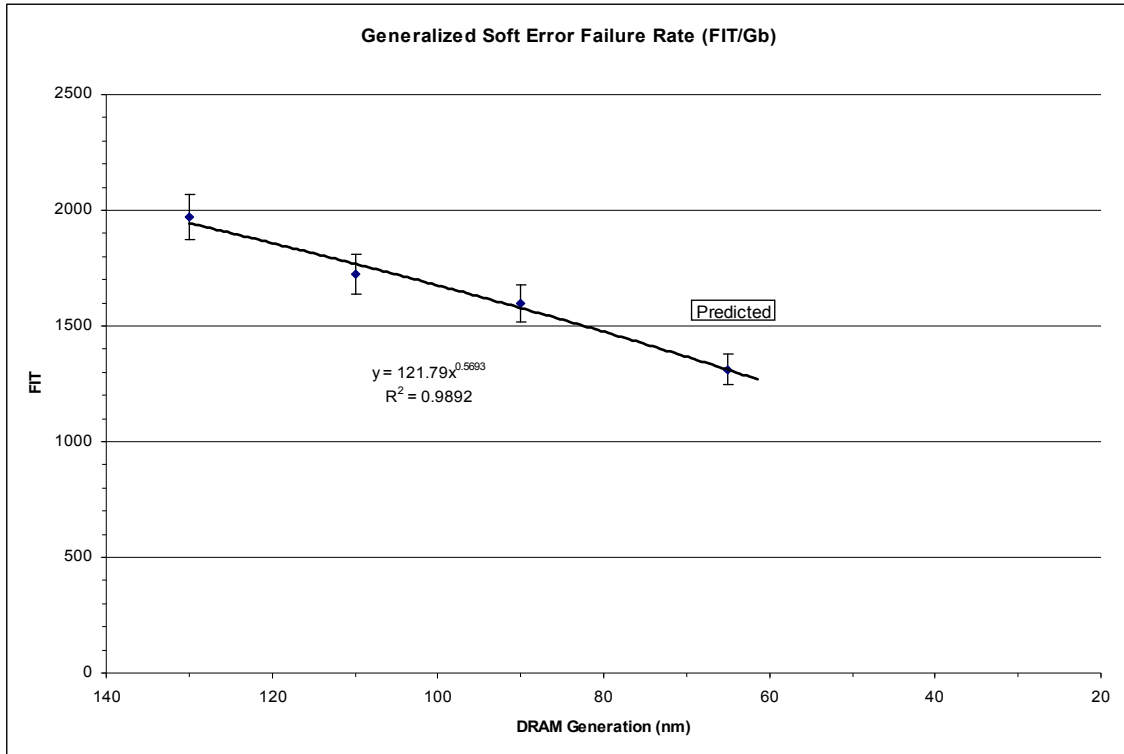


Figure 37. Generalized Soft Error Failure Rate Model for Scaled DRAM (FIT/Gb).

Data was also normalized to FIT/cm² and analyses of the soft error failure rate of the random bits are presented in Figure 38 and Table 16. The graph shows how the soft error failure rate of retention time behaves for scaled DRAM at multiple stress conditions per area of memory in cm². Curves were fit to the data with a power function.

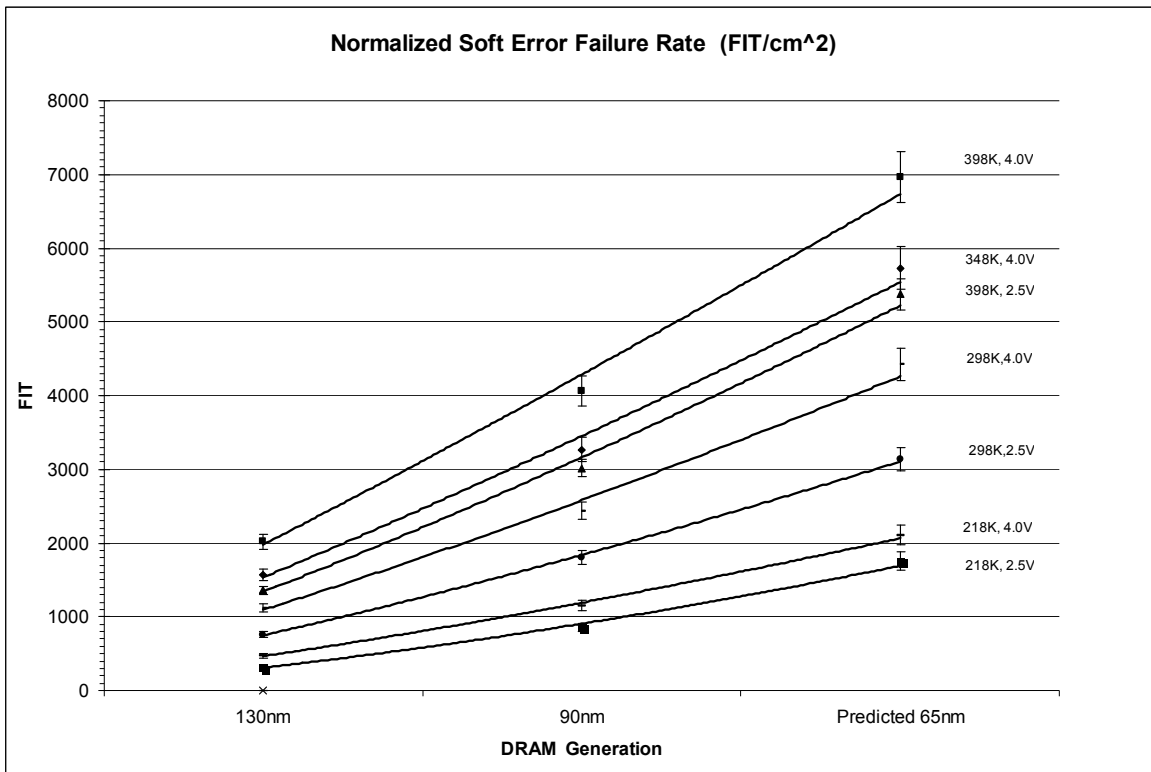


Figure 38. Normalized Soft Error Failure Rate for Scaled DRAM (FIT/cm²).

Table 16. Normalized Soft Error Failure Rate for Scaled DRAM (FIT/cm²).

Stress Condition	130nm	90nm	Predicted 65nm	Relation	Function	R ²
218K, 2.5V	318	855	1753	Pwr	$y = 311.77x^{1.5388}$	0.9965
298K, 2.5V	755	1807	3140	Pwr	$y = 750.37x^{1.2931}$	0.9996
398K, 2.5V	1364	3019	5375	Pwr	$y = 1341x^{1.2373}$	0.9966
218K, 4.0V	472	1152	2109	Pwr	$y = 465.98x^{1.3548}$	0.9984
298K, 4.0V	1119	2436	4418	Pwr	$y = 1095.2x^{1.2365}$	0.9946
348K, 4.0V	1569	3266	5733	Pwr	$y = 1537.1x^{1.1666}$	0.9945
398K, 4.0V	2021	4066	6960	Pwr	$y = 1981.7x^{1.1131}$	0.9944

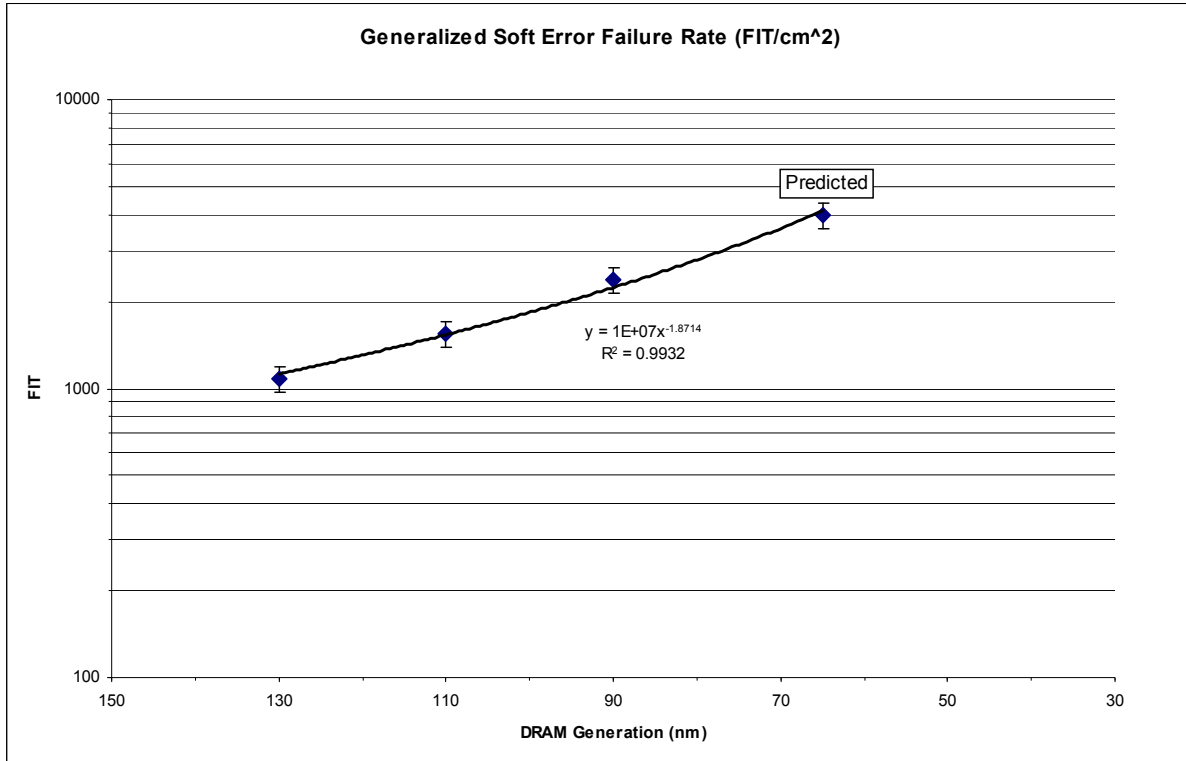


Figure 39. Generalized Soft Error Failure Rate Model for Scaled DRAM (FIT/cm²).

A generalized model of the scaling effect relationship on the SER of scaled DRAM in FIT/cm² may be expressed as a power function:

$$y = 1E+07x^{-1.8714} \quad (4.11)$$

where x is the technology node. Reference Figure 39.

The SER FIT/cm² is increasing at a greater rate per generation than the FIT/Gb. For each full node generation, e.g., 130nm to 90nm, where the density doubles as the area per transistor is reduced by S^2 (50% if $S = 0.707$), Figure 38 confirms that there is an approximate doubling of FIT/cm². As scaling progresses further, however, e.g., real world scaling as opposed to ideal scaling, gate voltages are scaled more slowly (approximately 0.85x/generation) than gate oxide

thickness in order to maintain transistor saturation currents and signal speed. In general, the ITRS roadmap shows the density progression for each successive technology and should be considered in future generation projections.

The reliability (FIT/Gb) and quality (DD) of the DRAM parts with respect to retention time characteristics is improving with each technology generation under equivalent stress conditions. The observed difference in soft error failure rate, however, is more pronounced at higher stress conditions. The normalized SER (FIT/cm²) is increasing with each progressive generation, therefore, the SER FIT for the product, or system has to take this into account, e.g. the density factor in Eq. 5.10. The user should consider these trends in the selection of a scaled DRAM product for a given application and the anticipated operating conditions. Increases in operating frequency, power dissipation, and junction temperature will each have a detrimental effect in determining the product reliability for a given application. The user must also consider the impact of SER on the increasing product density with each newer generation.

Chapter 5: Conclusion

5.1 Background

A description of the historical and modern approaches in assessing and predicting microelectronics reliability, including the motivation for further investigation into this important field of study, particularly for high reliability applications such as NASA spacecraft avionics is provided. A synopsis of microelectronics derating and reliability modeling and simulation is presented. CMOS technology scaling has an impact on circuit performance, power, circuit design, burn-in and long term reliability in modern day microelectronics; these effects and trends on microelectronics reliability are discussed. In addition, the Physics-of-Failure methodology, competing mechanism theory, common intrinsic failure mechanisms and statistical models, and the multiple failure mechanism model, are discussed and different approaches to calculate acceleration factors are summarized.

5.2 Conclusion

A design of experiments and an accelerated stress test on scaled commercial SDRAMs was performed. The goal of the SDRAM experiment was to investigate failure mechanism induced degradation at the product level, and determine if long term performance is random (constant rate process) or degrades over time (increasing failure rate). Additionally, characterization of product sensitivities to temperature and voltage at the product level across different scaled technologies was conducted.

Technology and construction analysis, device characterization, and data analysis led to a degradation and predictive model, reliability assessment and defect density calculations of three current SDRAM technologies for different stress conditions. Product, or system level soft error rates for data retention were calculated, and an AF test matrix with the acceleration factors for different combinations of temperature and voltage stresses is proposed. A methodology to determine the density of random defects per cm^2 of DRAM memory, and a forecast for the next technology generation of scaled DRAM is included. This technique may be applied to other scaled microelectronic devices and key parameters.

Retention time margin of several product generations is measured using a Q-ratio of the time-to-first-failure distribution (t_I) to the maximum specified refresh time, (t_M). This ratio provides insight into the tolerance of each technology generation to degradation with respect to voltage and temperature stresses. The ratio also provides a quality factor demonstrating the amount of margin between actual soft breakdown of a memory cell, and the manufacturer's specified refresh time.

A direct comparison of the data retention characteristics across three DRAM product technologies reveals that a recoverable soft error breakdown occurs with each memory cell, and that memory retention time gradually degrades over time. Two distinct populations are evident with data retention breakdown; the main population soft error rate of each product generation follows a Weibull distribution with a β slope ≥ 2.4 , while early failures are randomly distributed with a β slope ~ 1.0 . Data retention breakdown is accelerated by both temperature and voltage stresses as is shown in Chapter 4. The study shows that up to 0.58% of the 130nm memory cells

in the scaled DRAM products studied are statistically random defective bits, and that the percentage of random defective bits decreases to 0.32% for the 90nm memory cells. A prediction is made for the number of random defective bits for the 65nm technology node given the ever tighter process controls needed for nanometer scaled semiconductors and memory products. By incorporating the defect rates for each representative technology with the cell characteristics, the defect density per cm^2 of DRAM memory ranges from 3.19×10^6 bits/ cm^2 for the 130nm product technology, to 4.768×10^6 bits/ cm^2 for the 90nm product technology. A defect density prediction is made for the next generation 65nm technology node.

Early soft errors and acceleration factors from each of the different temperature and voltage conditions were analyzed against existing competing and multiple mechanism physical failure models. The multiple failure mechanism AF model using the Power Law for AFv best fits the DRAM retention time data and suggests a single temperature and voltage activated breakdown mechanism.

Data was normalized to FIT/Gb and FIT/ cm^2 for the soft error rates to compare technology generations, and a generalized model of the scaling effect relationship was developed. It was shown that the reliability in FIT/Gb and quality (defect density) of the DRAM parts with respect to retention time characteristics is improving with each technology generation under equivalent stress conditions. The observed difference in soft error failure rate, however, is more pronounced at higher stress conditions. The normalized SER (FIT/ cm^2) is increasing with each progressive generation, therefore, the SER FIT for the product, or system must be considered. The user must balance this knowledge with the anticipated application operating conditions.

Increases in operating frequency, power dissipation, and junction temperature will each have a detrimental effect in determining the product reliability for a given application.

The data and the derived acceleration and derating factors demonstrate that a combination of temperature and voltage stresses are better for screening out and/or qualification of scaled DRAM products for defects that may lead to premature failure in the application.

A summary of the nonlinear regression analysis for the SDRAM study is included in Appendix A.

The DRAM experimental results are particularly important for several reasons:

- 1) For the same density memory chip and equivalent stress conditions, the product or system reliability should increase for each successive technology generation as manufacturers strive to maintain product FIT rates for higher density memories. The DRAM results support this trend.
- 2) NASA and the aerospace industry have historically used temperature only as a stress driver to screen and qualify parts. This data supports that a combination of temperature and voltage stresses better accelerates both thermally and voltage driven mechanisms that could impact long term parts reliability. This method also better identifies the weak memory cells that lead to early breakdown.

- 3) A temperature and voltage stress test matrix approach shows the expected acceleration factor or derating factor for different temperature and voltage stress combinations on the data retention soft error rate for 130nm, 110nm and 90nm SDRAM product technologies. A similar screening and/or qualification approach may be adapted for other parts and newer product generations. The user should use caution and test the specific product family, technology, and manufacturer to determine accurate acceleration and derating factors at different stress combinations, especially for critical applications. Differences in over-voltage protection schemes, device layout, design, and other factors can impact the level of voltage stress actually applied deep inside the core of the chip circuitry. In many cases, discrete level testing is desirable and preferred to determine accurate voltage acceleration factors for the core circuitry, as these may be different than those observed at the product level.
- 4) Results show that early failures are dominated by CFR, Beta = 1, for each technology in the study.
- 5) Results show that the reliability is improving and failure rate (FIT/Gb) is decreasing with each new technology under equivalent stress conditions.
- 6) Results show that for the same size memory, e.g. 512Mb, the quality (defect density) is improving with each new technology generation. Therefore, the 90nm products exhibit better retention time characteristics and fewer defects/cm² than the larger 110nm and 130nm technologies.

- 7) Results show that the normalized soft error rate (FIT/cm²) is increasing with each new technology generations.

5.3 Future Work

Ongoing research, accelerated stress testing, and modeling of scaling effects on microelectronics reliability continues throughout the industry. Newer product technologies, including 65nm, 45nm, and 32nm need to be studied to determine if developments in materials, design, layout, and processing will inherently affect the reliability of next generation microelectronics. The evaluation methodology described herein, however, may be applied to other product technologies.

Appendix A

Nonlinear Regression: 90nm, 298.15K, 2.5V

```
[Variables]
x = col(2)
y = col(3)
reciprocal_y = 1/abs(y)
reciprocal_ysquare = 1/y^2
'Automatic Initial Parameter Estimate Functions
xnear0(q) = max(abs(q))-abs(q)
yatxnear0(q,r) = xatymax(q,xnear0(r))
[Parameters]
a = yatxnear0(y,x) "Auto {{previous: 8.55057}}
b = if(x50(x,y)-min(x)=0, 1, -ln(.5)/(x50(x,y)-min(x))) "Auto {{previous: 8.3314e-005}}
[Equation]
f = a*exp(-b*x)
fit f to y
"fit f to y with weight reciprocal_y
"fit f to y with weight reciprocal_ysquare
[Constraints]
b>0
[Options]
tolerance=0.0001
stepsize=100
iterations=100
```

R = 0.96296200 Rsqr = 0.92729580 Adj Rsqr = 0.91921756

Standard Error of Estimate = 0.0667

	Coefficient	Std. Error	t	P
a	8.5506	0.0383	223.3188	<0.0001
b	0.0001	0.0000	10.7438	<0.0001

Analysis of Variance:

	DF	SS	MS	F	P
Regression	1	0.5105	0.5105	114.7893	<0.0001
Residual	9	0.0400	0.0044		
Total	10	0.5506	0.0551		

PRESS = 0.0689

Durbin-Watson Statistic = 0.3805

Normality Test: K-S Statistic = 0.1884 Significance Level = 0.7865

Constant Variance Test: Passed (P = 0.7755)

Power of performed test with alpha = 0.0500: 0.9999

Regression Diagnostics:

Row	Predicted	Residual	Std. Res.	Stud. Res.	Stud. Del. Res.
4	8.5505	0.0845	1.2671	1.5474	1.7029
5	8.4796	0.0504	0.7553	0.8663	0.8531
6	8.4093	0.0007	0.0109	0.0120	0.0113
7	8.3395	-0.0395	-0.5923	-0.6334	-0.6110
8	8.2703	-0.0603	-0.9044	-0.9526	-0.9472
9	8.2017	-0.0717	-1.0750	-1.1276	-1.1472
10	8.1336	-0.0536	-0.8044	-0.8486	-0.8342
11	8.0662	-0.0562	-0.8422	-0.9024	-0.8921
12	7.9992	-0.0092	-0.1386	-0.1524	-0.1439
13	7.9329	0.0471	0.7066	0.8067	0.7896
14	7.8671	0.1080	1.6201	1.9459	2.4105

Influence Diagnostics:

Row	Cook'sDist	Leverage	DFFITS
4	0.5884	0.3295	1.1938
5	0.1184	0.2399	0.4793
6	0.0000	0.1722	0.0051
7	0.0288	0.1255	-0.2314
8	0.0497	0.0987	-0.3135
9	0.0637	0.0910	-0.3631
10	0.0407	0.1015	-0.2803
11	0.0604	0.1291	-0.3435
12	0.0024	0.1731	-0.0658
13	0.0986	0.2326	0.4347
14	0.8382	0.3069	1.6039

95% Confidence:

Row	Predicted	Regr. 5%	Regr. 95%	Pop. 5%	Pop. 95%
4	8.5505	8.4639	8.6371	8.3765	8.7245
5	8.4796	8.4057	8.5535	8.3116	8.6476
6	8.4093	8.3467	8.4719	8.2459	8.5726
7	8.3395	8.2861	8.3929	8.1795	8.4996
8	8.2703	8.2229	8.3177	8.1122	8.4285
9	8.2017	8.1562	8.2472	8.0441	8.3593
10	8.1336	8.0856	8.1817	7.9753	8.2920
11	8.0662	8.0120	8.1204	7.9059	8.2265
12	7.9992	7.9365	8.0620	7.8358	8.1626
13	7.9329	7.8601	8.0056	7.7654	8.1004
14	7.8671	7.7835	7.9506	7.6946	8.0395

Nonlinear Regression: 90nm, 348.15K, 2.5V

```
[Variables]
x = col(6)
y = col(7)
reciprocal_y = 1/abs(y)
reciprocal_ysquare = 1/y^2
'Automatic Initial Parameter Estimate Functions
xnear0(q) = max(abs(q))-abs(q)
yatxnear0(q,r) = xatymax(q,xnear0(r))
[Parameters]
a = yatxnear0(y,x) "Auto {{previous: 7.17615}}
b = if(x50(x,y)-min(x)=0, 1, -ln(.5)/(x50(x,y)-min(x))) "Auto {{previous: 0.000135366}}
[Equation]
f = a*exp(-b*x)
fit f to y
"fit f to y with weight reciprocal_y
"fit f to y with weight reciprocal_ysquare
[Constraints]
b>0
[Options]
tolerance=0.0001
stepsize=100
iterations=100
```

R = 0.99126396 Rsqr = 0.98260423 Adj Rsqr = 0.98067137

Standard Error of Estimate = 0.0422

	Coefficient	Std. Error	t	P
a	7.1762	0.0245	292.7811	<0.0001
b	0.0001	0.0000	22.5331	<0.0001

Analysis of Variance:

	DF	SS	MS	F	P
Regression	1	0.9069	0.9069	508.3672	<0.0001
Residual	9	0.0161	0.0018		
Total	10	0.9229	0.0923		

PRESS = 0.0236

Durbin-Watson Statistic = 1.2438

Normality Test: K-S Statistic = 0.1407 Significance Level = 0.9710

Constant Variance Test: Passed (P = 0.1987)

Power of performed test with alpha = 0.0500: 1.0000

Regression Diagnostics:

Row	Predicted	Residual	Std. Res.	Stud. Res.	Stud. Del. Res.
4	7.1761	-0.0214	-0.5056	-0.6208	-0.5982
5	7.0797	0.0203	0.4815	0.5530	0.5305
6	6.9845	-0.0045	-0.1060	-0.1165	-0.1099
7	6.8906	0.0194	0.4601	0.4917	0.4699
8	6.7979	0.0321	0.7595	0.7997	0.7823
9	6.7065	0.0435	1.0295	1.0799	1.0913
10	6.6163	-0.0663	-1.5709	-1.6581	-1.8759
11	6.5274	-0.0574	-1.3588	-1.4569	-1.5714
12	6.4396	-0.0296	-0.7014	-0.7714	-0.7526
13	6.3530	0.0070	0.1647	0.1878	0.1774
14	6.2676	0.0570	1.3490	1.6122	1.8024

Influence Diagnostics:

Row	Cook'sDist	Leverage	DFFITs
4	0.0978	0.3367	-0.4262
5	0.0488	0.2420	0.2997
6	0.0014	0.1718	-0.0500
7	0.0172	0.1244	0.1771
8	0.0348	0.0980	0.2579
9	0.0585	0.0912	0.3458
10	0.1569	0.1024	-0.6338
11	0.1589	0.1302	-0.6080
12	0.0623	0.1732	-0.3445
13	0.0053	0.2302	0.0970
14	0.5566	0.2998	1.1795

95% Confidence:

Row	Predicted	Regr. 5%	Regr. 95%	Pop. 5%	Pop. 95%
4	7.1761	7.1206	7.2315	7.0656	7.2865
5	7.0797	7.0327	7.1267	6.9732	7.1861
6	6.9845	6.9449	7.0241	6.8811	7.0879
7	6.8906	6.8569	6.9243	6.7893	6.9919
8	6.7979	6.7680	6.8278	6.6978	6.8980
9	6.7065	6.6777	6.7354	6.6067	6.8063
10	6.6163	6.5858	6.6469	6.5160	6.7167
11	6.5274	6.4929	6.5619	6.4258	6.6290
12	6.4396	6.3999	6.4794	6.3361	6.5431
13	6.3530	6.3072	6.3989	6.2471	6.4590
14	6.2676	6.2153	6.3199	6.1587	6.3766

Nonlinear Regression: 90nm, 398.15K, 2.5V

```
[Variables]
x = col(10)
y = col(11)
reciprocal_y = 1/abs(y)
reciprocal_ysquare = 1/y^2
'Automatic Initial Parameter Estimate Functions
xnear0(q) = max(abs(q))-abs(q)
yatxnear0(q,r) = xatymax(q,xnear0(r))
[Parameters]
a = yatxnear0(y,x) "Auto {{previous: 6.16959}}
b = if(x50(x,y)-min(x)=0, 1, -ln(.5)/(x50(x,y)-min(x))) "Auto {{previous: 0.00016254}}
[Equation]
f = a*exp(-b*x)
fit f to y
"fit f to y with weight reciprocal_y
```

"fit f to y with weight reciprocal_square

[Constraints]

b>0

[Options]

tolerance=0.0001

stepsize=100

iterations=100

R = 0.98318715 Rsqr = 0.96665697 Adj Rsqr = 0.96295219

Standard Error of Estimate = 0.0599

	Coefficient	Std. Error	t	P
a	6.1696	0.0349	176.6067	<0.0001
b	0.0002	0.0000	16.1867	<0.0001

Analysis of Variance:

	DF	SS	MS	F	P
Regression	1	0.9351	0.9351	260.9215	<0.0001
Residual	9	0.0323	0.0036		
Total	10	0.9674	0.0967		

PRESS = 0.0510

Durbin-Watson Statistic = 0.6007

Normality Test: K-S Statistic = 0.1920 Significance Level = 0.7668

Constant Variance Test: Passed (P = 0.6731)

Power of performed test with alpha = 0.0500: 1.0000

Regression Diagnostics:

Row	Predicted	Residual	Std. Res.	Stud. Res.	Stud. Del. Res.
4	6.1695	0.0454	0.7586	0.9340	0.9267
5	6.0701	0.0799	1.3344	1.5337	1.6824
6	5.9723	0.0177	0.2965	0.3257	0.3089
7	5.8760	-0.0760	-1.2689	-1.3556	-1.4326
8	5.7812	-0.0712	-1.1898	-1.2525	-1.2996
9	5.6880	-0.0380	-0.6351	-0.6662	-0.6442
10	5.5963	-0.0463	-0.7736	-0.8168	-0.8003
11	5.5061	-0.0361	-0.6028	-0.6465	-0.6242
12	5.4173	0.0027	0.0449	0.0494	0.0465
13	5.3300	0.0500	0.8357	0.9516	0.9461
14	5.2440	0.0725	1.2104	1.4428	1.5515

Influence Diagnostics:

Row	Cook'sDist	Leverage	DFBETS
4	0.2251	0.3404	0.6657
5	0.3776	0.2430	0.9534
6	0.0110	0.1715	0.1406
7	0.1298	0.1238	-0.5385
8	0.0849	0.0977	-0.4277
9	0.0223	0.0914	-0.2043
10	0.0383	0.1030	-0.2712
11	0.0315	0.1308	-0.2422
12	0.0003	0.1733	0.0213
13	0.1344	0.2289	0.5154
14	0.4380	0.2962	1.0065

95% Confidence:

Row	Predicted	Regr. 5%	Regr. 95%	Pop. 5%	Pop. 95%
4	6.1695	6.0905	6.2485	6.0127	6.3263
5	6.0701	6.0034	6.1369	5.9191	6.2211
6	5.9723	5.9162	6.0283	5.8257	6.1188
7	5.8760	5.8283	5.9236	5.7324	6.0195
8	5.7812	5.7389	5.8236	5.6393	5.9231
9	5.6880	5.6471	5.7290	5.5465	5.8295
10	5.5963	5.5529	5.6398	5.4541	5.7385
11	5.5061	5.4571	5.5551	5.3621	5.6501

12	5.4173	5.3609	5.4737	5.2706	5.5640
13	5.3300	5.2652	5.3948	5.1798	5.4801
14	5.2440	5.1703	5.3177	5.0899	5.3982

Nonlinear Regression: 90nm, 298.15K, 4.05V

```
[Variables]
x = col(2)
y = col(3)
reciprocal_y = 1/abs(y)
reciprocal_ysquare = 1/y^2
'Automatic Initial Parameter Estimate Functions
xnear0(q) = max(abs(q))-abs(q)
yatxnear0(q,r) = xatymax(q,xnear0(r))
[Parameters]
a = yatxnear0(y,x) "Auto {{previous: 6.85286}}
b = if(x50(x,y)-min(x)=0, 1, -ln(.5)/(x50(x,y)-min(x))) "Auto {{previous: 9.11558e-005}}
[Equation]
f = a*exp(-b*x)
fit f to y
"fit f to y with weight reciprocal_y
"fit f to y with weight reciprocal_ysquare
[Constraints]
b>0
[Options]
tolerance=0.0001
stepsize=100
iterations=100
```

R = 0.98384944 Rsqr = 0.96795972 Adj Rsqr = 0.96439969

Standard Error of Estimate = 0.0379

	Coefficient	Std. Error	t	P
a	6.8529	0.0218	314.5287	<0.0001
b	0.0001	0.0000	16.5178	<0.0001

Analysis of Variance:

	DF	SS	MS	F	P
Regression	1	0.3903	0.3903	271.8964	<0.0001
Residual	9	0.0129	0.0014		
Total	10	0.4033	0.0403		

PRESS = 0.0228

Durbin-Watson Statistic = 0.4847

Normality Test: K-S Statistic = 0.2474 Significance Level = 0.4524

Constant Variance Test: Passed (P = 0.2569)

Power of performed test with alpha = 0.0500: 1.0000

Regression Diagnostics:

Row	Predicted	Residual	Std. Res.	Stud. Res.	Stud. Del. Res.
4	6.8529	0.0613	1.6189	1.9788	2.4822
5	6.7907	0.0293	0.7740	0.8879	0.8764
6	6.7291	-0.0191	-0.5029	-0.5527	-0.5302
7	6.6680	-0.0380	-1.0028	-1.0722	-1.0823
8	6.6075	-0.0275	-0.7255	-0.7641	-0.7450
9	6.5475	-0.0375	-0.9905	-1.0390	-1.0442
10	6.4881	-0.0281	-0.7421	-0.7829	-0.7646
11	6.4292	-0.0192	-0.5079	-0.5443	-0.5218
12	6.3709	0.0091	0.2401	0.2640	0.2499
13	6.3131	0.0169	0.4462	0.5093	0.4872
14	6.2558	0.0529	1.3960	1.6755	1.9043

Influence Diagnostics:

Row	Cook'sDist	Leverage	DFBETS
4	0.9672	0.3307	1.7446
5	0.1246	0.2402	0.4928
6	0.0318	0.1721	-0.2418
7	0.0823	0.1253	-0.4096
8	0.0319	0.0986	-0.2464
9	0.0541	0.0911	-0.3305
10	0.0347	0.1016	-0.2571
11	0.0220	0.1293	-0.2010
12	0.0073	0.1731	0.1143
13	0.0392	0.2323	0.2680
14	0.6183	0.3058	1.2639

95% Confidence:

Row	Predicted	Regr. 5%	Regr. 95%	Pop. 5%	Pop. 95%
4	6.8529	6.8036	6.9021	6.7540	6.9517
5	6.7907	6.7487	6.8327	6.6952	6.8861
6	6.7291	6.6935	6.7646	6.6363	6.8219
7	6.6680	6.6377	6.6983	6.5771	6.7589
8	6.6075	6.5806	6.6344	6.5176	6.6973
9	6.5475	6.5217	6.5734	6.4580	6.6371
10	6.4881	6.4608	6.5154	6.3982	6.5781
11	6.4292	6.3984	6.4601	6.3382	6.5203
12	6.3709	6.3352	6.4066	6.2781	6.4637
13	6.3131	6.2718	6.3544	6.2179	6.4082
14	6.2558	6.2084	6.3032	6.1579	6.3538

Nonlinear Regression: 90nm, 348.15K, 4.05V

[Variables]

x = col(6)

y = col(7)

reciprocal_y = 1/abs(y)

reciprocal_ysquare = 1/y^2

'Automatic Initial Parameter Estimate Functions

xnear0(q) = max(abs(q))-abs(q)

yatxnear0(q,r) = xatymax(q,xnear0(r))

[Parameters]

a = yatxnear0(y,x) "Auto {{previous: 5.49431}}

b = if(x50(x,y)-min(x)=0, 1, -ln(.5)/(x50(x,y)-min(x))) "Auto {{previous: 7.28894e-005}}

[Equation]

f = a*exp(-b*x)

fit f to y

"fit f to y with weight reciprocal_y

"fit f to y with weight reciprocal_ysquare

[Constraints]

b>0

[Options]

tolerance=0.0001

stepsize=100

iterations=100

R = 0.98239160 Rsqr = 0.96509326 Adj Rsqr = 0.96121474

Standard Error of Estimate = 0.0257

	Coefficient	Std. Error	t	P
a	5.4943	0.0147	373.8763	<0.0001
b	0.0001	0.0000	15.7850	<0.0001

Analysis of Variance:

	DF	SS	MS	F	P
Regression	1	0.1638	0.1638	248.8299	<0.0001
Residual	9	0.0059	0.0007		
Total	10	0.1697	0.0170		

PRESS = 0.0099

Durbin-Watson Statistic = 0.8447

Normality Test: K-S Statistic = 0.1741 Significance Level = 0.8587

Constant Variance Test: Passed (P = 0.2096)

Power of performed test with alpha = 0.0500: 1.0000

Regression Diagnostics:

Row	Predicted	Residual	Std. Res.	Stud. Res.	Stud. Del. Res.
4	5.4943	0.0457	1.7808	2.1726	2.9703
5	5.4544	0.0056	0.2178	0.2497	0.2363
6	5.4148	-0.0248	-0.9667	-1.0625	-1.0712
7	5.3755	-0.0255	-0.9930	-1.0620	-1.0706
8	5.3364	-0.0264	-1.0305	-1.0855	-1.0979
9	5.2977	-0.0177	-0.6892	-0.7229	-0.7022
10	5.2592	0.0008	0.0309	0.0326	0.0308
11	5.2210	0.0090	0.3504	0.3754	0.3567
12	5.1831	0.0369	1.4386	1.5819	1.7553
13	5.1455	0.0045	0.1773	0.2024	0.1913
14	5.1081	-0.0081	-0.3151	-0.3789	-0.3601

Influence Diagnostics:

Row	Cook'sDist	Leverage	DFBETS
4	1.1526	0.3281	2.0758
5	0.0098	0.2395	0.1326
6	0.1175	0.1723	-0.4887
7	0.0811	0.1257	-0.4059
8	0.0647	0.0989	-0.3637
9	0.0262	0.0910	-0.2222
10	0.0001	0.1013	0.0103
11	0.0104	0.1289	0.1372
12	0.2619	0.1731	0.8030
13	0.0062	0.2331	0.1054
14	0.0320	0.3083	-0.2404

95% Confidence:

Row	Predicted	Regr. 5%	Regr. 95%	Pop. 5%	Pop. 95%
4	5.4943	5.4611	5.5276	5.4274	5.5612
5	5.4544	5.4260	5.4828	5.3898	5.5190
6	5.4148	5.3907	5.4389	5.3520	5.4776
7	5.3755	5.3549	5.3961	5.3139	5.4370
8	5.3364	5.3182	5.3547	5.2756	5.3973
9	5.2977	5.2802	5.3152	5.2371	5.3583
10	5.2592	5.2407	5.2777	5.1983	5.3201
11	5.2210	5.2002	5.2418	5.1594	5.2827
12	5.1831	5.1590	5.2072	5.1202	5.2460
13	5.1455	5.1174	5.1735	5.0810	5.2099
14	5.1081	5.0759	5.1403	5.0417	5.1745

Nonlinear Regression: 90nm, 398.15K, 4.05V

[Variables]

x = col(10)

y = col(11)

reciprocal_y = 1/abs(y)

reciprocal_ysquare = 1/y^2

'Automatic Initial Parameter Estimate Functions

xnear0(q) = max(abs(q))-abs(q)

yatxnear0(q,r) = xatymax(q,xnear0(r))

[Parameters]

a = yatxnear0(y,x) "Auto {{previous: 4.86817}}

b = if(x50(x,y)-min(x)=0, 1, -ln(.5)/(x50(x,y)-min(x))) "Auto {{previous: 0.000156699}}

[Equation]

f = a*exp(-b*x)

fit f to y

"fit f to y with weight reciprocal_y

"fit f to y with weight reciprocal_ysquare

[Constraints]
 b>0
 [Options]
 tolerance=0.0001
 stepsize=100
 iterations=100

R = 0.98191836 Rsqr = 0.96416367 Adj Rsqr = 0.96018186

Standard Error of Estimate = 0.0474

	Coefficient	Std. Error	t	P
a	4.8682	0.0276	176.1274	<0.0001
b	0.0002	0.0000	15.5904	<0.0001

Analysis of Variance:

	DF	SS	MS	F	P
Regression	1	0.5446	0.5446	242.1418	<0.0001
Residual	9	0.0202	0.0022		
Total	10	0.5649	0.0565		

PRESS = 0.0381

Durbin-Watson Statistic = 0.8096

Normality Test: K-S Statistic = 0.2390 Significance Level = 0.4974

Constant Variance Test: Passed (P = 0.3241)

Power of performed test with alpha = 0.0500: 1.0000

Regression Diagnostics:

Row	Predicted	Residual	Std. Res.	Stud. Res.	Stud. Del. Res.
4	4.8682	0.1018	2.1472	2.6424	5.2617
5	4.7925	-0.0025	-0.0522	-0.0600	-0.0566
6	4.7180	-0.0380	-0.8005	-0.8795	-0.8673
7	4.6446	-0.0446	-0.9407	-1.0050	-1.0056
8	4.5724	-0.0624	-1.3157	-1.3852	-1.4723
9	4.5013	-0.0113	-0.2384	-0.2501	-0.2366
10	4.4313	-0.0013	-0.0279	-0.0294	-0.0277
11	4.3624	-0.0024	-0.0511	-0.0548	-0.0517
12	4.2946	-0.0046	-0.0969	-0.1066	-0.1006
13	4.2278	0.0222	0.4676	0.5325	0.5102
14	4.1621	0.0435	0.9174	1.0941	1.1078

Influence Diagnostics:

Row	Cook's Dist	Leverage	DFFITS
4	1.7959	0.3397	3.7738
5	0.0006	0.2428	-0.0321
6	0.0801	0.1716	-0.3947
7	0.0714	0.1239	-0.3782
8	0.1040	0.0978	-0.4847
9	0.0031	0.0914	-0.0750
10	0.0000	0.1029	-0.0094
11	0.0002	0.1307	-0.0200
12	0.0012	0.1733	-0.0460
13	0.0421	0.2291	0.2781
14	0.2528	0.2970	0.7200

95% Confidence:

Row	Predicted	Regr. 5%	Regr. 95%	Pop. 5%	Pop. 95%
4	4.8682	4.8056	4.9307	4.7440	4.9923
5	4.7925	4.7396	4.8453	4.6729	4.9121
6	4.7180	4.6735	4.7624	4.6018	4.8341
7	4.6446	4.6068	4.6824	4.5309	4.7583
8	4.5724	4.5389	4.6059	4.4600	4.6848
9	4.5013	4.4689	4.5337	4.3892	4.6134
10	4.4313	4.3969	4.4657	4.3187	4.5440
11	4.3624	4.3236	4.4012	4.2483	4.4765
12	4.2946	4.2499	4.3393	4.1784	4.4108

13	4.2278	4.1765	4.2792	4.1089	4.3468
14	4.1621	4.1036	4.2206	4.0399	4.2843

Nonlinear Regression: 110nm, 298.15K, 2.5V

```
[Variables]
x = col(2)
y = col(3)
reciprocal_y = 1/abs(y)
reciprocal_ysquare = 1/y^2
'Automatic Initial Parameter Estimate Functions
xnear0(q) = max(abs(q))-abs(q)
yatxnear0(q,r) = xatymax(q,xnear0(r))
[Parameters]
a = yatxnear0(y,x) "Auto {{previous: 8.31352}}
b = if(x50(x,y)-min(x)=0, 1, -ln(.5)/(x50(x,y)-min(x))) "Auto {{previous: 8.16831e-005}}
[Equation]
f = a*exp(-b*x)
fit f to y
"fit f to y with weight reciprocal_y
"fit f to y with weight reciprocal_ysquare
[Constraints]
b>0
[Options]
tolerance=0.0001
stepsize=100
iterations=100
```

R = 0.99297544 Rsqr = 0.98600023 Adj Rsqr = 0.98444470

Standard Error of Estimate = 0.0271

	Coefficient	Std. Error	t	P
a	8.3135	0.0156	533.9676	<0.0001
b	0.0001	0.0000	25.1983	<0.0001

Analysis of Variance:

	DF	SS	MS	F	P
Regression	1	0.4665	0.4665	633.8679	<0.0001
Residual	9	0.0066	0.0007		
Total	10	0.4731	0.0473		

PRESS = 0.0117

Durbin-Watson Statistic = 0.5723

Normality Test: K-S Statistic = 0.1620 Significance Level = 0.9102

Constant Variance Test: Passed (P = 0.7965)

Power of performed test with alpha = 0.0500: 1.0000

Regression Diagnostics:

Row	Predicted	Residual	Std. Res.	Stud. Res.	Stud. Del. Res.
4	8.3135	0.0291	1.0720	1.3090	1.3716
5	8.2459	0.0141	0.5202	0.5966	0.5740
6	8.1788	0.0112	0.4126	0.4535	0.4325
7	8.1123	-0.0123	-0.4524	-0.4837	-0.4621
8	8.0463	-0.0263	-0.9686	-1.0203	-1.0230
9	7.9808	-0.0208	-0.7675	-0.8050	-0.7879
10	7.9159	-0.0259	-0.9546	-1.0070	-1.0079
11	7.8515	-0.0215	-0.7925	-0.8492	-0.8348
12	7.7876	-0.0076	-0.2812	-0.3092	-0.2931
13	7.7243	0.0057	0.2110	0.2409	0.2278
14	7.6614	0.0544	2.0038	2.4072	3.8029

Influence Diagnostics:

Row	Cook'sDist	Leverage	DFFITs
4	0.4207	0.3294	0.9612
5	0.0562	0.2398	0.3224
6	0.0214	0.1722	0.1973
7	0.0168	0.1255	-0.1751
8	0.0570	0.0988	-0.3386
9	0.0324	0.0910	-0.2493
10	0.0572	0.1014	-0.3386
11	0.0534	0.1291	-0.3214
12	0.0100	0.1731	-0.1341
13	0.0088	0.2327	0.1255
14	1.2840	0.3071	2.5316

95% Confidence:

Row	Predicted	Regr. 5%	Regr. 95%	Pop. 5%	Pop. 95%
4	8.3135	8.2783	8.3487	8.2428	8.3843
5	8.2459	8.2158	8.2759	8.1776	8.3142
6	8.1788	8.1533	8.2043	8.1124	8.2453
7	8.1123	8.0905	8.1340	8.0472	8.1774
8	8.0463	8.0270	8.0656	7.9819	8.1106
9	7.9808	7.9623	7.9993	7.9167	8.0449
10	7.9159	7.8964	7.9354	7.8515	7.9803
11	7.8515	7.8295	7.8735	7.7863	7.9167
12	7.7876	7.7621	7.8132	7.7212	7.8541
13	7.7243	7.6947	7.7539	7.6561	7.7924
14	7.6614	7.6274	7.6954	7.5913	7.7316

Nonlinear Regression: 110nm, 348.15K, 2.5V

[Variables]

x = col(6)

y = col(7)

reciprocal_y = 1/abs(y)

reciprocal_ysquare = 1/y^2

'Automatic Initial Parameter Estimate Functions

xnear0(q) = max(abs(q))-abs(q)

yatxnear0(q,r) = xatymax(q,xnear0(r))

[Parameters]

a = yatxnear0(y,x) "Auto {{previous: 6.84254}}

b = if(x50(x,y)-min(x)=0, 1, -ln(.5)/(x50(x,y)-min(x))) "Auto {{previous: 0.000120308}}

[Equation]

f = a*exp(-b*x)

fit f to y

"fit f to y with weight reciprocal_y

"fit f to y with weight reciprocal_ysquare

[Constraints]

b>0

[Options]

tolerance=0.0001

stepsize=100

iterations=100

R = 0.95758184 Rsqr = 0.91696299 Adj Rsqr = 0.90773665

Standard Error of Estimate = 0.0812

	Coefficient	Std. Error	t	P
a	6.8425	0.0470	145.6813	<0.0001
b	0.0001	0.0000	10.0099	<0.0001

Analysis of Variance:

	DF	SS	MS	F	P
Regression	1	0.6552	0.6552	99.3854	<0.0001
Residual	9	0.0593	0.0066		
Total	10	0.7145	0.0714		

PRESS = 0.1004

Durbin-Watson Statistic = 0.3621

Normality Test: K-S Statistic = 0.1456 Significance Level = 0.9606

Constant Variance Test: Passed (P = 0.8601)

Power of performed test with alpha = 0.0500: 0.9997

Regression Diagnostics:

Row	Predicted	Residual	Std. Res.	Stud. Res.	Stud. Del. Res.
4	6.8425	0.1219	1.5009	1.8400	2.1965
5	6.7607	0.0493	0.6070	0.6970	0.6756
6	6.6799	0.0001	0.0017	0.0018	0.0017
7	6.6000	-0.0600	-0.7388	-0.7896	-0.7717
8	6.5211	-0.1011	-1.2447	-1.3107	-1.3738
9	6.4431	-0.0831	-1.0232	-1.0733	-1.0836
10	6.3660	-0.0760	-0.9363	-0.9882	-0.9867
11	6.2899	-0.0299	-0.3682	-0.3947	-0.3754
12	6.2147	0.0153	0.1888	0.2076	0.1962
13	6.1404	0.0596	0.7346	0.8377	0.8225
14	6.0669	0.1043	1.2843	1.5371	1.6875

Influence Diagnostics:

Row	Cook'sDist	Leverage	DFBETS
4	0.8515	0.3347	1.5578
5	0.0773	0.2414	0.3811
6	0.0000	0.1719	0.0008
7	0.0444	0.1247	-0.2912
8	0.0936	0.0982	-0.4534
9	0.0578	0.0912	-0.3432
10	0.0555	0.1022	-0.3328
11	0.0116	0.1299	-0.1450
12	0.0045	0.1732	0.0898
13	0.1053	0.2309	0.4506
14	0.5108	0.3019	1.1096

95% Confidence:

Row	Predicted	Regr. 5%	Regr. 95%	Pop. 5%	Pop. 95%
4	6.8425	6.7363	6.9488	6.6304	7.0547
5	6.7607	6.6705	6.8510	6.5561	6.9654
6	6.6799	6.6037	6.7560	6.4810	6.8787
7	6.6000	6.5351	6.6648	6.4052	6.7948
8	6.5211	6.4635	6.5786	6.3286	6.7135
9	6.4431	6.3876	6.4985	6.2512	6.6349
10	6.3660	6.3073	6.4247	6.1732	6.5588
11	6.2899	6.2237	6.3561	6.0947	6.4851
12	6.2147	6.1382	6.2911	6.0157	6.4136
13	6.1404	6.0521	6.2286	5.9366	6.3441
14	6.0669	5.9660	6.1678	5.8574	6.2765

Nonlinear Regression: 110nm, 398.15K, 2.5V

[Variables]

x = col(10)

y = col(11)

reciprocal_y = 1/abs(y)

reciprocal_ysquare = 1/y^2

'Automatic Initial Parameter Estimate Functions

xnear0(q) = max(abs(q))-abs(q)

yatxnear0(q,r) = xatymax(q,xnear0(r))

[Parameters]

a = yatxnear0(y,x) "Auto {{previous: 6.03454}}

b = if(x50(x,y)-min(x)=0, 1, -ln(.5)/(x50(x,y)-min(x))) "Auto {{previous: 0.000153988}}

[Equation]

f = a*exp(-b*x)

fit f to y

"fit f to y with weight reciprocal_y

"fit f to y with weight reciprocal_ysquare

[Constraints]
 b>0
 [Options]
 tolerance=0.0001
 stepsize=100
 iterations=100

R = 0.99286227 Rsqr = 0.98577550 Adj Rsqr = 0.98419500

Standard Error of Estimate = 0.0361

	Coefficient	Std. Error	t	P
a	6.0345	0.0210	286.8718	<0.0001
b	0.0002	0.0000	24.9744	<0.0001

Analysis of Variance:

	DF	SS	MS	F	P
Regression	1	0.8134	0.8134	623.7110	<0.0001
Residual	9	0.0117	0.0013		
Total	10	0.8252	0.0825		

PRESS = 0.0194

Durbin-Watson Statistic = 1.2077

Normality Test: K-S Statistic = 0.1836 Significance Level = 0.8119

Constant Variance Test: Passed (P = 0.7755)

Power of performed test with alpha = 0.0500: 1.0000

Regression Diagnostics:

Row	Predicted	Residual	Std. Res.	Stud. Res.	Stud. Del. Res.
4	6.0345	0.0488	1.3502	1.6611	1.8807
5	5.9423	-0.0123	-0.3414	-0.3923	-0.3730
6	5.8515	-0.0315	-0.8729	-0.9591	-0.9543
7	5.7621	-0.0121	-0.3353	-0.3582	-0.3402
8	5.6741	0.0259	0.7184	0.7563	0.7368
9	5.5874	0.0226	0.6271	0.6579	0.6357
10	5.5020	-0.0520	-1.4392	-1.5194	-1.6614
11	5.4179	-0.0379	-1.0495	-1.1256	-1.1448
12	5.3351	-0.0151	-0.4184	-0.4601	-0.4390
13	5.2536	0.0164	0.4546	0.5178	0.4956
14	5.1733	0.0474	1.3124	1.5656	1.7304

Influence Diagnostics:

Row	Cook's Dist	Leverage	DFFITS
4	0.7085	0.3393	1.3477
5	0.0247	0.2427	-0.2112
6	0.0953	0.1716	-0.4344
7	0.0091	0.1240	-0.1280
8	0.0310	0.0978	0.2426
9	0.0218	0.0913	0.2016
10	0.1323	0.1028	-0.5624
11	0.0952	0.1306	-0.4438
12	0.0222	0.1733	-0.2010
13	0.0399	0.2293	0.2703
14	0.5186	0.2973	1.1256

95% Confidence:

Row	Predicted	Regr. 5%	Regr. 95%	Pop. 5%	Pop. 95%
4	6.0345	5.9870	6.0821	5.9400	6.1291
5	5.9423	5.9021	5.9826	5.8513	6.0334
6	5.8515	5.8177	5.8854	5.7631	5.9399
7	5.7621	5.7333	5.7909	5.6755	5.8487
8	5.6741	5.6485	5.6996	5.5885	5.7597
9	5.5874	5.5627	5.6120	5.5020	5.6727
10	5.5020	5.4758	5.5282	5.4162	5.5878
11	5.4179	5.3884	5.4474	5.3310	5.5048
12	5.3351	5.3011	5.3691	5.2466	5.4236

13	5.2536	5.2145	5.2927	5.1630	5.3442
14	5.1733	5.1288	5.2179	5.0803	5.2664

Nonlinear Regression: 110nm, 298.15K, 4.05V

```
[Variables]
x = col(2)
y = col(3)
reciprocal_y = 1/abs(y)
reciprocal_ysquare = 1/y^2
'Automatic Initial Parameter Estimate Functions
xnear0(q) = max(abs(q))-abs(q)
yatxnear0(q,r) = xatymax(q,xnear0(r))
[Parameters]
a = yatxnear0(y,x) "Auto {{previous: 6.61935}}
b = if(x50(x,y)-min(x)=0, 1, -ln(.5)/(x50(x,y)-min(x))) "Auto {{previous: 9.73741e-005}}
[Equation]
f = a*exp(-b*x)
fit f to y
"fit f to y with weight reciprocal_y
"fit f to y with weight reciprocal_ysquare
[Constraints]
b>0
[Options]
tolerance=0.0001
stepsize=100
iterations=100
```

R = 0.99404435 Rsqr = 0.98812417 Adj Rsqr = 0.98680463

Standard Error of Estimate = 0.0235

	Coefficient	Std. Error	t	P
a	6.6194	0.0135	489.0502	<0.0001
b	0.0001	0.0000	27.3844	<0.0001

Analysis of Variance:

	DF	SS	MS	F	P
Regression	1	0.4138	0.4138	748.8418	<0.0001
Residual	9	0.0050	0.0006		
Total	10	0.4188	0.0419		

PRESS = 0.0081

Durbin-Watson Statistic = 0.6441

Normality Test: K-S Statistic = 0.1696 Significance Level = 0.8791

Constant Variance Test: Passed (P = 0.2209)

Power of performed test with alpha = 0.0500: 1.0000

Regression Diagnostics:

Row	Predicted	Residual	Std. Res.	Stud. Res.	Stud. Del. Res.
4	6.6194	0.0192	0.8188	1.0015	1.0017
5	6.5552	0.0248	1.0546	1.2101	1.2468
6	6.4917	-0.0017	-0.0718	-0.0789	-0.0744
7	6.4288	-0.0188	-0.7990	-0.8542	-0.8401
8	6.3665	-0.0065	-0.2759	-0.2906	-0.2753
9	6.3048	-0.0148	-0.6293	-0.6601	-0.6380
10	6.2437	-0.0237	-1.0081	-1.0637	-1.0725
11	6.1832	-0.0332	-1.4122	-1.5135	-1.6526
12	6.1233	-0.0033	-0.1396	-0.1535	-0.1449
13	6.0639	0.0261	1.1083	1.2647	1.3149
14	6.0052	0.0319	1.3576	1.6285	1.8281

Influence Diagnostics:

Row	Cook'sDist	Leverage	DFFITS
------------	-------------------	-----------------	---------------

4	0.2487	0.3315	0.7054
5	0.2318	0.2405	0.7015
6	0.0006	0.1721	-0.0339
7	0.0522	0.1252	-0.3178
8	0.0046	0.0985	-0.0910
9	0.0218	0.0911	-0.2020
10	0.0641	0.1017	-0.3609
11	0.1702	0.1294	-0.6371
12	0.0025	0.1731	-0.0663
13	0.2415	0.2320	0.7226
14	0.5818	0.3050	1.2109

95% Confidence:

Row	Predicted	Regr. 5%	Regr. 95%	Pop. 5%	Pop. 95%
4	6.6194	6.5887	6.6500	6.5580	6.6807
5	6.5552	6.5291	6.5813	6.4960	6.6144
6	6.4917	6.4696	6.5137	6.4341	6.5493
7	6.4288	6.4100	6.4476	6.3724	6.4852
8	6.3665	6.3498	6.3832	6.3107	6.4222
9	6.3048	6.2887	6.3208	6.2492	6.3603
10	6.2437	6.2267	6.2607	6.1879	6.2995
11	6.1832	6.1641	6.2023	6.1267	6.2397
12	6.1233	6.1012	6.1454	6.0657	6.1809
13	6.0639	6.0383	6.0896	6.0049	6.1230
14	6.0052	5.9758	6.0346	5.9444	6.0659

Nonlinear Regression: 110nm, 348.15K, 4.05V

```
[Variables]
x = col(6)
y = col(7)
reciprocal_y = 1/abs(y)
reciprocal_ysquare = 1/y^2
'Automatic Initial Parameter Estimate Functions
xnear0(q) = max(abs(q))-abs(q)
yatxnear0(q,r) = xatymax(q,xnear0(r))
[Parameters]
a = yatxnear0(y,x) "Auto {{previous: 5.53632}}
b = if(x50(x,y)-min(x)=0, 1, -ln(.5)/(x50(x,y)-min(x))) "Auto {{previous: 0.000132161}}
[Equation]
f = a*exp(-b*x)
fit f to y
"fit f to y with weight reciprocal_y
"fit f to y with weight reciprocal_ysquare
[Constraints]
b>0
[Options]
tolerance=0.0001
stepsize=100
iterations=100
```

R = 0.98683279 Rsqr = 0.97383896 Adj Rsqr = 0.97093217

Standard Error of Estimate = 0.0393

	Coefficient	Std. Error	t	P
a	5.5363	0.0228	242.6812	<0.0001
b	0.0001	0.0000	18.2529	<0.0001

Analysis of Variance:

	DF	SS	MS	F	P
Regression	1	0.5185	0.5185	335.0230	<0.0001
Residual	9	0.0139	0.0015		
Total	10	0.5324	0.0532		

PRESS = 0.0206

Durbin-Watson Statistic = 1.0134

Normality Test: K-S Statistic = 0.1706 Significance Level = 0.8749

Constant Variance Test: Passed (P = 0.0762)

Power of performed test with alpha = 0.0500: 1.0000

Regression Diagnostics:

Row	Predicted	Residual	Std. Res.	Stud. Res.	Stud. Del. Res.
4	5.5363	0.0056	0.1418	0.1740	0.1644
5	5.4636	-0.0336	-0.8550	-0.9819	-0.9797
6	5.3919	-0.0119	-0.3026	-0.3325	-0.3154
7	5.3211	-0.0211	-0.5366	-0.5735	-0.5509
8	5.2513	0.0087	0.2224	0.2342	0.2215
9	5.1823	0.0177	0.4498	0.4718	0.4504
10	5.1143	0.0557	1.4167	1.4953	1.6262
11	5.0471	0.0729	1.8525	1.9863	2.4989
12	4.9809	-0.0209	-0.5302	-0.5831	-0.5604
13	4.9155	-0.0255	-0.6472	-0.7378	-0.7176
14	4.8509	-0.0478	-1.2160	-1.4537	-1.5668

Influence Diagnostics:

Row	Cook'sDist	Leverage	DFBETS
4	0.0077	0.3363	0.1170
5	0.1538	0.2418	-0.5533
6	0.0115	0.1718	-0.1436
7	0.0234	0.1244	-0.2077
8	0.0030	0.0981	0.0730
9	0.0112	0.0912	0.1427
10	0.1275	0.1024	0.5492
11	0.2952	0.1302	0.9666
12	0.0356	0.1732	-0.2565
13	0.0814	0.2303	-0.3926
14	0.4534	0.3003	-1.0263

95% Confidence:

Row	Predicted	Regr. 5%	Regr. 95%	Pop. 5%	Pop. 95%
4	5.5363	5.4847	5.5879	5.4334	5.6392
5	5.4636	5.4199	5.5074	5.3645	5.5628
6	5.3919	5.3550	5.4288	5.2956	5.4882
7	5.3211	5.2897	5.3525	5.2267	5.4155
8	5.2513	5.2234	5.2791	5.1580	5.3445
9	5.1823	5.1554	5.2092	5.0893	5.2753
10	5.1143	5.0858	5.1427	5.0208	5.2077
11	5.0471	5.0150	5.0792	4.9525	5.1417
12	4.9809	4.9438	5.0179	4.8845	5.0773
13	4.9155	4.8728	4.9582	4.8168	5.0142
14	4.8509	4.8022	4.8997	4.7494	4.9524

Nonlinear Regression: 110nm, 398.15K, 4.05V

```
[Variables]
x = col(10)
y = col(11)
reciprocal_y = 1/abs(y)
reciprocal_ysquare = 1/y^2
'Automatic Initial Parameter Estimate Functions
xnear0(q) = max(abs(q))-abs(q)
yatxnear0(q,r) = xatymax(q,xnear0(r))
[Parameters]
a = yatxnear0(y,x) "Auto {{previous: 4.80363}}
b = if(x50(x,y)-min(x)=0, 1, -ln(.5)/(x50(x,y)-min(x))) "Auto {{{previous: 0.000163859}}}
[Equation]
f = a*exp(-b*x)
fit f to y
"fit f to y with weight reciprocal_y
"fit f to y with weight reciprocal_ysquare
[Constraints]
b>0
[Options]
```

tolerance=0.0001
 stepsize=100
 iterations=100

R = 0.99731150 Rsqr = 0.99463023 Adj Rsqr = 0.99403359

Standard Error of Estimate = 0.0186

	Coefficient	Std. Error	t	P
a	4.8036	0.0109	441.6168	<0.0001
b	0.0002	0.0000	40.7878	<0.0001

Analysis of Variance:

	DF	SS	MS	F	P
Regression	1	0.5790	0.5790	1667.0493	<0.0001
Residual	9	0.0031	0.0003		
Total	10	0.5821	0.0582		

PRESS = 0.0057

Durbin-Watson Statistic = 1.4607

Normality Test: K-S Statistic = 0.2475 Significance Level = 0.4523

Constant Variance Test: Passed (P = 0.0883)

Power of performed test with alpha = 0.0500: 1.0000

Regression Diagnostics:

Row	Predicted	Residual	Std. Res.	Stud. Res.	Stud. Del. Res.
4	4.8036	0.0372	1.9942	2.4560	4.0320
5	4.7256	-0.0156	-0.8352	-0.9599	-0.9553
6	4.6488	-0.0188	-1.0068	-1.1061	-1.1219
7	4.5732	-0.0132	-0.7088	-0.7572	-0.7378
8	4.4989	-0.0089	-0.4767	-0.5019	-0.4799
9	4.4258	-0.0058	-0.3094	-0.3246	-0.3079
10	4.3538	0.0162	0.8672	0.9157	0.9066
11	4.2831	0.0169	0.9080	0.9740	0.9709
12	4.2135	-0.0135	-0.7226	-0.7948	-0.7771
13	4.1450	-0.0050	-0.2677	-0.3048	-0.2889
14	4.0776	0.0105	0.5622	0.6700	0.6481

Influence Diagnostics:

Row	Cook'sDist	Leverage	DFBETTS
4	1.5582	0.3407	2.8982
5	0.1480	0.2431	-0.5413
6	0.1266	0.1715	-0.5104
7	0.0405	0.1237	-0.2773
8	0.0136	0.0977	-0.1579
9	0.0053	0.0914	-0.0976
10	0.0482	0.1030	0.3072
11	0.0714	0.1308	0.3767
12	0.0662	0.1733	-0.3557
13	0.0138	0.2288	-0.1573
14	0.0944	0.2960	0.4202

95% Confidence:

Row	Predicted	Regr. 5%	Regr. 95%	Pop. 5%	Pop. 95%
4	4.8036	4.7790	4.8282	4.7548	4.8524
5	4.7256	4.7048	4.7463	4.6786	4.7726
6	4.6488	4.6313	4.6662	4.6031	4.6944
7	4.5732	4.5584	4.5880	4.5285	4.6179
8	4.4989	4.4857	4.5121	4.4547	4.5431
9	4.4258	4.4130	4.4385	4.3817	4.4698
10	4.3538	4.3403	4.3674	4.3096	4.3981
11	4.2831	4.2678	4.2983	4.2382	4.3279
12	4.2135	4.1959	4.2310	4.1678	4.2591
13	4.1450	4.1248	4.1652	4.0983	4.1917
14	4.0776	4.0547	4.1006	4.0296	4.1256

Nonlinear Regression: 130nm, 298.15K, 2.5V

```
[Variables]
x = col(2)
y = col(3)
reciprocal_y = 1/abs(y)
reciprocal_ysquare = 1/y^2
'Automatic Initial Parameter Estimate Functions
xnear0(q) = max(abs(q))-abs(q)
yatxnear0(q,r) = xatymax(q,xnear0(r))
[Parameters]
a = yatxnear0(y,x) "Auto {{previous: 8.34415}}
b = if(x50(x,y)-min(x)=0, 1, -ln(.5)/(x50(x,y)-min(x))) "Auto {{previous: 0.000192898}}
[Equation]
f = a*exp(-b*x)
fit f to y
"fit f to y with weight reciprocal_y
"fit f to y with weight reciprocal_ysquare
[Constraints]
b>0
[Options]
tolerance=0.0001
stepsize=100
iterations=100
```

R = 0.97546068 Rsqr = 0.95152354 Adj Rsqr = 0.94613727

Standard Error of Estimate = 0.1159

	Coefficient	Std. Error	t	P
a	8.3441	0.0681	122.6069	<0.0001
b	0.0002	0.0000	13.2135	<0.0001

Analysis of Variance:

	DF	SS	MS	F	P
Regression	1	2.3740	2.3740	176.6571	<0.0001
Residual	9	0.1209	0.0134		
Total	10	2.4950	0.2495		

PRESS = 0.1766

Durbin-Watson Statistic = 0.8093

Normality Test: K-S Statistic = 0.0966 Significance Level = 0.9999

Constant Variance Test: Passed (P = 0.9676)

Power of performed test with alpha = 0.0500: 1.0000

Regression Diagnostics:

Row	Predicted	Residual	Std. Res.	Stud. Res.	Stud. Del. Res.
4	8.3441	-0.1048	-0.9044	-1.1172	-1.1350
5	8.1847	-0.0647	-0.5584	-0.6423	-0.6199
6	8.0284	-0.0184	-0.1584	-0.1740	-0.1643
7	7.8750	0.0550	0.4746	0.5068	0.4848
8	7.7245	0.1155	0.9961	1.0484	1.0550
9	7.5770	0.1830	1.5790	1.6567	1.8735
10	7.4322	0.0878	0.7574	0.8000	0.7826
11	7.2902	0.0098	0.0845	0.0907	0.0855
12	7.1509	-0.1909	-1.6470	-1.8114	-2.1424
13	7.0143	-0.1023	-0.8825	-1.0040	-1.0045
14	6.8803	0.0289	0.2493	0.2963	0.2807

Influence Diagnostics:

Row	Cook'sDist	Leverage	DFFITs
4	0.3282	0.3447	-0.8231
5	0.0666	0.2442	-0.3523

6	0.0031	0.1712	-0.0747
7	0.0180	0.1231	0.1817
8	0.0593	0.0974	0.3465
9	0.1384	0.0916	0.5949
10	0.0370	0.1036	0.2661
11	0.0006	0.1315	0.0333
12	0.3439	0.1733	-0.9809
13	0.1483	0.2274	-0.5449
14	0.0181	0.2921	0.1803

95% Confidence:

Row	Predicted	Regr. 5%	Regr. 95%	Pop. 5%	Pop. 95%
4	8.3441	8.1902	8.4981	8.0401	8.6482
5	8.1847	8.0551	8.3143	7.8922	8.4772
6	8.0284	7.9198	8.1369	7.7446	8.3122
7	7.8750	7.7830	7.9670	7.5971	8.1529
8	7.7245	7.6427	7.8064	7.4498	7.9992
9	7.5770	7.4976	7.6563	7.3030	7.8509
10	7.4322	7.3478	7.5166	7.1567	7.7077
11	7.2902	7.1951	7.3853	7.0113	7.5692
12	7.1509	7.0418	7.2601	6.8669	7.4350
13	7.0143	6.8893	7.1394	6.7238	7.3048
14	6.8803	6.7386	7.0220	6.5822	7.1784

Nonlinear Regression: 130nm, 348.15K, 2.5V

[Variables]

x = col(6)

y = col(7)

reciprocal_y = 1/abs(y)

reciprocal_ysquare = 1/y^2

'Automatic Initial Parameter Estimate Functions

xnear0(q) = max(abs(q))-abs(q)

yatxnear0(q,r) = xatymax(q,xnear0(r))

[Parameters]

a = yatxnear0(y,x) "Auto {{previous: 6.74299}}

b = if(x50(x,y)-min(x)=0, 1, -ln(.5)/(x50(x,y)-min(x))) "Auto {{previous: 0.000307091}}

[Equation]

f = a*exp(-b*x)

fit f to y

"fit f to y with weight reciprocal_y

"fit f to y with weight reciprocal_ysquare

[Constraints]

b>0

[Options]

tolerance=0.0001

stepsize=100

iterations=100

R = 0.98137920 Rsqr = 0.96310513 Adj Rsqr = 0.95900570

Standard Error of Estimate = 0.1210

	Coefficient	Std. Error	t	P
a	6.7430	0.0726	92.8213	<0.0001
b	0.0003	0.0000	15.3632	<0.0001

Analysis of Variance:

	DF	SS	MS	F	P
Regression	1	3.4393	3.4393	234.9363	<0.0001
Residual	9	0.1318	0.0146		
Total	10	3.5711	0.3571		

PRESS = 0.2217

Durbin-Watson Statistic = 0.4790

Normality Test: K-S Statistic = 0.1130 Significance Level = 0.9979

Constant Variance Test: Passed (P = 0.6531)

Power of performed test with alpha = 0.0500: 1.0000

Regression Diagnostics:

Row	Predicted	Residual	Std. Res.	Stud. Res.	Stud. Del. Res.
4	6.7430	0.1588	1.3126	1.6414	1.8487
5	6.5391	0.0609	0.5037	0.5809	0.5582
6	6.3413	-0.0313	-0.2587	-0.2840	-0.2690
7	6.1495	-0.0195	-0.1614	-0.1721	-0.1626
8	5.9636	-0.1136	-0.9385	-0.9873	-0.9857
9	5.7832	-0.1832	-1.5141	-1.5895	-1.7670
10	5.6083	-0.0983	-0.8125	-0.8593	-0.8456
11	5.4387	-0.0587	-0.4851	-0.5212	-0.4990
12	5.2742	0.0258	0.2131	0.2344	0.2216
13	5.1147	0.0753	0.6223	0.7053	0.6841
14	4.9600	0.1886	1.5585	1.8328	2.1827

Influence Diagnostics:

Row	Cook'sDist	Leverage	DFFITs
4	0.7593	0.3605	1.3880
5	0.0557	0.2482	0.3208
6	0.0083	0.1700	-0.1217
7	0.0020	0.1208	-0.0603
8	0.0520	0.0963	-0.3219
9	0.1289	0.0926	-0.5645
10	0.0438	0.1061	-0.2914
11	0.0210	0.1339	-0.1962
12	0.0057	0.1731	0.1014
13	0.0708	0.2215	0.3649
14	0.6432	0.2769	1.3507

95% Confidence:

Row	Predicted	Regr. 5%	Regr. 95%	Pop. 5%	Pop. 95%
4	6.7430	6.5787	6.9073	6.4237	7.0622
5	6.5391	6.4027	6.6754	6.2333	6.8449
6	6.3413	6.2285	6.4542	6.0452	6.6374
7	6.1495	6.0544	6.2447	5.8598	6.4393
8	5.9636	5.8786	6.0485	5.6770	6.2501
9	5.7832	5.6999	5.8665	5.4971	6.0693
10	5.6083	5.5191	5.6975	5.3204	5.8962
11	5.4387	5.3385	5.5388	5.1472	5.7301
12	5.2742	5.1603	5.3881	4.9778	5.5707
13	5.1147	4.9859	5.2435	4.8122	5.4172
14	4.9600	4.8160	5.1041	4.6507	5.2693

Nonlinear Regression: 130nm, 398.15K, 2.5V

```
[Variables]
x = col(10)
y = col(11)
reciprocal_y = 1/abs(y)
reciprocal_ysquare = 1/y^2
'Automatic Initial Parameter Estimate Functions
xnear0(q) = max(abs(q))-abs(q)
yatxnear0(q,r) = xatymax(q,xnear0(r))
[Parameters]
a = yatxnear0(y,x) "Auto {{previous: 5.44426}}
b = if(x50(x,y)-min(x)=0, 1, -ln(.5)/(x50(x,y)-min(x))) "Auto {{previous: 0.000319428}}
[Equation]
f = a*exp(-b*x)
fit f to y
"fit f to y with weight reciprocal_y
"fit f to y with weight reciprocal_ysquare
[Constraints]
b>0
[Options]
```

tolerance=0.0001
 stepsize=100
 iterations=100

R = 0.89745925 Rsqr = 0.80543310 Adj Rsqr = 0.78381455

Standard Error of Estimate = 0.2520

	Coefficient	Std. Error	t	P
a	5.4443	0.1517	35.8959	<0.0001
b	0.0003	0.0001	6.1554	0.0002

Analysis of Variance:

	DF	SS	MS	F	P
Regression	1	2.3663	2.3663	37.2566	0.0002
Residual	9	0.5716	0.0635		
Total	10	2.9379	0.2938		

PRESS = 1.2230

Durbin-Watson Statistic = 1.3834

Normality Test: K-S Statistic = 0.2084 Significance Level = 0.6724

Constant Variance Test: Failed (P = 0.0290)

Power of performed test with alpha = 0.0500: 0.9849

Regression Diagnostics:

Row	Predicted	Residual	Std. Res.	Stud. Res.	Stud. Del. Res.
4	5.4443	0.6001	2.3813	2.9817	25.4908
5	5.2731	-0.2731	-1.0837	-1.2502	-1.2966
6	5.1073	-0.2073	-0.8227	-0.9029	-0.8927
7	4.9468	-0.1668	-0.6617	-0.7056	-0.6845
8	4.7912	-0.1212	-0.4811	-0.5061	-0.4841
9	4.6406	-0.0606	-0.2405	-0.2525	-0.2389
10	4.4947	-0.0447	-0.1775	-0.1878	-0.1774
11	4.3534	-0.0434	-0.1723	-0.1852	-0.1749
12	4.2166	0.0434	0.1724	0.1895	0.1791
13	4.0840	0.1060	0.4206	0.4765	0.4550
14	3.9556	0.1752	0.6952	0.8166	0.8001

Influence Diagnostics:

Row	Cook'sDist	Leverage	DFBETS
4	2.5241	0.3622	19.2085
5	0.2586	0.2486	-0.7458
6	0.0834	0.1698	-0.4038
7	0.0341	0.1206	-0.2535
8	0.0136	0.0963	-0.1580
9	0.0033	0.0927	-0.0764
10	0.0021	0.1064	-0.0612
11	0.0027	0.1341	-0.0688
12	0.0038	0.1731	0.0819
13	0.0322	0.2208	0.2422
14	0.1267	0.2753	0.4931

95% Confidence:

Row	Predicted	Regr. 5%	Regr. 95%	Pop. 5%	Pop. 95%
4	5.4443	5.1012	5.7874	4.7789	6.1097
5	5.2731	4.9888	5.5574	4.6361	5.9102
6	5.1073	4.8724	5.3423	4.4907	5.7240
7	4.9468	4.7488	5.1447	4.3433	5.5503
8	4.7912	4.6144	4.9681	4.1943	5.3882
9	4.6406	4.4670	4.8142	4.0447	5.2366
10	4.4947	4.3087	4.6807	3.8951	5.0944
11	4.3534	4.1446	4.5622	3.7463	4.9606
12	4.2166	3.9794	4.4537	3.5991	4.8340
13	4.0840	3.8161	4.3519	3.4541	4.7139
14	3.9556	3.6565	4.2547	3.3118	4.5994

Nonlinear Regression: 130nm, 298.15K, 4.05V

```
[Variables]
x = col(2)
y = col(3)
reciprocal_y = 1/abs(y)
reciprocal_ysquare = 1/y^2
'Automatic Initial Parameter Estimate Functions
xnear0(q) = max(abs(q))-abs(q)
yatxnear0(q,r) = xatymax(q,xnear0(r))
[Parameters]
a = yatxnear0(y,x) "Auto {{previous: 6.52409}}
b = if(x50(x,y)-min(x)=0, 1, -ln(.5)/(x50(x,y)-min(x))) "Auto {{previous: 0.000249826}}
[Equation]
f = a*exp(-b*x)
fit f to y
"fit f to y with weight reciprocal_y
"fit f to y with weight reciprocal_ysquare
[Constraints]
b>0
[Options]
tolerance=0.0001
stepsize=100
iterations=100
```

R = 0.99420186 Rsqr = 0.98843734 Adj Rsqr = 0.98715260

Standard Error of Estimate = 0.0544

	Coefficient	Std. Error	t	P
a	6.5241	0.0323	202.0870	<0.0001
b	0.0002	0.0000	27.7099	<0.0001

Analysis of Variance:

	DF	SS	MS	F	P
Regression	1	2.2745	2.2745	769.3677	<0.0001
Residual	9	0.0266	0.0030		
Total	10	2.3011	0.2301		

PRESS = 0.0437

Durbin-Watson Statistic = 0.8986

Normality Test: K-S Statistic = 0.1885 Significance Level = 0.7860

Constant Variance Test: Passed (P = 0.9676)

Power of performed test with alpha = 0.0500: 1.0000

Regression Diagnostics:

Row	Predicted	Residual	Std. Res.	Stud. Res.	Stud. Del. Res.
4	6.5241	0.0136	0.2502	0.3110	0.2948
5	6.3631	0.0469	0.8621	0.9930	0.9922
6	6.2061	0.0539	0.9908	1.0880	1.1007
7	6.0530	-0.0430	-0.7909	-0.8440	-0.8293
8	5.9037	-0.0537	-0.9868	-1.0384	-1.0435
9	5.7580	-0.0380	-0.6988	-0.7334	-0.7130
10	5.6159	-0.0159	-0.2929	-0.3096	-0.2935
11	5.4774	-0.0474	-0.8711	-0.9354	-0.9282
12	5.3422	-0.0322	-0.5926	-0.6518	-0.6295
13	5.2104	0.0096	0.1763	0.2002	0.1892
14	5.0819	0.1073	1.9743	2.3340	3.5025

Influence Diagnostics:

Row	Cook'sDist	Leverage	DFFITs
4	0.0263	0.3525	0.2175
5	0.1611	0.2462	0.5671
6	0.1218	0.1706	0.4993

7	0.0495	0.1220	-0.3091
8	0.0578	0.0968	-0.3416
9	0.0273	0.0920	-0.2270
10	0.0056	0.1048	-0.1004
11	0.0669	0.1327	-0.3630
12	0.0445	0.1733	-0.2882
13	0.0058	0.2245	0.1018
14	1.0830	0.2845	2.2086

95% Confidence:

Row	Predicted	Regr. 5%	Regr. 95%	Pop. 5%	Pop. 95%
4	6.5241	6.4511	6.5971	6.3810	6.6671
5	6.3631	6.3021	6.4242	6.2258	6.5004
6	6.2061	6.1553	6.2569	6.0730	6.3392
7	6.0530	6.0100	6.0960	5.9227	6.1833
8	5.9037	5.8654	5.9419	5.7748	6.0325
9	5.7580	5.7207	5.7953	5.6295	5.8865
10	5.6159	5.5761	5.6558	5.4866	5.7452
11	5.4774	5.4326	5.5222	5.3465	5.6083
12	5.3422	5.2910	5.3934	5.2090	5.4754
13	5.2104	5.1521	5.2687	5.0743	5.3465
14	5.0819	5.0163	5.1475	4.9425	5.2213

Nonlinear Regression: 130nm, 348.15K, 4.05V

[Variables]

x = col(6)

y = col(7)

reciprocal_y = 1/abs(y)

reciprocal_ysquare = 1/y^2

'Automatic Initial Parameter Estimate Functions

xnear0(q) = max(abs(q))-abs(q)

yatxnear0(q,r) = xatymax(q,xnear0(r))

[Parameters]

a = yatxnear0(y,x) "Auto {{previous: 5.47147}}

b = if(x50(x,y)-min(x)=0, 1, -ln(.5)/(x50(x,y)-min(x))) "Auto {{previous: 0.000372677}}

[Equation]

f = a*exp(-b*x)

fit f to y

"fit f to y with weight reciprocal_y

"fit f to y with weight reciprocal_ysquare

[Constraints]

b>0

[Options]

tolerance=0.0001

stepsize=100

iterations=100

R = 0.99709819 Rsqr = 0.99420480 Adj Rsqr = 0.99356089

Standard Error of Estimate = 0.0453

	Coefficient	Std. Error	t	P
a	5.4715	0.0276	198.5888	<0.0001
b	0.0004	0.0000	39.0512	<0.0001

Analysis of Variance:

	DF	SS	MS	F	P
Regression	1	3.1710	3.1710	1544.0089	<0.0001
Residual	9	0.0185	0.0021		
Total	10	3.1895	0.3190		

PRESS = 0.0305

Durbin-Watson Statistic = 1.1364

Normality Test: K-S Statistic = 0.2382 Significance Level = 0.5019

Constant Variance Test: Passed (P = 0.1017)

Power of performed test with alpha = 0.0500: 1.0000

Regression Diagnostics:

Row	Predicted	Residual	Std. Res.	Stud. Res.	Stud. Del. Res.
4	5.4715	0.0049	0.1087	0.1369	0.1292
5	5.2713	0.0087	0.1916	0.2213	0.2092
6	5.0785	0.0415	0.9161	1.0050	1.0057
7	4.8927	-0.0027	-0.0597	-0.0636	-0.0600
8	4.7137	-0.0137	-0.3027	-0.3184	-0.3019
9	4.5413	-0.0313	-0.6903	-0.7250	-0.7044
10	4.3752	-0.0252	-0.5551	-0.5876	-0.5649
11	4.2151	-0.0151	-0.3333	-0.3584	-0.3403
12	4.0609	-0.0709	-1.5646	-1.7203	-1.9798
13	3.9124	0.0076	0.1688	0.1909	0.1803
14	3.7692	0.0977	2.1552	2.5195	4.3758

Influence Diagnostics:

Row	Cook'sDist	Leverage	DFFITS
4	0.0055	0.3696	0.0989
5	0.0082	0.2503	0.1209
6	0.1028	0.1692	0.4538
7	0.0003	0.1196	-0.0221
8	0.0054	0.0960	-0.0984
9	0.0271	0.0934	-0.2261
10	0.0208	0.1077	-0.1963
11	0.0100	0.1352	-0.1346
12	0.3092	0.1728	-0.9050
13	0.0051	0.2179	0.0952
14	1.1637	0.2683	2.6495

95% Confidence:

Row	Predicted	Regr. 5%	Regr. 95%	Pop. 5%	Pop. 95%
4	5.4715	5.4091	5.5338	5.3515	5.5915
5	5.2713	5.2200	5.3226	5.1567	5.3860
6	5.0785	5.0363	5.1206	4.9676	5.1893
7	4.8927	4.8573	4.9282	4.7842	5.0012
8	4.7137	4.6820	4.7455	4.6064	4.8210
9	4.5413	4.5100	4.5726	4.4341	4.6485
10	4.3752	4.3415	4.4088	4.2673	4.4831
11	4.2151	4.1774	4.2528	4.1059	4.3243
12	4.0609	4.0183	4.1035	3.9499	4.1719
13	3.9124	3.8645	3.9602	3.7992	4.0255
14	3.7692	3.7161	3.8223	3.6538	3.8847

Nonlinear Regression: 130nm, 398.15K, 4.05V

```
[Variables]
x = col(10)
y = col(11)
reciprocal_y = 1/abs(y)
reciprocal_ysquare = 1/y^2
'Automatic Initial Parameter Estimate Functions
xnear0(q) = max(abs(q))-abs(q)
yatxnear0(q,r) = xatymax(q,xnear0(r))
[Parameters]
a = yatxnear0(y,x) "Auto {{previous: 4.75819}}
b = if(x50(x,y)-min(x)=0, 1, -ln(.5)/(x50(x,y)-min(x))) "Auto {{previous: 0.000438572}}
[Equation]
f = a*exp(-b*x)
fit f to y
"fit f to y with weight reciprocal_y
"fit f to y with weight reciprocal_ysquare
[Constraints]
b>0
[Options]
tolerance=0.0001
stepsize=100
```

iterations=100

R = 0.99727239 Rsqr = 0.99455223 Adj Rsqr = 0.99394692

Standard Error of Estimate = 0.0436

	Coefficient	Std. Error	t	P
a	4.7582	0.0268	177.3685	<0.0001
b	0.0004	0.0000	40.1613	<0.0001

Analysis of Variance:

	DF	SS	MS	F	P
Regression	1	3.1216	3.1216	1643.0509	<0.0001
Residual	9	0.0171	0.0019		
Total	10	3.1387	0.3139		

PRESS = 0.0267

Durbin-Watson Statistic = 1.3963

Normality Test: K-S Statistic = 0.1552 Significance Level = 0.9339

Constant Variance Test: Failed (P = 0.0234)

Power of performed test with alpha = 0.0500: 1.0000

Regression Diagnostics:

Row	Predicted	Residual	Std. Res.	Stud. Res.	Stud. Del. Res.
4	4.7582	0.0407	0.9339	1.1849	1.2160
5	4.5540	0.0560	1.2843	1.4852	1.6117
6	4.3586	-0.0586	-1.3447	-1.4745	-1.5962
7	4.1716	-0.0516	-1.1835	-1.2605	-1.3096
8	3.9926	-0.0426	-0.9770	-1.0274	-1.0310
9	3.8213	-0.0213	-0.4879	-0.5127	-0.4906
10	3.6573	0.0527	1.2091	1.2811	1.3358
11	3.5004	-0.0004	-0.0084	-0.0091	-0.0085
12	3.3502	-0.0002	-0.0039	-0.0042	-0.0040
13	3.2064	-0.0064	-0.1472	-0.1660	-0.1568
14	3.0688	0.0336	0.7702	0.8951	0.8842

Influence Diagnostics:

Row	Cook'sDist	Leverage	DFFITs
4	0.4281	0.3788	0.9496
5	0.3722	0.2523	0.9363
6	0.2199	0.1683	-0.7180
7	0.1067	0.1184	-0.4799
8	0.0559	0.0957	-0.3354
9	0.0137	0.0943	-0.1583
10	0.1007	0.1093	0.4680
11	0.0000	0.1365	-0.0034
12	0.0000	0.1724	-0.0018
13	0.0038	0.2143	-0.0819
14	0.1405	0.2597	0.5237

95% Confidence:

Row	Predicted	Regr. 5%	Regr. 95%	Pop. 5%	Pop. 95%
4	4.7582	4.6975	4.8189	4.6424	4.8740
5	4.5540	4.5045	4.6036	4.4437	4.6644
6	4.3586	4.3182	4.3991	4.2520	4.4652
7	4.1716	4.1377	4.2055	4.0673	4.2759
8	3.9926	3.9621	4.0231	3.8894	4.0958
9	3.8213	3.7910	3.8516	3.7181	3.9244
10	3.6573	3.6247	3.6899	3.5534	3.7612
11	3.5004	3.4639	3.5368	3.3953	3.6055
12	3.3502	3.3092	3.3911	3.2434	3.4569
13	3.2064	3.1608	3.2521	3.0978	3.3151
14	3.0688	3.0186	3.1191	2.9582	3.1795

References

- [1] NASA Jet Propulsion Laboratory Derating Guidelines JPL-D-8545.
- [2] J. D. Walter, "Methods to account for accelerated semiconductor device wearout in long life aerospace applications," UMD Ph.D. Dissertation, 2003.
- [3] W. H. Roadstrum and D. H. Wolaver, *Electrical Engineering For All Engineers*. Harper & Row, Publishers, Inc, 1987.
- [4] J. M. Galbraith, et al., "Reliability challenges for low voltage/low power integrated circuits," *Quality and Reliability Engineering International*, vol. 12, pp. 271–279, 1996.
- [5] P. Pop, "TDTS 51: Advance computer architecture lecture 11." [/webhttp://www.ida.liu.se/TDTS51/lectures/lecture11.pdf](http://www.ida.liu.se/TDTS51/lectures/lecture11.pdf), 2000.
- [6] T. Givargis, "Uci/ics253 lecture 9." [<www.ics.uci.edu/_givargis/courses/253/notes/lecture9.pdf>](http://www.ics.uci.edu/_givargis/courses/253/notes/lecture9.pdf), 2002.
- [7] W. J. Hsu, et al., "Computer-aided VLSI circuit reliability assurance," *International Journal of Modeling and Simulation*, vol. 9, no. 4, pp. 118-123, 1989.
- [8] B. S. Chun, et al., "Circuit-level reliability simulation and its applications," *Journal of the Korean Institute of Telematics and Electronics*, vol. 31A, no. 1, pp. 93-102, 1994.
- [9] S.M. Alam, et al., "Electromigration reliability comparison of Cu and Al interconnects," *Proceedings. 6th International Symposium on Quality Electronic Design*, pp. 303-308, 2005.
- [10] P. C. Li, et al., "iProbe-d: a hot-carrier and oxide reliability simulator," *32nd IEEE International Reliability Physics Proceedings*, pp. 274-279, 1994.
- [11] X. Xuan and A. Chatterjee, "Sensitivity and Reliability Evaluation for Mixed-Signal ICs under Electromigration and Hot-Carrier Effects," *IEEE ISDFT*, 2001.
- [12] J.W. Lathrop, et al., "Design rules hold key to future VLSI reliability," *Proceedings of the Seventh Biennial University/Government/Industry Microelectronics Symposium*, pp. 91-94, 1987.
- [13] C. Hu, "Berkeley reliability simulator BERT: An IC reliability simulator," *Microelectronics Journal*, vol. 23, no. 2, pp. 97-102, 1992.
- [14] W. Bornstein, et al., "Field Degradation of Memory Components from Hot Carriers," *IEEE IRPS*, 2006.
- [15] University of Maryland - Center for Reliability Engineering, AVSI 17 Project, 2002-2006.
- [16] X. Li, et al., "Simulating and Improving Microelectronic Device Reliability by Scaling Voltage and Temperature," *IEEE ISQED*, 2005.

- [17] J. Srinivasan, et al., "The Impact of Technology Scaling on Lifetime Reliability," *International Conference on Dependable Systems and Networks*, June 2004.
- [18] Failure Mechanisms and Models for Semiconductor Devices. JEDEC Publication JEP122-A, 2002.
- [19] S.V. Kumar, et al., "Impact of NBTI on SRAM Read Stability and Design for Reliability," *IEEE ISQED*, 2006.
- [20] V. Reddy, et al., "Impact of NBTI on Digital Circuit Reliability," *IEEE IRPS*, 2002.
- [21] N.K. Jha, et al., "NBTI Degradation and its Impact for Analog Circuit Reliability," *IEEE Transactions on Electron Devices*, Dec. 2005.
- [22] J. Stathis, "Physical Models of Ultra-thin Oxide Reliability in CMOS Devices and Implications for Circuit Reliability," *IEEE IRPS*, 2001.
- [23] E. Rosenbaum, et al., "Circuit Reliability Simulator Oxide Breakdown Module," Technical Digest, of International Electron Devices Meeting, pp. 331-334, 1989.
- [24] L.B. Khin, et al., "Circuit Reliability Simulator for Interconnect, Via, and Contact Electromigration", *IEEE Transactions on Electron Devices*, vol. 39, no. 11, pp. 2472-2479, 1992.
- [25] X. Li, "Deep Submicron CMOS VLSI Circuit Reliability Modeling, Simulation and Design," UMD Ph.D. Dissertation, 2005.
- [26] J. Qin, "A New Physics-of-Failure Based VLSI Circuits Reliability Simulation and Prediction Methodology," UMD Ph.D. Dissertation, 2007.
- [27] T.A. Mazzuchi and R. Soyer, "A Bayes Method for Assessing Product-Reliability During Development Testing," *IEEE Transactions on Reliability*, Vol. 42, No. 3, Sept. 1993.
- [28] A. Jee, et al., "Optimizing Memory Tests by Analyzing Defect Coverage," IEEE, 2000.
- [29] L.C. Tang, et al., "Planning of Step-stress Accelerated Degradation Test," *IEEE RAMS*, 2004.
- [30] M. Kraisch, "Accelerated Testing for Demonstration of Product Lifetime Reliability," *IEEE RAMS*, 2003.
- [31] A. Turner, "Product Reliability in 90nm CMOS and Beyond," *IEEE IRW*, 2005.
- [32] C.J. Lu and W.Q. Meeker, "Using Degradation Measures to Estimate a Time-to-Failure Distribution," *Technometrics*, 35(2), 161-174, 1993.
- [33] C.J. Lu, et al., "Statistical Inference of a Time-to-Failure Distribution Derived from Linear Degradation Data," *Technometrics*, 39(4), 391-400, 1997.
- [34] H. Guo and A. Mettas, "Improved Reliability Using Accelerated Degradation & Design of Experiments," *IEEE RAMS*, 2007.
- [35] C. Mead, "Fundamental limitations in microelectronics – I. MOS technology", *Solid State Electronics*, vol. 15, pp 819-829, 1972.

- [36] R. H. Dennard, F. H. Gaensslen, H-N, Yu, V.I. Rideout, E. Bassous, and A. R. LeBlanc, "Design of ion-implanted MOSFET's with very small physical dimensions," *IEEE Journal of Solid-State Circuits*, SC-9, pp.256-268, 1974.
- [37] H. Iwai, "CMOS Scaling towards its Limits", *IEEE*, pp. 31-34, 1998.
- [38] R.D. Isaac, "Reaching the Limits of CMOS Technology", *IEEE*, pp. 3, 1998.
- [39] S. Borkar, "Design Challenges of Technology Scaling", *IEEE Micro*, pp. 23-29, 1999.
- [40] Y. Taur, "CMOS Scaling Beyond 0.1 μ m: How Far Can it Go", *VLSI-TSA*, pp. 6-9, 1999.
- [41] G. G. Shahidi, "Challenges of CMOS scaling at below 0.1 μ m", *The 12th International Conference on Microelectronics*, October 31 – November 2, 2000.
- [42] L. Chang, et al., "Moore's Law Lives on", *IEEE Circuits and Devices Magazine*, pp. 35-42, January, 2003.
- [43] D. Foty, et al., "CMOS Scaling Theory – Why Our Theory of Everything Still Works and What that Means for the Future", *IEEE*, 2004.
- [44] T. Skotnicki, et al., "The End of CMOS Scaling", *IEEE Circuits and Devices Magazine*, pp. 16-26, January, 2005.
- [45] K. Lee, et al., "The Impact of Semiconductor Technology Scaling on CMOS RF and Digital Circuits for Wireless Application", *IEEE Transactions on Electron Devices*, Vol. 52, No.7, July 2005.
- [46] T. Chen, et al., "Overcoming Research Challenges for CMOS Scaling: Industry Directions", *IEEE*, 2006.
- [47] R. Puri, T. Karnik, R. Joshi, "Technology Impacts on sub-90nm CMOS Circuit Design & Design methodologies", *Proceedings of the 19th International Conference on VLSI Design*, 2006.
- [48] Intel news release, 2007.
- [49] S. Nassif, "Design for Variability in DSM Technologies", *Proc ISQED*, 2000.
- [50] D. Sylvester, et al., "Future Performance Challenges in Nanometer Design", *Proceedings of the 38th DAC*, pp. 3-8.
- [51] D. Duarte, et al., "Impact of Scaling on the Effectiveness of Dynamic Power Reduction Schemes", *Proceedings of the 2002 IEEE International Conference on Computer Design: VLSI in Computers and Processors*, 2002.
- [52] R. Viswanath, et al., "Thermal Performance Challenges from Silicon to Systems", *Intel Technology Journal*, 3rd quarter, 2000.
- [53] P. Zarkesh-Ha et al., "Chip Clock Distribution Networks", *Proc. IITC*, June, 1999.
- [54] V. Mehrotra et al., "Modeling the Effects of Manufacturing Variation on High-speed Microprocessor Interconnect Performance", *Proceedings of IEDM*, December, 1998.
- [55] V. Mehrotra et al., "Technology Scaling Impact of Variation on Clock Skew and Interconnect Delay", *IEEE*, 2001.

- [56] A. Vassighi, et al., “CMOS IC Technology Scaling and Its Impact on Burn-in”, *IEEE Transactions on Device and Materials Reliability*, Vol. 4, No. 2, pp. 208-221, June 2004.
- [57] M. White, et al., “Microelectronics Reliability: Physics-of-Failure Based Modeling and Lifetime Evaluation”, JPL Publication 08-5 2/08, 2008.
- [58] IEDM.
- [59] Y. Chen, et al, “Stress-Induced MOSFET Mismatch for Analog Circuit”, *IEEE International Integrated Reliability Workshop*, 2001.
- [60] H. Yang, et al, “Effect of Gate Oxide Breakdown on RF Device and Circuit Performance”, *IEEE International Reliability and Physics Symposium*, 2003.
- [61] C. Schlunder, et al, “On the Degradation of P-MOSFETS in Analog and RF Circuit Under Inhomogeneous Negative Bias Temperature Stress”, *International Reliability and Physics Symposium*, 2003.
- [62] R. Rodriguez, et al, “Modeling and Experimental Verification of the Effect of Gate Oxide Breakdown on CMOS Inverters”, *International Reliability and Physics Symposium*, 2003.
- [63] M. Agostinelli, et al, “PMOS NBTI-Induced Circuit Mismatch in Advanced Technologies”, *IEEE International Reliability and Physics Symposium*, 2004.
- [64] J. Maiz, “Reliability Challenges: Preventing Them from Becoming Limiters to Technology Scaling”, *IEEE International Integrated Reliability Workshop*, 2006.
- [65] A. Krishnan, “NBTI: Process, Device, and Circuits”, *IEEE International Reliability Physics Symposium*, 2005.
- [66] A. Haggag, et al., “Realistic Projection of Product Fails from NBTI and TDDB”, *IEEE International Reliability Physics Symposium*, pp. 541-544, 2006.
- [67] A. Haggag, et al., “Understanding SRAM High-Temperature-Operating-Life NBTI: Statistics and Permanent vs Recoverable Damage”, *IEEE International Reliability Physics Symposium*, pp 452-456, 2007.
- [68] J. Bernstein, AVSI Quarter Report, 2006.
- [69] M. White and Y. Chen, NASA Scaled CMOS Technology Reliability Users Guide, JPL Publication 08-14 3/08, 2008.
- [70] M. White and J. Bernstein, Microelectronics Reliability: Physics-of-Failure Based Modeling and Lifetime Evaluation, JPL Publication 08-5 2/08, 2008.
- [71] M. Ohring, Reliability and Failure of Electronic Materials and Devices, Academic Press, pp 330-338, 1998.
- [72] E. Takeda, et al., Hot-Carrier Effects in MOS Devices, Academic Press, ch. 2, pp. 49–58. 1995.
- [73] M. Song, et al., “Comparison of NMOS and PMOS Hot Carrier Effects from 300 to 77 k,” *IEEE Transactions on Electron Devices*, vol. 44, pp. 268–276, 1997.

- [74] E. S. Snyder, et al., "The Impact of Statistics on Hot Carrier Lifetime Estimates of n-Channel MOSFETs," *SPIE – Microelectronics Manufacturing and Reliability*, vol. 1802, pp. 180–187, 1992.
- [75] E. Takeda, et al., *Hot-Carrier Effects in MOS Devices*, Academic Press ch. 5, pp. 124–125, Academic Press, 1995.
- [76] A. Acovic, et al., "A Review of Hot Carrier Degradation Mechanisms in MOSFETs," *Microelectronics Reliability*, vol. 36, pp. 845–869, 1996.
- [77] C. Hu, et al., "Hot Electron-induced MOSFET Degradation-Model, Monitor, and Improvement," *IEEE Journal of Solid-State Circuits*, vol. SC-20, pp. 295–305, 1985.
- [78] JEDEC, *Failure Mechanisms and Models for Semiconductor Devices*. JEDEC Solid State Technology Association, 2003.
- [79] Ibid. M. Ohring, p. 281.
- [80] J. B. Lai, et al., "A Study of Bimodal Distributions of time-to-Failure of Copper via Electromigration," *International Symposium on VLSI Technology, Systems, and Applications*, pp. 271–274, 2001.
- [81] E. T. Ogawa, et al., "Statistics of Electromigration Early Failures in Cu/Oxide Dual-Damascene Interconnects," *39th Annual International Reliability Physics Symposium*, pp. 341–349, 2001.
- [82] Ibid. M. Ohring, p. 278.
- [83] S. Tsujikawa, et al., "Evidence for Bulk Trap Generation During NBTI Phenomenon in pMOSFETs with Ultrathin SiON Gate Dielectrics," *IEEE Transactions on Electron Devices*, Vol. 1, No. 1, Jan. 2006.
- [84] S. Mahapatra, et al. "Investigation and Modeling of Interfact and Bulk Trap Generation during NBTI of p-MOSFETs," *IEEE Transactions on Electron Devices*, Vol. 51, No. 9, Sept. 2004.
- [85] Y.F. Chen, "NBTI in Deep Sub-micron p-gate p-MOSFETs," *IEEE Integrated Reliability Workshop*, 2000.
- [86] G. Haller, et al., "Bias Temperature Stress on Metal-Oxide-Semiconductor Structures as Compared to Ionizing Irradiation and Tunnel Injection," *Journal of Applied Physics*, vol. 56, p. 184, 1984.
- [87] P. Chaparala, et al., "Threshold Voltage Drift in PMOSFETS due to NBTI and HCI," *IEEE Integrated Reliability Workshop*, pp. 95–97, IEEE, 2000.
- [88] M. White and J. Bernstein, *Microelectronics Reliability: Physics-of-Failure Based Modeling and Lifetime Evaluation*, JPL Publication 08-5 2/08, p52, 2008.
- [89] H. Iwai, et al., "The Future of Ultra-Small-Geometry MOSFETs beyond 0.1 micron," *Microelectronic Engineering*, vol. 28, pp. 147–154, 1995.
- [90] J. B. Bernstein, et al. "Electronic Circuit Reliability Modeling," *Microelectronics Reliability*, No. 46, pp. 1957-1979, 2006.

- [91] Electronic Derating for Optimum Performance, Reliability Analysis Center under contract to Defense Supply Center Columbus (DSCC), p104, 2000.
- [92] M. White, et al., "Impact of Junction Temperature on Microelectronics Device Reliability and Considerations for Space Applications," *IEEE Integrated Reliability Workshop*, 2003.
- [93] M. White, Supplier Survey with eight major microelectronics suppliers, Appendix A, 2003.
- [94] M. White, et al., "Impact of Device Scaling on Deep Sub-Micron Transistor Reliability – A Study of Reliability Trends Using SRAM," *IEEE Integrated Reliability Workshop*, 2005.
- [95] W. Meeker and L. Escobar, *Statistical Methods for Reliability Data*, John Wiley and Sons, 1998.
- [96] M. Talmer, et al. "Competing Failure Modes in Microelectronic Devices and Acceleration Factors Modeling," *Intl. Symposium on Stochastic Models in Reliability, Safety, Security and Logistics Proceedings*, Israel. Feb. 2005.
- [97] M. White, et al., "Product Reliability trends, Derating Considerations and Failure Mechanisms with Scaled CMOS," *IEEE Integrated Reliability Workshop*, 2006.
- [98] A. Tossi, et al., "Hot-Carrier Photo emission in Scaled CMOS Technologies: A Challenge for Emission Based Testing and Diagnostics," *IEEE International Reliability Physics Symposium*, 2006.
- [99] J. Baker, "The 1T1C DRAM and its Impact on Society," Dept. of Electrical and Computer Engineering, Boise State University, 2008.
- [100] A. Sharma, *Semiconductor Memories – Technology, Testing, and Reliability*, John Wiley and Sons, pp. 40-45, 1997.
- [101] IDC, *Isuppli, IC Insights*, Q1, 2006.
- [102] Manufacturer's data sheet.
- [103] M. Modarres, et al., *Reliability Engineering and Risk Analysis, A Practical Guide*. Marcel Dekker, Inc., pp 112-121, 1999.
- [104] M. Modarres, ENRE-641 Accelerated Testing Course Notes, UMD, pp 448-458, 2005.
- [105] J.B. Bernstein, ENRE-653 Electronic Reliability Engineering Principles, UMD, L. 3, pg. 29.
- [106] D.C. Shaw, et al. "Radiation Effects in Five Volt Advanced Lower Voltage DRAMs," *IEEE Transactions on Nuclear Science*, No. 41, pg. 2259, 1994.
- [107] ITRS 2007.